APPENDIX B: UFI MODELING REPORT

MATHEMATICAL MODELS TO SUPPORT EVALUATION OF TWO MANAGEMENT ALTERNATIVES FOR SCHOHARIE RESERVOIR: MULTI-LEVEL INTAKE FACILITY AND BAFFLE

Upstate Freshwater Institute, Syracuse, N.Y.

September 2006

Table of Contents

1. SYSTEM DESCRIPTION, MANAGEMENT ISSUES AND ALTERNATIVES

Schoharie Reservoir is located (latitude 42º 23´ N; longitude 74º 26´ W) in the Catskill Mountains of southwestern New York, 190 km from New York City (NYC; Figure 1a). The reservoir was initially filled in 1927 and is part of a network of nineteen reservoirs that supplies water to nine million people in the NYC area. The impoundment is 8 km long, has a maximum width of 1 km, and lacks dendritic features (Figure 1b). When full, the reservoir has an area of 4.6 km^2, a volume of 79 x 10^6 m^3, a maximum depth of 41 m, and a surface elevation of 344.43 m. These morphometric features often vary associated with drawdown of the impoundment's surface (water surface elevation, WSE), that occurs in response to withdrawals for the water supply (single bottom intake, Figure 1b) exceeding inputs from the watershed (815 km^2). The greatest drawdown is usually observed in September and October, as illustrated for the 1989-2002 period (Figure 2a). The substantial interannual variability in WSE, depicted here through monthly means and ranges for this period (Figure 2a), and by temporally detailed daily time series for 1998 (Figure 2b) and 2002 (Figure 2c), is driven primarily by natural variations in runoff. The reservoir has a dimictic stratification regime, and it flushes (on average) about 10 times per year, on a completely mixed basis.

Schoharie Creek, the major tributary (drains ~ 75% of the watershed) and source of sediment, enters the southern end of the reservoir (Figure 1b). Glacial lake silt and clay deposits in the watershed are greatest in valley bottoms along the present stream channels, including Schoharie Creek and its tributaries. These deposits are poorly armored (Smith 2002); exposure of these fine sediments along meander bends and channel troughs promotes elevated concentrations (and loads) of suspended sediment (Smith 2002; Effler et al. 2006a) and levels of turbidity (O'Donnell and Effler 2006) in the stream during runoff events. The vast majority of the particles responsible for these conditions are clay minerals (Peng et al. 2004).

Conspicuous increases in turbidity (T_n) occur in the reservoir's water column in response to tributary inputs received during runoff events (Effler et al. 2006b), and from resuspension of deposited terrigenous inputs during drawdown intervals from up-reservoir portions of the impoundment. The turbid stream waters enter as a plunging density current during summer and fall because of the cooler temperatures of Schoharie Creek relative to the reservoir (O'Donnell and Effler 2006), forming an underflow in up-reservoir areas and an interflow down-reservoir (Effler et al. 2006a). These impacts diminish along the axis of the reservoir for minor and moderate runoff events, but can be greater and more persistent in down-reservoir portions of the reservoir for larger (i.e., more rare) events (Effler et al. 2006a). The extent and persistence of lateral differences in turbidity are modest compared to observed longitudinal patterns (Effler et al. 2006b).

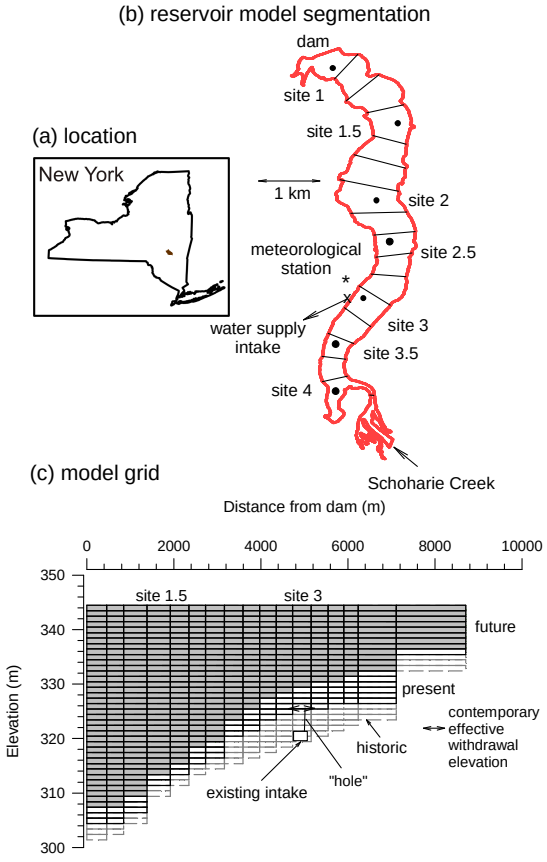

Figure 1. Schoharie Reservoir: (a) Location in New York, (b) Reservoir Shoreline, Longitudinal Model Segments, and Other Selected features, and (c) Vertical and Longitudinal Model Segments.

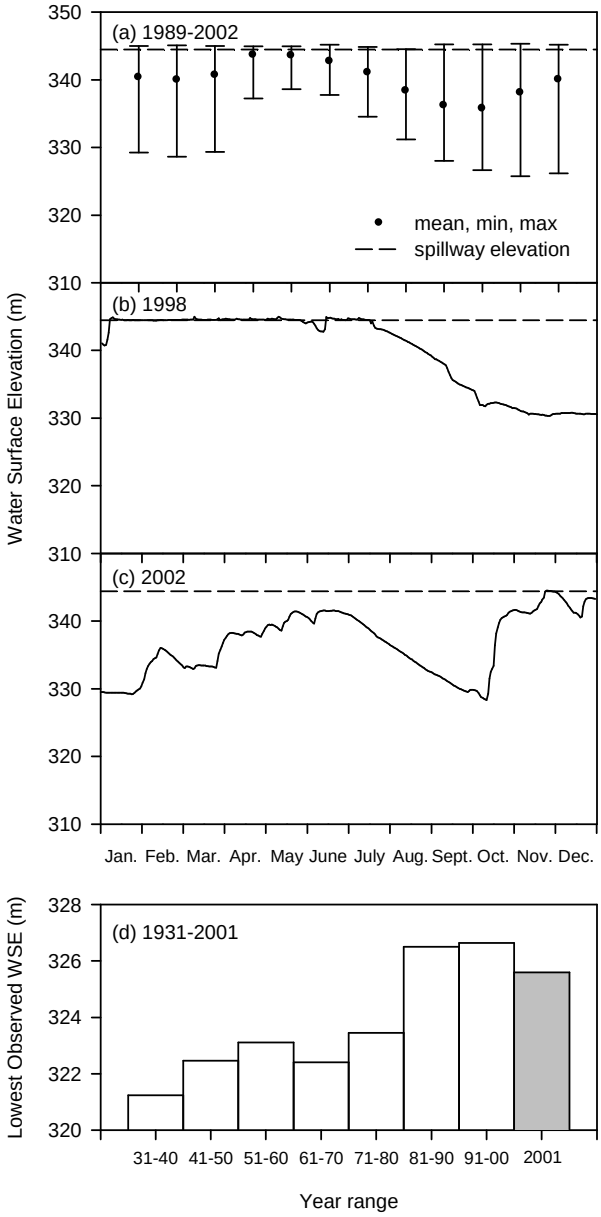

Figure 2. Variations in water surface elevation (WSE) in Schoharie Reservoir: (a) monthly means and ranges for the 1989-2002 period, (b) time series of daily values in 1998, (c) time series of daily values in 2002, (d) maximum drawdown observed for 10 y intervals since 1931, and in 2001.

Schoharie Reservoir is an upstream impoundment within the network of NYC reservoirs, as the water withdrawn for the water supply travels 29 km through an underground (Shandaken) tunnel, 20 km in Esopus Creek that receives the discharge, and subsequently two reservoirs, before delivery to the City. Esopus Creek supports a salmonid fishery. Water quality concerns for this discharge, and thus Schoharie Reservoir, are potential impacts on the stream's fishery associated with high temperature (T_w) or turbidity ($T_{n,w}$) (e.g., Newcombe 2003) of this input. Tentative water quality goals for this discharge, on a daily average basis, are $T_w \leq 70$ ºF (21.1ºC) and $T_{n,w}$ not more than 15 NTU higher than the level in Esopus Creek upstream of the point of entry of this inflow. Monitoring of the withdrawal establishes that these goals have been exceeded irregularly in recent years. These occurrences follow runoff events in the case of $T_{n,w}$ (Gelda and Effler 2006b), while $T_w >$ 21.1º C has been observed in the late summer of certain years of extensive drawdown (Gelda and Effler 2006a). The disparate runoff conditions that drive these two features of water quality confound identification of a single set of critical conditions.

NYC is evaluating a number of management alternatives to improve conditions with respect to T_w and $T_{n,w}$ in the Schoharie Reservoir withdrawal relative to emerging goals (Gannett Fleming & Hazen and Sawyer 2004). Two of these alternatives are evaluated here through the development, testing and application of mathematical models (1) a multi-level intake facility, with various possible longitudinal locations and vertical positions of the intakes, and (2) a baffle positioned adjoining the existing intake to avoid short-circuited turbid inflows reaching the intake and to promote deposition of turbidity before reaching the withdrawal. MLI facilities offer the potential benefit of providing some avoidance of layers of undesirable water quality (Hanna et al. 1999; Martin and McCutcheon 1999). A version of the MLI option that positions the facility ~ 5 km down-reservoir (e.g., site 1.5, Figure 1b) of the existing intake (e.g., site 3, Figure 1b) was identified as a preferred alternative (Skinner et al. 2003), based on analysis of limited monitoring data, and without the benefit of a mathematical model. Location of a MLI facility at this down-reservoir position would cost substantially more than if it was positioned at the present intake site, associated primarily with tunneling costs (Gannett Fleming & Hazen and Sawyer 2004).

2. MODELS TO EVALUATE MULTI-LEVEL INTAKE ALTERNATIVES

2.1. Submodels and Integrated Modeling Frameworks

2.1.1. Hydrothermal/Transport Submodel

An appropriate predictive framework is necessary to simulate fundamental transport processes and temperature patterns. Transport processes are critical in regulating T_n patterns in time and space in the reservoir, and therefore the withdrawal ($T_{n,w}$), particularly related to the behavior of turbid density currents formed during runoff events. Simulation of temperature patterns are necessary to predict temperatures in the reservoir withdrawal (T_w)

and the status with respect to the goal ($T_w \leq 21.1$ ºC). Moreover, the thermal stratification regime, a ubiquitous phenomenon in deep reservoirs and lakes, is a fundamental regulator of ecosystem metabolism and commonly monitored features of water quality.

Here the set-up and testing of a 2D hydrothermal/transport model (W2/T) to address related issues in Schoharie Reservoir at its withdrawals are documented. Two different time scales of performance of W2/T are important to address the water quality issues of this reservoir: (1) seasonal, to quantify the thermal stratification regime of the reservoir and T_w, and (2) day-to-day to describe the impacts of runoff events on T_n patterns within the reservoir and $T_{n,w}$.

2.1.1.1 Model description

The adopted computer code was the hydrothermal/transport submodel of CE-QUAL-W2 (subsequently identified as W2/T), a dynamic, laterally averaged, two-dimensional (longitudinal-vertical) model (Edinger and Buchak 1975; Cole and Wells 2002). The model is based on the finite-difference solution of partial differential equations for laterally averaged fluid motion and mass transport. The model's basic equations that describe horizontal momentum, free water surface elevation, hydrostatic pressure, continuity, equation of state, and constituent transport have been presented by Cole and Wells (2002), Chung and Gu (1998), and Gu and Chung (1998). The model assumes that vertical velocities are sufficiently small to allow the vertical momentum equation to be simplified to the hydrostatic equation. The heat budget of W2/T includes terms for evaporative heat loss, short- and long-wave radiation, convection, conduction, and back radiation (Cole and Wells 2002). The model has been successfully applied to a number of systems and issues (Chung and Gu 1998; Gelda et al. 1998; Gu and Chung 1998; Hanna et al. 1999; Gelda and Effler 2002; Ahlfeld et al. 2003).

The model represents the reservoir in the form of a grid of cells consisting of longitudinal segments and vertical layers. The geometry of the computational grid is determined by the boundaries of the longitudinal segments, the depth interval of the vertical layers, and average cross sectional width. Certain features of outflow structures are also represented, such as spillway length, and elevations of the water supply withdrawal and dam outlet(s). Required meteorological inputs for W2/T include air temperature, dew point temperature, wind speed and direction, and cloud cover (or direct measurements of solar radiation). The value of the light attenuation coefficient for downwelling irradiance (k_d, m^{-1}), that quantifies the vertical limit of the penetration of solar energy in the water column of the reservoir, is also a required input. Inflows, inflow temperatures, and outflows must also be specified. The model has six coefficients that may be adjusted in the calibration process (Table 1). The values of the coefficients for longitudinal eddy viscosity, eddy diffusivity, and wind sheltering directly affect simulated hydrodynamics which in turn affect the distribution of heat. The other two coefficients, the fraction of incident solar radiation absorbed at the water surface and the coefficient for bottom heat exchange, directly influence the heat budget. Experience with application of W2/T to multiple reservoirs in this region (Upstate Freshwater Institute 2001) and elsewhere (personal communication, T. Cole, U.S. Army Corps of Engineers, Vicksburg, MS) indicates values of these coefficients generally do

not differ greatly, with the exception of the wind sheltering coefficient that reflects local topography.

Table 1. Two-dimensional hydrothermal/hydrodynamic model (W2/T) coefficients for Schoharie Reservoir.

Coefficient	Value
Longitudinal eddy viscosity	1 $m^2 \cdot s^{-1}$
longitudinal eddy diffusivity	10 $m^2 \cdot s^{-1}$
Chezy coefficient	70 $m^{0.5} \cdot s^{-1}$
wind sheltering coefficient	1.0
fraction of incident solar radiation absorbed at the water surface	0.45
coefficient of bottom exchange	7.0 x 10^{-8} $W \cdot m^{-2} \cdot s^{-1}$

2.1.1.2 Model specifications, development of inputs and supporting data for hydrothermal testing

The guidelines of Cole and Wells (2002) for defining the computational grid were followed. Schoharie Reservoir is represented by 17 longitudinal segments (Figure 1b), with a layer thickness of 1 m (maximum of 40 layers). Contemporary morphometric features of the grid (Figure 1c), including dimensions of individual layers within the various longitudinal segments, were based on an analysis with ArcInfo® software of the digitized bathymetric map developed from a survey conducted in 1997 (GZA GeoEnvironmental of New York 2002) and augmented by subsequent partial surveys (unpublished data, Upstate Freshwater Institute).

The centerline elevation of the shoreline intake structure is 321.1 m, corresponding to a full reservoir depth of 23.3 m. The intake channel is ~ 10 m wide and ~ 75 m long (~ one tenth of the width of the reservoir at that location, Gannett Fleming and Hazen and Sawyer 2004). Topographic maps that represent the reservoir bottom at the time of construction (GZA GeoEnvironmental of New York 2002) establish that the intake had unobstructed access to waters at that elevation (e.g., down-reservoir.

However, subsequent sedimentation, as documented in recent bathymetric surveys and local borings to the original reservoir bottom (GZA GeoEnvironmental of New York 2002), has isolated the intake structure from access to water layers of that depth. The intake structure is now bounded by sediment deposits that are nearly 6 m higher (GZA GeoEnvironmental of New York 2002; Figure 1c) within relatively close proximity; e.g., within 40 m along the intake channel (Gannett Fleming and Hazen and Sawyer 2004). The contemporary reservoir bottom depths caused by sedimentation extend over substantial areas, as represented for the corresponding model segment (Figure 1c). The nearly 6 m deep "hole"

maintained by the turbulence associated with the operation of the withdrawal is small (~ 2,000 m^2) relative to that of the model segment. These conditions result in water being effectively withdrawn from an elevation corresponding to the bounding sediment plateau (e.g., Martin and McCutcheon 1999). This is represented in the model by specifying an "effective" withdrawal elevation of 326.9 m (i.e., 5.8 m shallower than the intake structure), that is consistent with both the most recent bathymetric data (GZA GeoEnvironmental of New York 2002; unpublished data, Upstate Freshwater Institute) and the results of model testing. Review of the reservoir WSE record for 10 y intervals (Figure 2d) depicts a reduction in maximum drawdown that is consistent with a progressive loss of access to water layers at the depth (elevation) of the existing intake. In the 1931-1940 interval the maximum drawdown approached the construction depth of the intake, but by the 1980s and 1990s the maximum drawdown had shifted more than 5 m higher (Figure 2d). The approximate closure of this value with the reported sedimentation bordering the intake provides additional support for the "effective" withdrawal depth adopted for the model to represent contemporary conditions.

Inflows and outflows directly enter and exit model segments according to their location. Ninety-five percent of the reservoir's watershed is gauged for flow by the United States Geologic Survey (USGS). Schoharie Creek and the second largest tributary have been gauged over the entire 14 y period of testing of the hydrothermal submodel (1989-2002). The third largest tributary (~ 6% of the total inflow) has been gauged since 1998. The minor ungauged inflows (< 5%) enter as spatially distributed inputs around the perimeter of the reservoir in the model. Outflows via the spillway (48% annually, on average) and the water supply withdrawal (52% annually, on average), were monitored earlier by the New York City Department of Environmental Protection (NYCDEP) and more recently by USGS. NYCDEP routinely monitors WSE. An analytical hydrologic model, operated outside of W2/T (e.g., Owens et al. 1998b), was used to maintain a hydrologic balance over the entire 14 y interval of model testing and to estimate surface inflows from the ungauged portion of the watershed. All inflows and outflows were specified as daily average values testing hydrothermal performance.

To support hydrothermal testing, tributary temperatures were specified based on routine monitoring conducted by NYCDEP near the mouths of the three largest tributaries either weekly or bi-weekly, depending on the year and stream. Daily T values, required as inputs to the model, were determined by linear interpolation. An exception was the hourly T values available to support specification of daily average T for Schoharie Creek for several months in 2002 (Effler et al. 2006a). Temperature profiles collected in the reservoir water column annually over the testing period represent the primary data used to evaluate the performance of the model. Profiles were collected at four sites along the axis of the reservoir (sites 1 - 4; Figure 1b). Frequencies of measurements over the April through October interval were monthly for the 1989-1992 period, weekly for 1993-1995, and bi-weekly thereafter. Profile measurements were generally collected at depth intervals of 1 m. The accuracy and resolution of tributary and reservoir T measurements was ± 0.15 and 0.01 ºC, respectively. Modest longitudinal T differences have been observed in April and October, when Schoharie Creek tends to be systematically warmer and cooler, respectively, than the reservoir (Effler et al. 2006a). Otherwise the residual of T values for sites 1 and 3 at equal

depths have approached zero. The temperature of the water withdrawn from the reservoir (T_w) is monitored by NYCDEP, representing an additional opportunity to test predictions at the intake depth and site. The frequency of T_w measurements has varied from 1 wk^{-1} to nearly daily.

A thermistor chain, or string (Aanderaa Model 2862; accuracy and resolution of ± 0.15 and 0.01 ºC, respectively), and a data logger (Aanderaa Model TR7), were deployed at site 1 over the interval August 4 to September 15, 1998. Measurements were made at 10 min intervals. The thermistor chain measurements provided a second type of data for evaluation of the model's performance related to internal waves (Lemmin and Mortimer 1986). Spectral analyses of the thermistor chain observations at a depth of 25.5 m and model predictions for this same site, time interval, depth and frequency were conducted to identify characteristic periods of oscillations associated with internal waves and evaluate the model's performance in this regard (e.g., Gelda et al. 1998).

Values of k_d were determined from profiles of downwelling irradiance (Kirk 1994) collected in 1992-1999 and 2002. Secchi disc measurements, collected routinely as part of the reservoir monitoring program, served as a surrogate estimator of k_d (Effler 1985) for other years. Values of k_d were specified according to $k_d \cdot SD = 1.26$, based on a linear least-squares regression analysis ($r^2 = 0.82$) of paired measurements collected in the reservoir in 1998. Values of k_d were specified daily though linear interpolation of the estimates.

Meteorological inputs were specified hourly, consistent with the recommendation of Cole and Wells (2002). On-site (Figure 1b) hourly meteorological measurements (including solar radiation) were available for the last 6 y of the 14 y modeling period. Simulations for the other 8 y were supported by off-site meteorological data collected at a National Weather Service station located ~ 60 km away (northeast of the reservoir) at Albany, NY. Strong linear least-squares regression relationships ($r^2 > 0.95$) were observed between the on-site and off-site measurements of air and dewpoint temperatures. In contrast, substantial differences in wind speed were observed, and a weaker linear least-squares relationship ($r^2 = 0.23$) prevailed, as was reported between paired off-site and on-site measurements elsewhere in this region (Gelda et al. 1998). These regression expressions were used to specify meteorological inputs for the 1989-1996 interval based on Albany observations.

2.1.1.3 Setup, testing, and evaluation of performance of hydrothermal simulations

The model's autostepping algorithm (Cole and Wells 2002) calculates a maximum time-step, within a specified range, based on hydrodynamic numerical stability requirements and then uses a fraction of this value for the actual time-step of calculations. The minimum and maximum time-steps used were 1 s and 1 h, respectively. Model validation was based on a set of coefficients (Table 1) that performed well for the entire 14 y period. These coefficient values correspond rather closely to those adopted elsewhere (Martin 1988; Gelda et al. 1998) and recommended by Cole and Wells (2002).

Model performance was evaluated both qualitatively and quantitatively. Salient features of the stratification regime on which model simulations were evaluated qualitatively

include (Owens and Effler 1989): (1) the timing of the onset of stratification in spring and turnover in fall, (2) the duration of stratification, (3) the dimensions of the stratified layers (e.g., epilimnion and hypolimnion), (4) the temperatures of the stratified layers, (5) T_w, (6) the overall temperature differences in the water column, and (7) the periods of internal wave oscillations in stratified layers. These features of performance are illustrated here in various graphical presentation formats.

The primary quantitative basis of evaluating model performance adopted was the "root mean square error" (RMSE) statistic (e.g., Thomann 1982), calculated according to

$$RMSE = \sqrt{\frac{\sum_{i=1}^{N} (T_{i,obs} - T_{i,prd})^2}{N}} \quad (1)$$

where N = number of observations, $T_{i,obs}$ = observed value of *i*th observations of T, and $T_{i,prd}$ = predicted value of *i*th observation of T. RMSE is statistically well behaved and is an indicator of the average error between observations and predictions. A lower RMSE indicates a better model fit to observations.

2.1.1.4 Performance of hydrothermal submodel

Predictions of thermal stratification matched measured T profiles well, as illustrated monthly for sites 1 and 3 in 1998 (Figure 3) and 2002 (Figure 4), two years with distinctly different WSE dynamics (Figure 2b and c). In contrast to common limnological protocols (Wetzel 2001), depths are represented in terms of elevations (Figures 3 and 4), rather than depth from the surface, to accommodate variations in WSE. The simulations track the observed progressions at site 1 in both years, including: (1) the near absence of stratification in mid-April (Figure 3a and Figure 4a), (2) the development of increasing stratification in May, June and July (Figure 3b-3d and Figure 4b-4d) and peak stratification in mid-August (Figure 3e and Figure 4e), (3) the subsequent diminishment of vertical T differences and deepening of the epilimnion in September and October (Figure 3f and g, Figure 4f and g), and (4) the establishment of fall turnover by mid-November (Figure 3h and Figure 4h). Timing, temperatures and dimensions of the layers are simulated well, despite noteworthy differences between these two years that included a deeper epilimnion in mid-June in 1998, but shallower in July of that year, and greater loss of stratification by mid-October in 2002 compared to 1998. Performance for the shallower upstream site 3 was also generally good (Figure 3i-3o and Figure 4i-4o), though some diminishment was apparent in mid-June (Figure 4k) and mid-July in 2002 (Figure 4l) that may reflect the effects of internal waves, the use of interpolation over extended intervals to specify the inflow temperature, variations in the layers affected by the water supply withdrawal (Martin and McCutcheon 1999) and local sedimentation conditions, and spatially varying wind-sheltering.

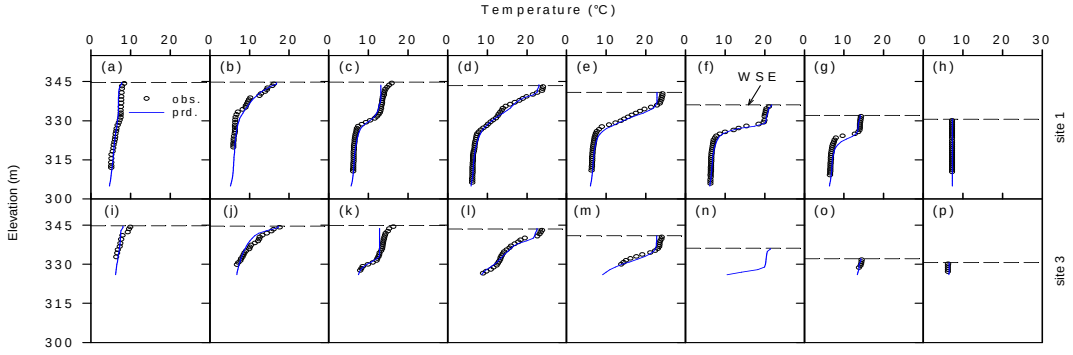

Figure 3. Performance of hydrothermal model for Schoharie Reservoir as monthly profiles in 1998: (a) site 1, April 21, (b) site 1, May 19, (c) site 1, June 16, (d) site 1, July 21, (e) site 1, August 18, (f) site 1, September 15, (g) site 1, October 13, and (h) site 1, November 17, (i) site 3, April 21, (j) site 3, May 19, (k) site 3, June 16, (l) site 3, July 21, (m) site 3, August 18, (n) site 3, September 15 (no observations available), (o) site 3, October 13, and (p) site 3, November 17.

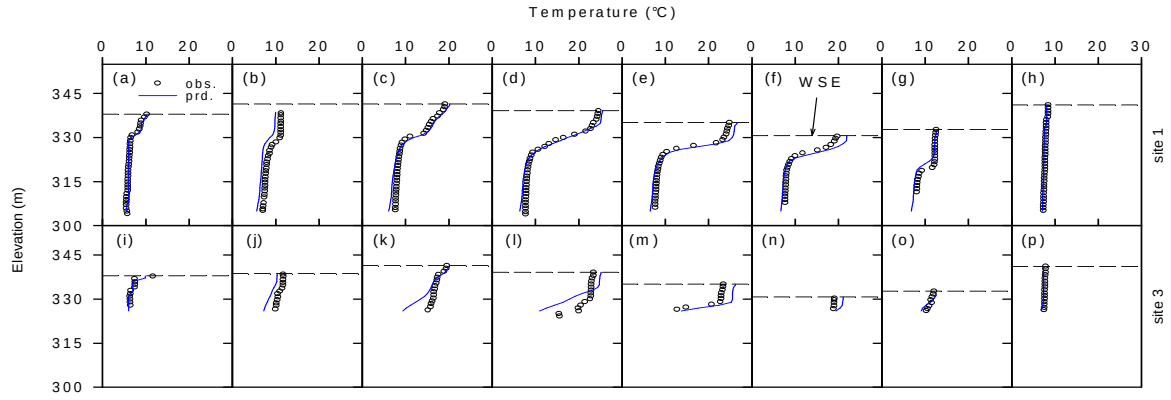

Figure 4. Performance of hydrothermal model for Schoharie Reservoir as monthly profiles in 2002: (a) site 1, April 15, (b) site 1, May 13, (c) site 1, June 10, (d) site 1, July 15, (e) site 1, August 12, (f) site 1, September 16, (g) site 1, October 15, and (h) site 1, November 12, (i) site 3, April 15, (j) site 3, May 13, (k) site 3, June 10, (l) site 3, July 21, (m) site 3, August 12, (n) site 3, September 16, (o) site 3, October 15, and (p) site 3, November 12.

Spectral analyses of the thermistor chain observations of 1998 indicate the presence of several characteristic or dominant periods of oscillation in stratified layers associated with internal waves (Owens 1998a). These periods were about 62, 42, and 28 h (Figure 5a). Spectral analysis of the model output for the same position and time interval yields very similar characteristic periods of about 59, 43 and 27 h (Figure 5b). A period of about 32 h was more prominent in the predictions than the observations. The similarities of the results

of these spectral analyses support the position that the model captured the characteristics of water motion which influence transport and mixing in the hypolimnion of this reservoir. The lower magnitude of the peaks for the model predictions indicates a modest level of underprediction of the magnitude of T fluctuations in stratified layers.

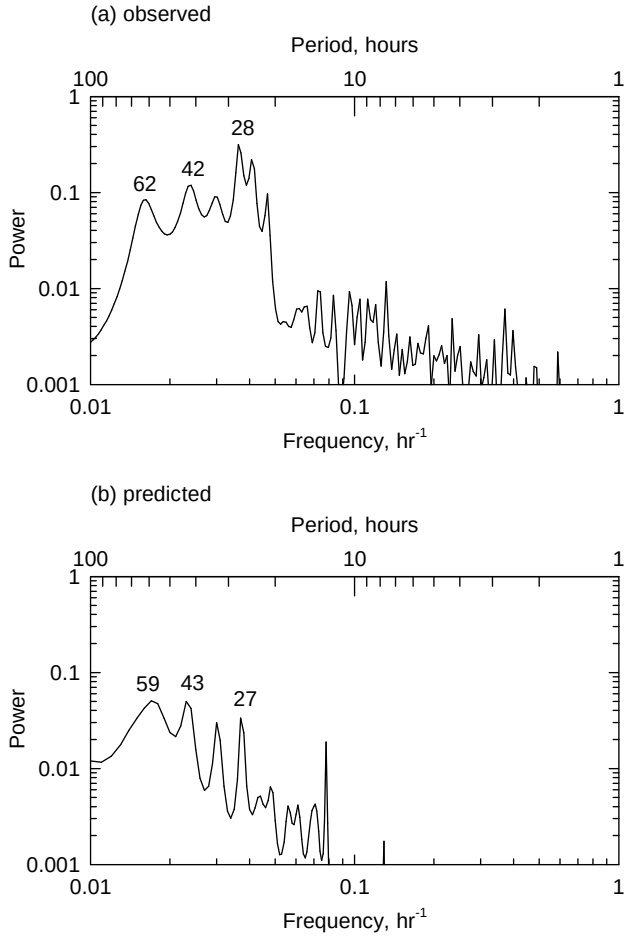

Figure 5. Spectra of time series of T in Schoharie Reservoir at site 1, depth of 25.5 m, over the August 4-September 15 interval of 1998: (a) observed, and (b) predicted by hydrothermal model.

Performance for the entire 14 y period is depicted through comparison of time series of observations and continuous model simulations of epilimnetic and hypolimnetic volume-weighted Ts for site 1 (Figure 6). The various features of the stratification regime were generally well simulated in all 14 y, including timing of turnover, duration of stratification, seasonal heating and cooling of the upper waters, and Ts of the layers. This 14 y simulation substantially extends the period covered in testing hydrothermal models beyond the longest intervals previously reported [e.g., 6 y, Onondaga Lake, NY (Owens and Effler 1996); 8 y, Cannonsville Reservoir, NY (Gelda et al. 1998)].

A strong relationship between predicted and observed T_w values prevails for the entire 14 y period, that depicts only modest deviations between predictions and observations (Figure 7). According to linear least squares regression analysis, variations in predicted T_w explain 95% of the observed variations. The RMSE of the predictions of T_w for the entire 14 y period is 1.89 ºC. These features of the model's performance support its appropriateness for management applications that focus on T_w.

Good model performance is also depicted by the calculated annual RMSE values for the 1989-2002 period (Table 2). Each of these values incorporate all the paired T measurements and predictions from all four of the monitored sites. The RMSE ranged from 0.85 (1994) to 1.75 (2001); the average for the entire period was 1.30. This level of performance compares favorably to two other cases where this representation of

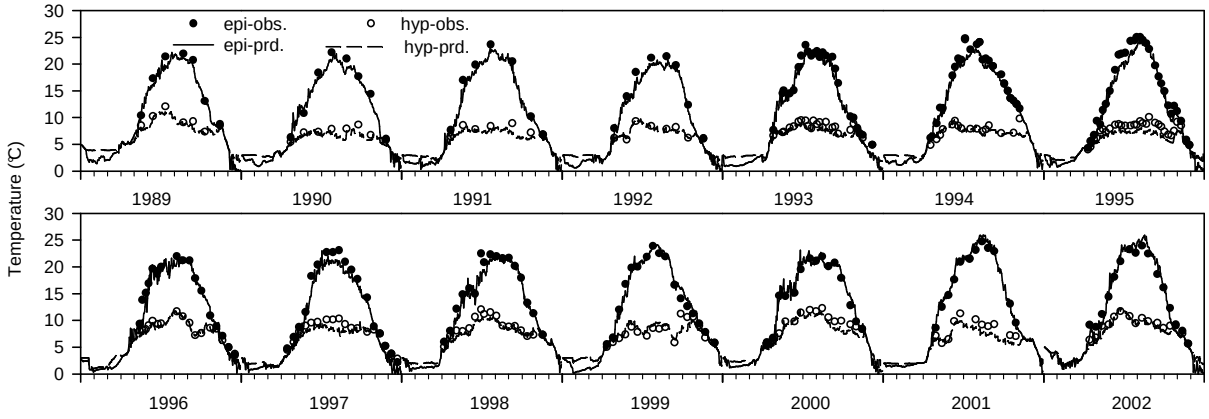

Figure 6. Comparison of observed and predicted epilimnetic and hypolimnetic Ts at site 1 in Schoharie Reservoir for the period of 1989-2002.

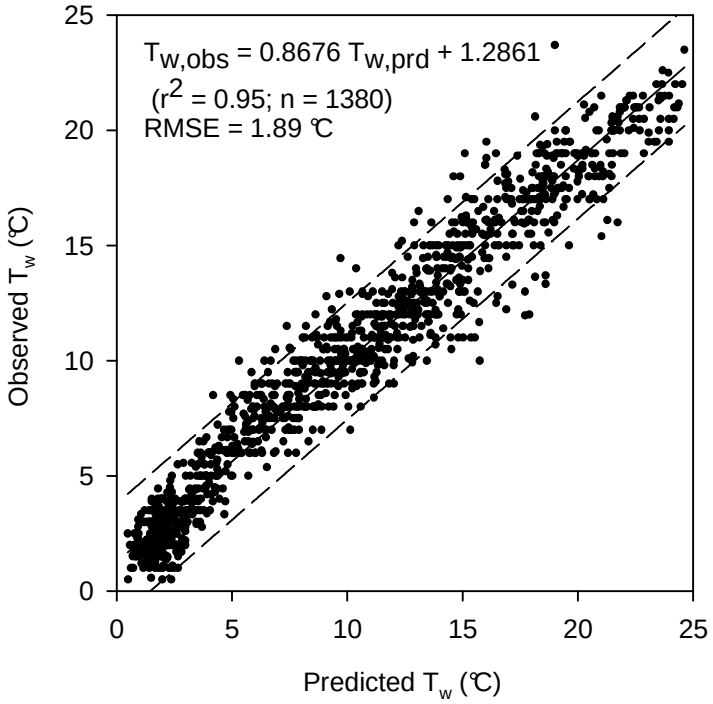

Figure 7. Performance of the hydrothermal model in simulating the withdrawal T (T_w) from Schoharie Reservoir for the 1989-2002 period.

Table 2. Performance of hydrothermal/transport model in predicting temperature patterns in Schoharie Reservoir annually, over the period 1989-2002, as represented by the root mean square error (RMSE).

Year	RMSE (ºC)
1989	1.06
1990	1.47
1991	1.49
1992	1.26
1993	1.19
1994	0.85
1995	1.33
1996	1.01
1997	1.54
1998	0.96
1999	1.43
2000	1.49
2001	1.75
2002	1.40

hydrothermal model performance was reported for multiple years (Gelda et al. 1998; Owens 1998a). No significant difference in model performance, based on the RMSE statistic, is associated with the years of off-site (but adjusted for wind differences) versus on-site meteorological data. Further, there is no significant relationship between the annual RMSE (Table 2) and average WSE (Figure 2a), indicating model performance was not substantively affected by the wide range of drawdown conditions included in the testing period. Based on the performance of the model for a wide range of forcing conditions embedded in this 14 y period (Figures 3-7, Table 2), using a single set of coefficients, the model is described as validated.

2.1.1.5 Development of inputs and supporting data to test transport simulations

Specific conductance (SC) serves as a valuable tracer of turbid density currents formed in the reservoir from runoff events, as noteworthy reductions in levels are observed in these inflows (O'Donnell and Effler 2006). Temporally detailed (e.g., 20 min intervals) measurements of flow (Q; USGS), T, and SC (O'Donnell and Effler 2006) were made at the mouth of Schoharie Creek in 2003 to support testing of the short-term (e.g., runoff event) transport simulation capabilities of W2/T. In-reservoir vertical profiles of T and SC were made at numerous sites with rapid profiling instrumentation (Effler et al. 2006b) following runoff events to support testing of the model. Time series of Q in the creek, and T and SC in the creek and surface waters of the reservoir are presented in Figure 8. The cooler temperature of Schoharie Creek relative to the reservoir in summer and fall is responsible for the plunging behavior of this tributary during that interval (Effler et al. 2006a). Eight runoff events in 2003 were evaluated for short-term transport submodel performance, which had recurrence (peak flow) frequencies ranging from 1 (relatively rare) to 17 y^{-1} (common). Model simulations were continuous from mid-July through mid-November. The same model coefficient (Table 1) used to validate the hydrothermal performance of the submodel were retained in testing its transport capabilities.

Transport performance was evaluated in the context of the submodel's ability to simulate patterns of the SC tracer imparted to the reservoir's water column, particularly associated with runoff events. Model performance was evaluated both qualitatively (e.g., graphically as vertical profiles, contours and time series), and quantitatively, through the root-mean-square-error statistic.

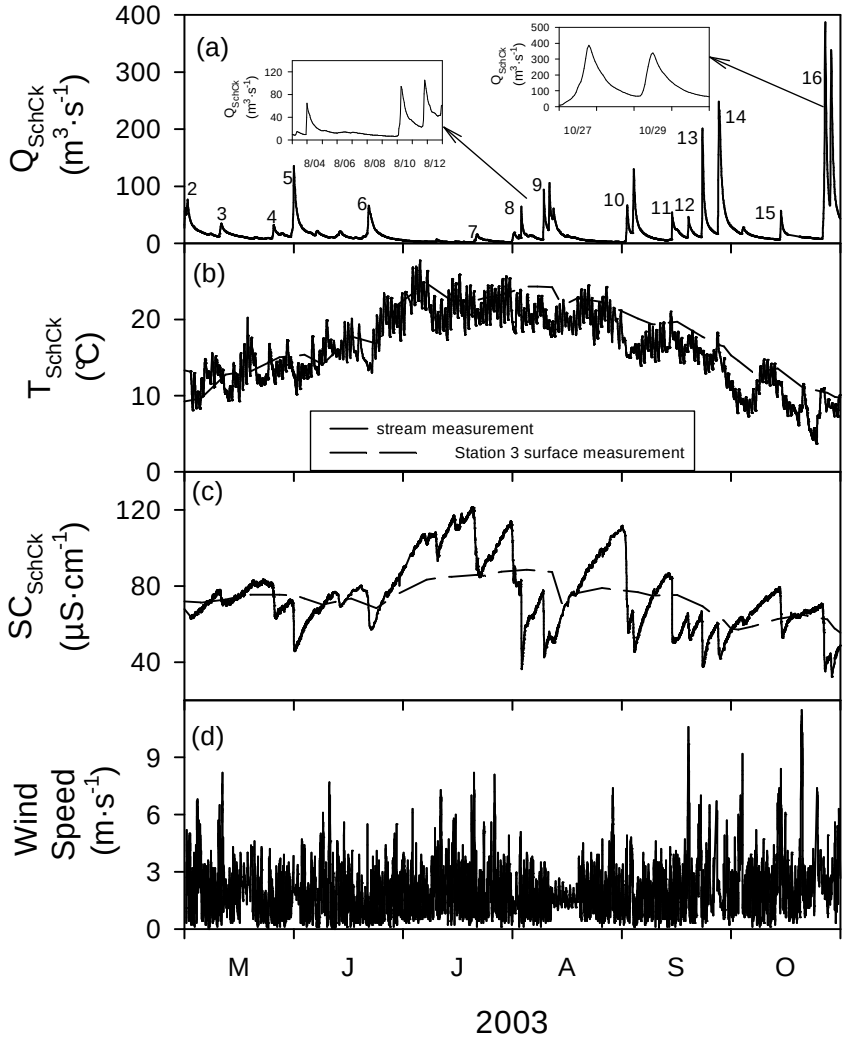

Figure 8. Time plots for selected model forcing conditions for Schoharie Reservoir 2003; (a) Schoharie Creek USGS flows, (b) temperatures for Schoharie Reservoir surface at station 3 and Schoharie Creek, and (c) specific conductance for Schoharie Reservoir surface at station 3 and Schoharie Creek.

2.1.1.6 Transport performance of submodel

The submodel performed well in simulating the distinct patterns in time and space of the SC tracer within the reservoir, establishing that features of transport and mixing, particularly related to density currents from runoff events, were well represented. Four forms of graphical representation support this position: (1) changes in vertical profiles of SC from before to after runoff events (Figure 9), (2) time series of observed and predicted SC values for multiple layers and longitudinal positions (Figures 10 and 11), (3) comparisons of

observed and predicted longitudinal patterns of SC (as isopleths) along the longitudinal axis of the reservoir for multiple days for a selected event (Figure 12), and (4) comparisons of observed and predicted temporal and vertical patterns of SC (as isopleths) at a site (No. 3) adjoining the intake (Figure 13). Rather well defined structures in observed SC patterns are manifested in each of these formats, supporting the position that these offer a robust test of the transport simulation capabilities of the model.

The changes in vertical patterns of SC brought about by runoff events were well represented for multiple positions along the reservoir's major axis, as illustrated for late

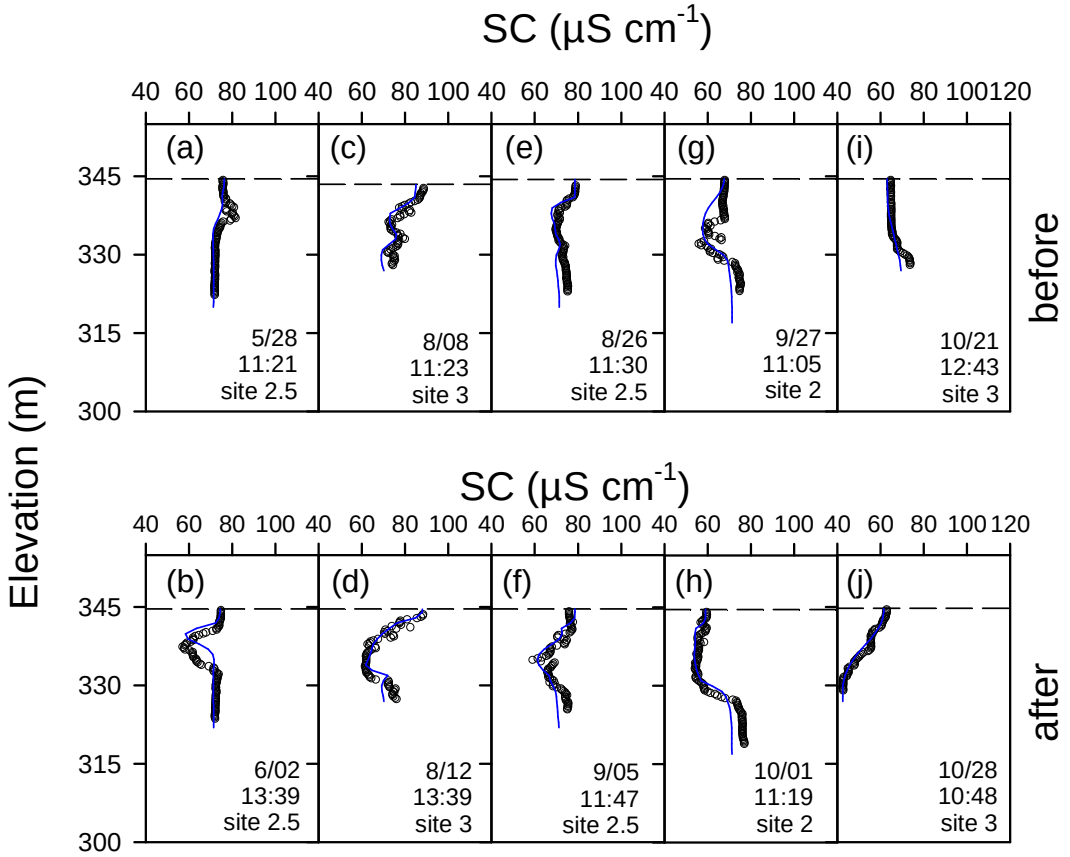

Figure 9. Model performance for specific conductance (SC; predictions as solid line) in Schoharie Reservoir as profiles demonstrating model performance before and after selected events (a) before event 5/28, (b) after event 6/02, (c) before event 8/08, (d) after event 8/12, (e) before event 8/26, (f) after event 9/05, (g) before event 9/27, (h) after event 10/01, (i) before event 10/21, (j) after event 10/28.

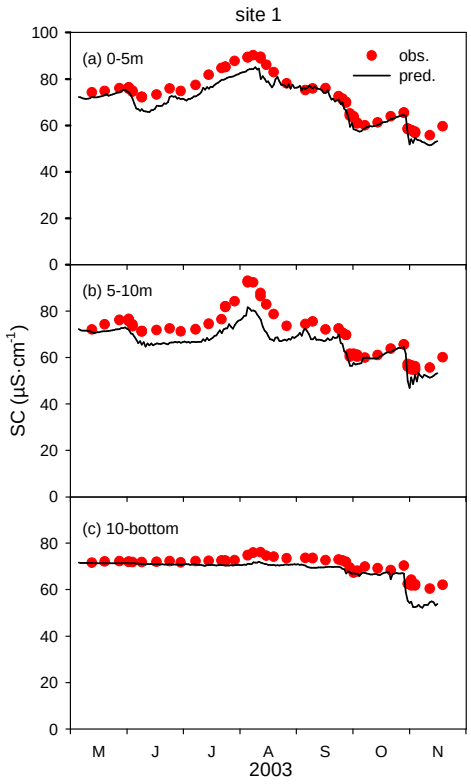

Figure 10. Comparison of time plots of volume weighted average specific conductance (SC), observed and predicted (solid lines), Schoharie Reservoir site 1: (a) 0-5m, (b) 5-10m, and (c)10 – bottom.

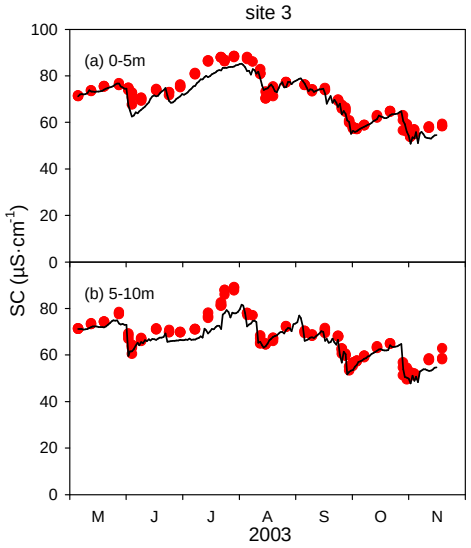

Figure 11. Comparison of time plots of volume weighted average specific conductance (SC), observed and predicted (solid lines), Schoharie Reservoir site 3: (a) 0-5 m, and (b) 5-10 m.

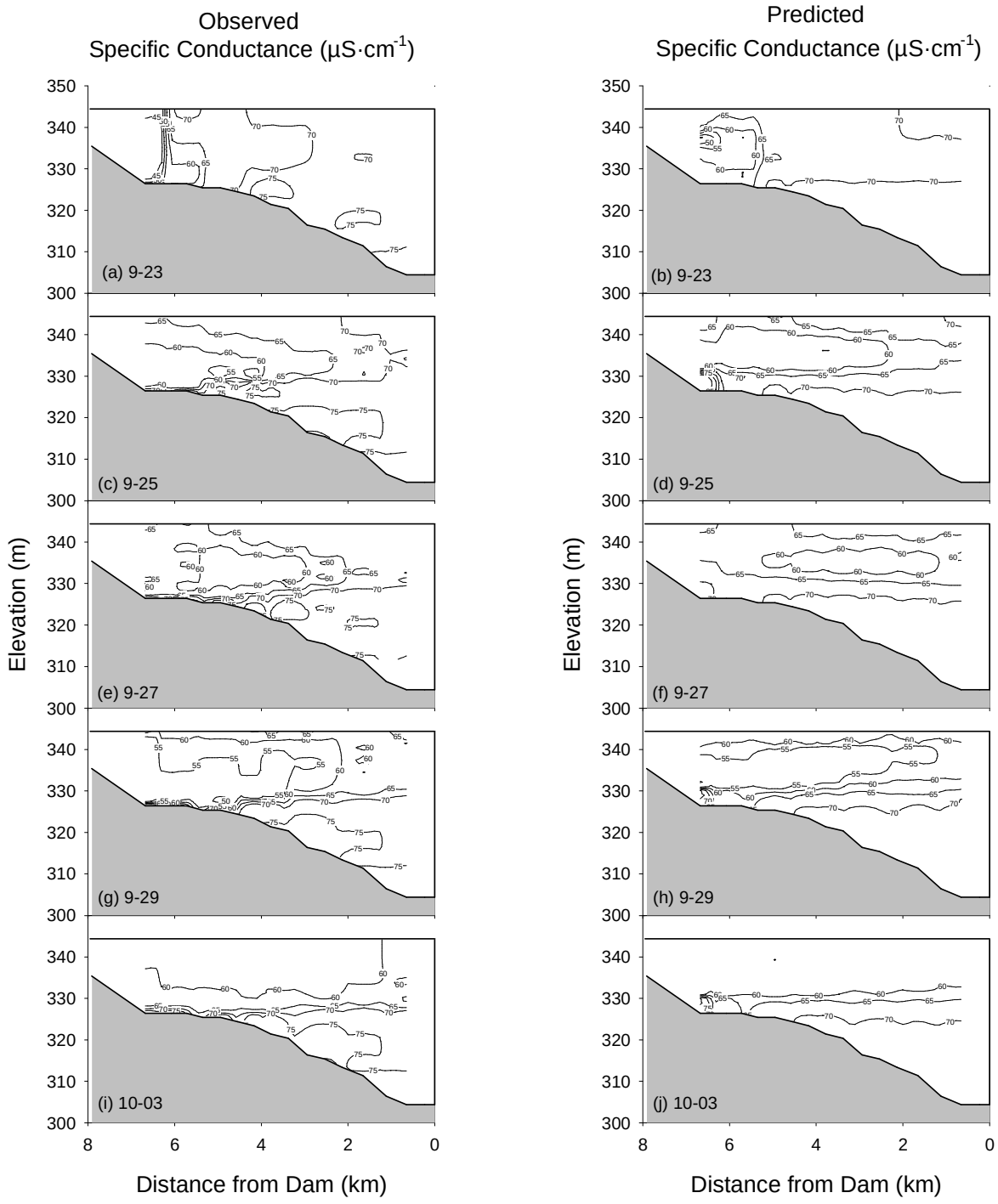

Figure 12: Comparison of predicted and observed longitudinal patterns of specific conductance (SC) along the major axis of the reservoir during a runoff event in 2003 (a) observed 9/23, (b) predicted 9/23, (c) observed 9/25, (d) predicted 9/25, (e) observed 9/27, (f) predicted 9/27, (g) observed 9/29, (h) predicted 9/29, (i) observed 10/03, (j) predicted 10/03.

May/early June (Figure 9a and b), mid-August (Figure 9c and d), late August/early September (Figure 9e and f), late September/early October (Figure 9g and h), and late October (Figure 9i and j) events. The dilution effects of the runoff events on SC is manifested in each of these cases. The plunging behavior is manifested both as interflows (in summer, Figure 9b, d and f) and an underflow (in fall, Figure 9j). Temporal patterns (as volume weighted values) in three depth strata were well represented at site No. 1 (Figure 10). Substantial temporal structure occurred in the upper two strata (0 - 5 m depth interval, and 5 - 10 m depth interval) in response to the dynamics of runoff and SC levels in the inflows. Even better model performance was observed at the shallower up-reservoir site 3 (Figure 11).

The observed longitudinal patterns of SC over the September 23 through October 3 interval of 2003 depict the entry of plunging dilute inflows in response to two runoff events (peak flows on September 23 and September 28). The front of the density current was about 5 to 6 km up-reservoir from the dam on September 23 (Figure 12a) and had approached the dam (1 to 2 km up-reservoir) by September 25 (Figure 12c). The plunging inflow of Schoharie Creek lifted off the bottom and entered the down-reservoir water column as an interflow for the first runoff peak about 5 km up-reservoir from the dam. This shifted further down-reservoir for the second runoff peak (Figure 12 g). This inflow had mixed into the epilimnion by October 3 (Figure 12i). The behavior of the density currents was generally well-represented throughout the interval (Figure 12b, d, f, h and j); e.g., SC levels, occurrence and thickness of the density currents, and longitudinal extent.

The model also performed well in simulating the combined vertical and temporal patterns of SC at various positions along the axis of the reservoir, illustrated here for site 3 (Figure 13a and b). The highly dynamic mid-depth structure starting in July and extending through September of 2003 is a manifestation of the entry of density currents from multiple runoff events, a feature that is well represented in model predictions. In contrast, the late October event was an underflow at this site (Figure 13a) because of the seasonal deepening of the epilimnion. This feature was also simulated well by the model (Figure 13b).

Root-mean-square-errors (RMSE) were determined for seven time intervals in 2003 that contained runoff events (Table 3), based on paired observations and predictions of SC throughout the reservoir through each interval. The average values for the seven intervals range from 3.89 to 6.70 $\mu S \cdot cm^{-1}$ (Table 3); the overall average is 5.27 $\mu S \cdot cm^{-1}$.

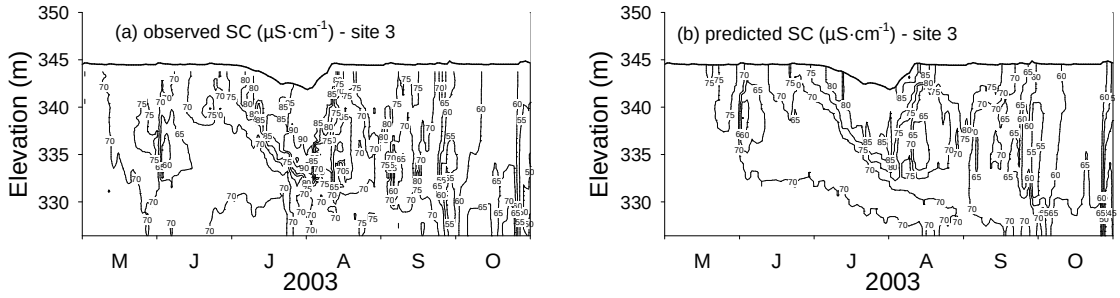

Figure 13 Comparison of predicted and observed temporal patterns of specific conductance (SC) at site 3 (a) observed, (b) predicted.

Table 3: Performance of hydrothermal/transport model in simulating specific conductance (SC) patterns in Schoharie Reservoir for seven runoff event intervals in 2003, as represented by the root-mean-square-error (RMSE).

Time Interval	RMSE (µS·cm^{-1})
June 1 - June 9	4.43
July 22 - July 24	6.64
August 3 - August 8	5.56
August 10 - August 15	5.59
September 4 - September 9	3.89
September 23 - October 3	4.06
October 27 - November 3	6.70

2.1.2. Modeling Turbidity

2.1.2.1 Approach and process

The alternative of simulating T_n indirectly through mass balance modeling of suspended solids (SS) has been rejected here for both conceptual and practical reasons. First, because larger sized particles make greater contributions to the particle assemblage during high runoff events in the primary tributary than in the water column of the reservoir (Gelda and Effler 2006b), the SS approach is fundamentally flawed. Accordingly, the SS approach would result in systematically false high loads within the context of reservoir T_n (light scattering) levels. Apparently, many of the larger particles mobilized in the stream during the high runoff interval are deposited before reaching lacustrine portions of the reservoir (Gelda and Effler 2006b). This size sorting process operates widely in reservoirs, manifested as higher sediment deposition (Effler et al. 2001; Effler and Matthews 2004) and accumulation rates, and greater contributions by coarser sediments (Pemberton and Blanton 1980), in riverine and transition zones of

reservoirs. Further, practical limitations in sampling and analysis for SS compromise resolution of loading and in-reservoir impacts associated with transient runoff events. Direct measurements of a surrogate metric of the light scattering coefficient **(b)** with appropriate modern instrumentation, as implemented here in supporting studies (Effler et al. 2006b), provides much greater resolution of patterns in time and space to support model testing.

This turbidity model is instead based on mass balance-type modeling of a surrogate metric of **b,** an approach that is supported by the additive character of components and sources of **b** (Davies-Colley et al. 1993). Implicit in this approach is the recognition that light scattering is regulated by characteristics of the particles of the water column, which in natural systems are heterogeneous with respect to size and often composition. The beam attenuation coefficient, **c,** is defined by the following summation

$$\mathbf{c} = \mathbf{a} + \mathbf{b} \tag{2}$$

where **a** = the absorption coefficient (m^{-1}). $\mathbf{a}_{660}$ is only ~ 3 to 6% of $\mathbf{c}_{660}$, and **b** does not vary greatly with λ (Babin et al. 2003), supporting $\mathbf{c}_{660}$ as a surrogate measure of **b**. The value of $\mathbf{c}_{660}$ (**c** is also additive; Davies-Colley et al. al 1993) is selected as the model state variable instead of T_n. This choice was also based on both conceptual and practical considerations. Several investigators have indicated that **c** has advantages over T_n as a measure of the magnitude of "turbidity" on scientific grounds (McCarthy et al. 1974; Davies-Colley and Smith 2001). Instruments that measure **c** are subject to absolute calibration, while T_n calibrations are based on an arbitrary standard (Davies-Colley and Smith 2001). Further, T_n values depend to some extent on the particular nephelometer used (Letterman et al. 2004). The $\mathbf{c}_{660}$ metric has the additional advantage of providing more complete spatial resolution (0.25 m vertically at multiple longitudinal positions) of light scattering levels in the reservoir, through implementation of rapid profiling field instrumentation (Effler et al. 2006b). Further, field measurements avoid potential biases from systematic changes associated with the unavoidable delay of laboratory analyses (e.g., aggregation; Effler et al. 2006b). Predictions of $\mathbf{c}_{660}$ can be converted to T_n values (Hach 2100 AN) for this reservoir according to the following linear relationship (Effler et al. 2006b)

$$T_n = 2.5 \cdot \mathbf{c}_{660} \tag{3}$$

Adoption of a light scattering metric instead of SS as the model state variable eliminates the substantial variability and uncertainty that accompanies the representation of light scattering by SS, associated with the different particle size dependencies of these measures.

Two kinetic processes are represented in the turbidity model settling (a loss process) and sediment resuspension (an internal source process), as specified by the settling velocity, v ($m \cdot d^{-1}$). The effect of settling has been represented in three ways. The simplest approach applies a single value of v to the entire $\mathbf{c}_{660}$ pool. The two more complex representations partition the pool into two and three fractions, respectively, each

with a different value of v (Table 4). Values of v and the partitioning of the $\mathbf{c}_{660}$ into multiple fractions were determined by model calibration. These different representations essentially treat the settling loss pathway for $\mathbf{c}_{660}$ as being regulated by either a single lumped particle size class or multiple size classes.

The values of v arrived at by calibration, correspond to particle diameters (assuming spherical) of approximately 0.42 and $\geq$ 6.6 µm according to Stokes Law (Table 4). The larger sizes represent much lower contributions (e.g., $\leq$ 1%) of the measured particle population of the water column (Peng et al. 2004) than the fractions determined from calibration (Table 4). The effective size of these particles may be even greater, and thus their occurrence even rarer than indicated by the Stokes Law estimates (Table 4), because of the plate-like (i.e., non-spherical) features of many (e.g., clay) of the particles (Peng et al. 2004). The need for such a high settling velocity indicates the operation of particle aggregation is effectively embedded within the rapid settling fractions.

Table 4: Values of Fractions and Settling Velocities (Adjusted for Temperature), for Selected Single and Multiple Component $\mathbf{c}_{660}$ Models, with Calculated Particle Diameters.

Model Component	Fractions (%)	Settling Vel. ($m \cdot d^{-1}$)	Diameter (µm)
1	100	1	4.17
2	35, 65	0.01, 3	0.42, 7.21
3	20, 45, 35	0.01, 2.5, 5	0.42, 6.59, 9.31

Resuspension of bottom sediment occurs when the bottom shear stress caused by water motion exceeds a critical value. The critical shear stress represents the resistance to suspension of an individual non-cohesive particle or a collection of cohesive particles. When this occurs, particles on the bed are lifted into the water column, acting as an internal source of particles and increasing the mass concentration of particles and optical measures of light scattering such as turbidity. Resuspended particles may later return to the bottom by settling and deposition.

WL/T has the capability to predict water motion associated with most hydrodynamic processes, including circulation driven by wind stress at the water surface and reservoir inflow and outflow. In particular, the model can predict bottom shear caused by tributary inflow from Schoharie Creek moving through the relatively shallow, narrow section of the reservoir near it's mouth. Resuspension associated with the water motion that is predicted by the 2D model is termed "circulation resuspension". The approach used here to simulate this process is similar to that used in other lake and reservoir models (Lick et al. 1994, Ziegler and Nisbet 1995).

A potentially important source of bottom shear stress which is not simulated in the 2D model is that associated with wind-driven progressive waves on the water surface. Such waves cause an oscillatory motion and stress in relatively shallow water, where the

water depth is less than about half the wavelength (Dean and Dalrymple 1991); in deeper water, surface waves have no effect. Mechanistic simulation of progressive waves in lakes and reservoir, and the associated bottom resuspension, has been accomplished by other (e.g., Luettich et al. 1990, Jin and Ji 2004). As described below, a mechanistic surface save model was developed and tested for Schoharie Reservoir (Owens 2006). This surface wave model was linked with W2/T in order to provide mechanistic simulations of resuspension and resulting particle concentrations and optical properties.

Both resuspension processes are represented in the Schoharie model. Wave conditions are simulated (Owens 2006) outside of W2/T by the Donelan/GLERL model (Schwab et al. 1984) and supplied to W2/T as driving conditions for wave-driven resuspension.

2.1.2.1.1 Supporting data and development of inputs

Testing of the turbidity model, without resuspension processes, focused on conditions encountered in 2003, a year with only a small degree of drawdown (i.e., minimal in part from resuspension processes). The hydrology of the reservoir is well quantified by comprehensive monitoring of inflows and outflows (United States Geologic Survey) and water surface elevation [WSE; New York City Department of Environmental Protection (NYCDEP)]. Measurements reported at a time step of 1 h are used here. Ungauged inflows were assumed to have dynamics that tracked those of Schoharie Creek (unpublished data, NYCDEP). Outflows and WSE values were specified at this time step, as the daily average values. Meteorological inputs for the transport submodel were specified at a 20 min time step, based on measurements made at a position along the reservoir's main axis on a monitoring platform located about 2.5 km north of the mouth of Schoharie Creek (Figure 1). Hourly measurements of temperature (T, ºC; accuracy ± 0.15 ºC, resolution 0.01 ºC) and $\mathbf{c}_{660}$ (accuracy ± 0.30 m^{-1}, resolution of 0.03 m^{-1}) were made with calibrated instrumentation near the mouth of Schoharie Creek for most of the study period.

Reservoir measurements of T (accuracy ± 0.002 ºC, resolution 0.003 ºC) and $\mathbf{c}_{660}$ (accuracy ± 0.30 m^{-1}, resolution 0.03 m^{-1}) were collected with field instrumentation on 42 occasions over the study period. Weekly measurements were made at four long-term monitoring sites (No.'s 1 - 4) along the main axis of the reservoir, which extend nearly its entire length (Figure 1). Additional monitoring was conducted during and following runoff events starting in early June (events No.'s 3 - 12, Table 5). All runoff event-based monitoring included at least 3 additional sites along the main axis, located approximately mid-way between the long-term sites (No.'s 1.5, 2.5, and 3.5; Figure 1). The measurements of T and $\mathbf{c}_{660}$ were made with rapid profiling instrumentation (Effler et al. 2006b). Eight measurements per second were collected for both parameters during profiling and stored in the instrument's data logger. The instrument was lowered on a cable at a rate of ~ 0.5 $m \cdot s^{-1}$; i.e., approximately 16 measurements were made with each sensor over each meter of depth. Measurements (n ~ 4) within 0.25 m intervals were averaged, producing detailed vertical profiles. Measurements at the multiple sites were completed within 4 h.

2.1.2.1.2 Setup, testing and evaluation of model performance

The model was initialized according to the measurements of May 6, 2003. The predictions presented here result from continuous simulations over the entire May - October interval of 2003, a much more rigorous test compared to multiple shorter term simulations that would depend on respecification of initial conditions before each of the runoff events.

Table 5: Characteristics of, and model performance for, twelve runoff events for Schoharie Creek for the study interval of 2003.

Event* No.	Runoff Event† Vol. (m^3 x 10^7)	Peak in-reservoir c_{660}	RMSE (RMSEN) No. of Components		
			1	2	3
1	0.48	3.7	0.5 (13)	0.4 (10)	0.5 (14)
2	0.41	3.6	0.8 (21)	0.6 (16)	0.8 (23)
3	1.61	8.2	1.4 (18)	1.1 (13)	1.2 (15)
4	1.12	7.0	1.1 (15)	0.9 (13)	1.0 (15)
5	0.18	12.1	1.5 (12)	1.1 (9)	1.2 (10)
6	0.88	7.7	2.2 (29)	1.4 (18)	1.0 (13)
7	1.88	20.1	3.5 (17)	2.5 (12)	2.1 (10)
8	1.95	12.3	3.3 (27)	2.1 (17)	1.7 (14)
9	0.74	12.3	3.2 (26)	2.3 (18)	1.8 (15)
10	0.62	72.8	15.1 (21)	14.6 (20)	14.8 (20)
11	1.57	72.8	11.8 (16)	10.9 (15)	10.7 (15)
12	3.23	79.4	6.5 (8)	6.7 (8)	7.4 (9)

* see Figure 2a
† from Effler et al. (2006b)

Model performance was evaluated both qualitatively, through analysis of graphical presentations, and quantitatively, based on statistical comparisons of observations and predictions. Salient features of the impact of runoff events on reservoir light scattering levels considered were: (1) peak levels following events, (2) vertical patterns, (3) longitudinal patterns, and (4) attenuation/diminishment following events. A quantitative basis of model evaluation was the root-mean-square-error (RMSE) statistic. RMSE is statistically well behaved (e.g., Thomann 1982), indicating the average error

between observations and predictions; lower values generally reflect better performance. The manner of application of the RMSE analysis reflects the emphasis on impact of runoff events. Analyses were conducted over intervals extending from the peak documented impact of an event to 7 d later. These values were "normalized" by the $\mathbf{c}_{660}$ maximum (RMSEN) observed for each event to depict relative performance across the wide range of magnitudes of runoff events and impacts.

2.1.2.1.3 Model performance and sensitivity: full reservoir without sediment resuspension

Graphical representations of model performance in simulating $\mathbf{c}_{660}$ levels in the reservoir are presented in two formats: (1) detailed vertical profiles for the four monitored sites for two days during event No. 8 (Figure 14), and (2) time series for three depth intervals of the water column (0 - 5 m, 5 - 10 m, and 10 m - bottom) of volume-weighted values at two reservoir sites for the entire study (Figure 15). Representations of performance in terms of the RMSE and RMSEN statistics are

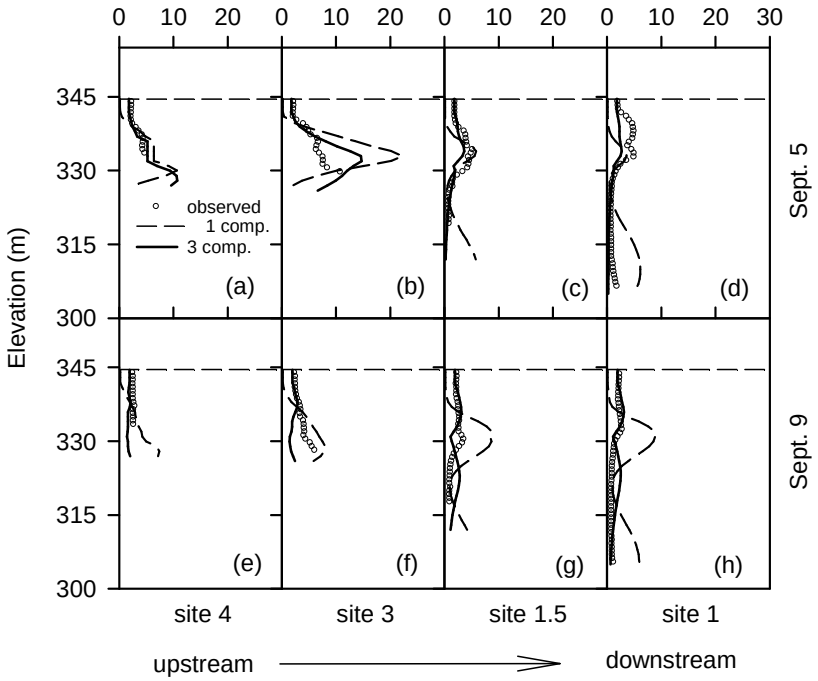

Figure 14. Performance of Model for Schoharie Reservoir for an Early September Runoff Event (No. 8) as Comparison of Predicted and Observed Vertical Profiles of $\mathbf{c}_{660}$ According to Monitored Sites (see Figure 1); for September 5 (a-d) and September 9 (e-h). Progression from Up-reservoir to Down-reservoir Moves Left to Right. Both 1 and 3 Component Simulation are Presented.

presented in tabular form for each of the runoff events and representations of component fractions and settling (Table 5). Comparison of the one and three component $\mathbf{c}_{660}$ models

is presented in the format of vertical profiles (Figure 14), while performance of the two and three component representations is contrasted in the time series simulations for the three strata (Figure 15). The performance of the multi-component models was generally superior to the single component representation for the overall study; e.g., the average RMSEN for the one component model was 18.6% compared to 14.0% and 14.4% for the two and three component approaches. Graphical comparisons further support this position.

Both the one and three component models performed well in simulating the vertical position of the $\mathbf{c}_{660}$ maxima along the longitudinal axis of the reservoir during the peak impact of event No. 8 (September 5; Figure 14a-d). Levels of $\mathbf{c}_{660}$ were overpredicted at site 3 (Figure 14b), but the attenuation of impact in downstream portions of the reservoir for this modest runoff event (Table 5) was well simulated for the three component model (Figure 14c and 14d). These performance features, immediately following the event, were largely controlled by the hydrodynamic transport model. The predictions presented for the single component $\mathbf{c}_{660}$ model correspond to a value of v = 1 $m \cdot d^{-1}$ (Table 4), from calibration that focused on performance within the depths of the maxima. Systematic short-comings in performance emerged for this simple kinetic framework even during peak impact. Levels of $\mathbf{c}_{660}$ were underpredicted in the near-surface waters along the entire reservoir (Figure 14a - d) and overpredicted, as a second maximum, in deeper layers in downstream segments (Figure 14c and d). No single value of v could eliminate both of these shortcomings. Performance of the single component approach worsened four days later (September 9) as impact diminished and kinetics (deposition) became relatively more important following the initial event driven transport (Figure 14e - h). The extent of diminishment in subsurface layers was underpredicted throughout the reservoir, as manifested by false high predictions of $\mathbf{c}_{660}$ at depth of ~ 15 m (elevation = 330 m). Levels in the surface waters continued to be underpredicted and those at depths > 30 m (elevation 315 m) were overpredicted.

Vertical features of performance improved substantially with both the two and three component frameworks, as illustrated here for the three component model (Figure 14a - h). Values of the fractions and the corresponding v for the multiple component models determined through calibration are presented tabularly, along with corresponding particle diameters calculated according to the Stokes' law (temperature adjusted; Reynolds Number $Re << 1$) for the spherical and inorganic (i.e., density ~ 2.6 $g \cdot cm^{-3}$) particle assumptions (Table 4). Qualitatively, the multiple component approach corresponds to a persistent (i.e., slow settling) fraction and a single or two rapidly settling fraction(s) of particles responsible for light scattering ($\mathbf{c}_{660}$). This approach resulted in much better simulation of levels in surface waters and in deep layers in downstream portions of the reservoir for both peak impact and diminishing effect intervals (Figure 14), and in terms of overall statistical metrics of performance (Table 5). The three component model somewhat underpredicted $\mathbf{c}_{660}$ at depths > 10 m in upstream portions of the reservoir for September 9.

The time series representation of model performance (Figure 15) is valuable in considering temporal features within the context of the entire study period. These time

series of observations and simulations also serve to demonstrate the distinct temporal and spatial patterns imparted by the runoff events of the study period (Table 5). Attenuation of the impact in both time and space (site 3 versus site 1) is clearly evident. These patterns were generally predicted by both the two and three component representations for the three strata at both upstream (site 3) and downstream (site 1) monitored locations. The model predictions explained 65 to 95% of the observed temporal variations within the defined strata (n = 6) of these two sites (Figure 15). The two component model

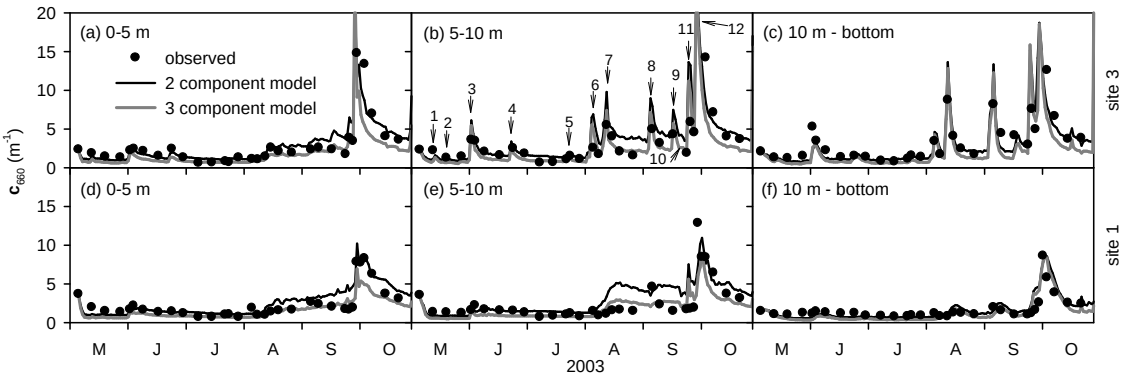

Figure 15. Performance of Model for Schoharie Reservoir as Comparisons of Predicted and Observed T ime Series of $\mathbf{c}_{660}$ for Three Vertical Segments (volume-weighted) for Two Monitoring Sites (a) 0-5 m, site 3, (b) 5-10 m, site 3, (c) 10 m-bottom, site 3, (d) 0-5 m, site 1, (e) 5-10 m, site 1, and (f) 10 m-bottom, site 1. Both 2 and 3 Component Simulations are Presented.

performed generally better over the May through July period, an interval of lower runoff and smaller events. However, the three component model tracked observations closer in August and September when severe runoff events occurred; an exception was the lower stratum at site 3 (Figure 15c). Improvements compared to the two component model were most noteworthy in the mid-depth stratum (Figure 15b and e). However, the two component model performed better for the largest runoff event (No. 12, Table 5) and subsequent diminishment. The three component model has been adopted in subsequent management applications. Without inclusion of sediment resuspension, the model underpredicted the occurrence of $T_{n,w} > 15$ NTU as documented for the 1987-2004 period (Figure 16). Inclusion of sediment resuspension, following calibration of both circulation and wave-based inputs, resulted in a good match with observations for $T_{n,w} > 10$ NTU (Figure 16). This overall turbidity model was applied in subsequent related modeling analyses of management alternatives.

The magnitude of the RMSE of model predictions generally increased with the magnitude of impact imparted by a runoff event, as reflected by the peak $\mathbf{c}_{660}$ observed in the reservoir (Table 5). However, when performance is considered relative to this metric of event impact, as RMSEN, much greater uniformity is indicated. For example, the RMSEN for the two component model ranged from 8 to 20% for the 12 events (Table 5) and the coefficient of variation for this performance metric for the events was only 27%. According to the RMSEN metric, performance of the multi-component models was the

best for events 5 and 12 and the worst for event 10. Model predictions were found to be sensitive to the specified fractions and corresponding settling velocities of the components of $\mathbf{c}_{660}$, and frequency of tributary measurements of $\mathbf{c}_{660}$ during events that specify external inputs.

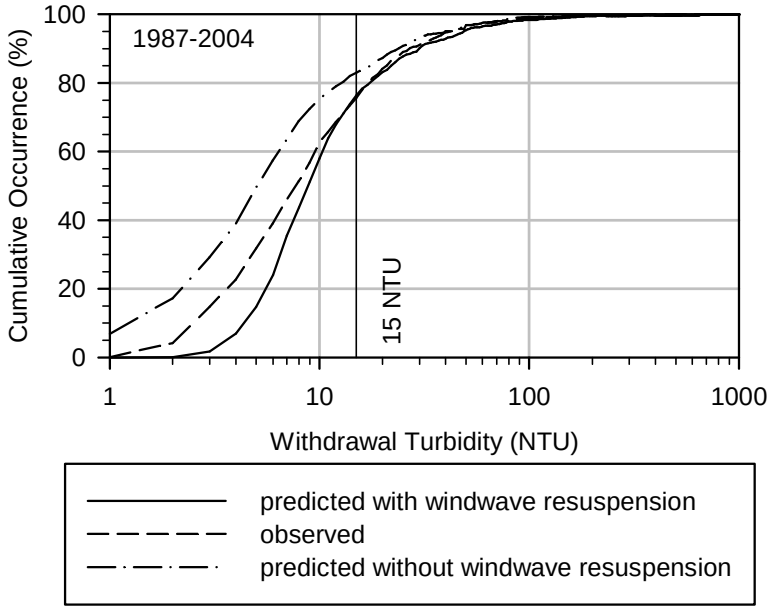

Figure 16. Comparison of Turbidity Model Predictions to Observed Values of Withdrawal Turbidity ($T_{n,w}$) for Schoharie Reservoir, for the 1987-2004 Period, in the Form of Cumulative Occurrence, Predictions are for the Cases of With and Without Resuspension Inputs.

2.1.3. Optimization framework

2.1.3.1 Description

An optimization framework (Figure 17a) was developed that links the reservoir simulation model for T and T_n with a heuristic operations algorithm (Figure 17b), to evaluate the benefits of a multi-level intake (MLI) structure on the quality of withdrawn water. The water quality features of interest in this case are the withdrawal temperature (T_w) and turbidity ($T_{n,w}$). The optimization algorithm reflects a strategy of using warmer (epilimnetic) waters earlier in the year, saving the colder hypolimnetic waters for late summer withdrawal, to avoid exceeding a specified goal for T_w in late summer and fall (e.g., Figure 17b). Required specifications include a time series of withdrawal flow (Q_w) that reflects historic observations or a scenario of interest, and T_w and $T_{n,w}$ goals (Figure 17a). Additional inputs include WSE and simulated vertical profiles of in-reservoir T and

T_n, from the model segment containing the intake (model output). The algorithm proceeds day by day, determining the combination of withdrawal levels and flows that meet, if possible,

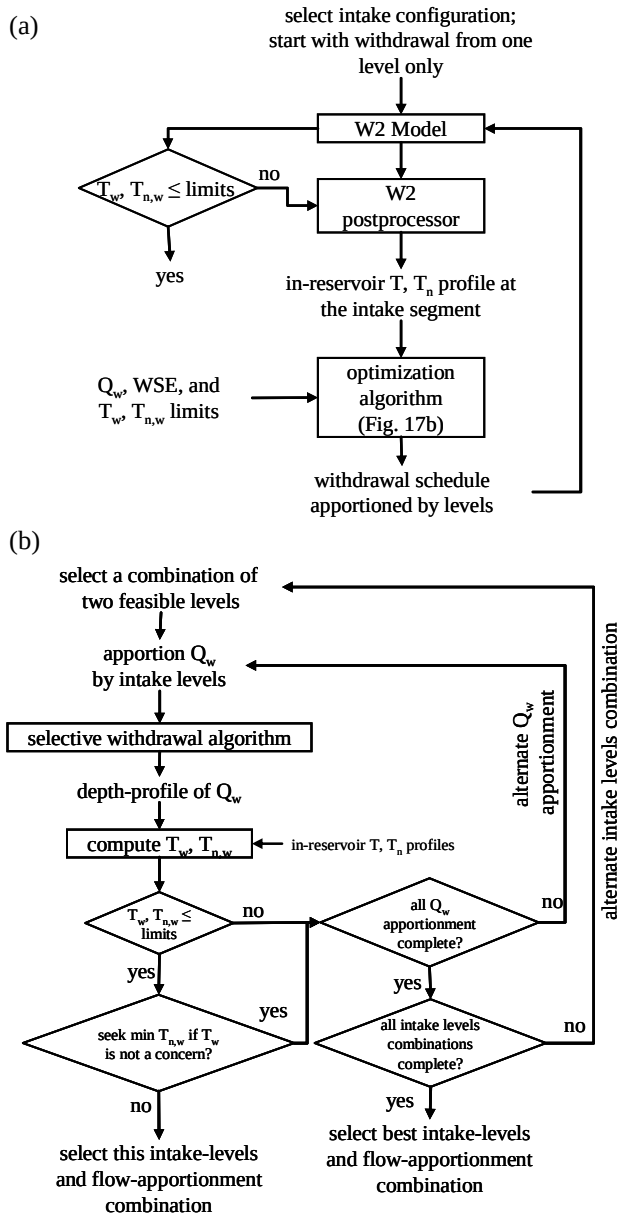

Figure 17. Optimization of Operation of Multi-level Intake Facility: (a) Linkage of Two-Dimensional Water Quality Model and Optimization Algorithm, and (b) Heuristic Optimization Algorithm for Blending of Withdrawals from Multiple Intakes to Meet T_W Goal and Minimize $T_{n,w}$.

the specified goals. The heuristic approach (Figure 17b) has advantages over other optimization techniques, such as dynamic programming, including computational efficiency and ready linkage with a simulation model such as W2/T.

Initially the algorithm establishes the intake levels that are available (i.e., positioned below the WSE; Figure 17b). The desired Q_w is then apportioned among the available intake levels for withdrawal. Two adjoining intake levels are selected for withdrawal, moving downward in the water column. For example, for a 4-level intake facility, intakes I and II are first selected (numbered according to shallowest, or highest elevation, as intake I, and deepest, or lowest elevation, as intake IV), consistent with the strategy of preserving the colder hypolimnetic water. High $T_{n,w}$ values at these intake levels would force shifts to deeper intakes. The apportionment (blending) of Q_w for the selected levels is done progressively, starting with 100% from the upper level and 0% from the deeper level, with shifts in this partitioning (increments of 0.5%) as necessary to meet the specified goals (Figure 17b). The relatively small size of the increments supports a "smooth" blending that reduces variations in T_w that could lead to irregular exceedences of the goal (e.g., Hanna et al. 1999).

The withdrawal algorithm is then used to calculate the effective withdrawal flow rate from each of the model layers, based on the combination of determined levels and flow apportionment (Figure 17b). Note that withdrawals are effectively taken from a rather broad depth interval adjoining an intake (Martin and McCutcheon 1999), as represented by W2/T (Cole and Wells 2002), and as illustrated through simulations for three different intake elevations for the conditions observed for June 16, 2002 (Figure 18). This, together with the model simulations of in-reservoir profiles of T and T_n for

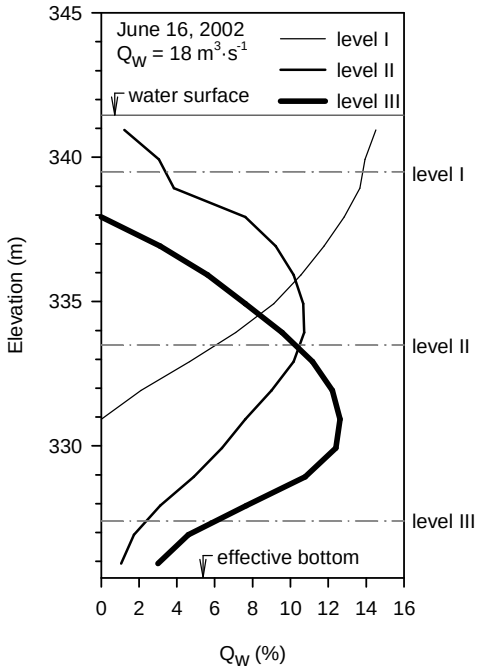

Figure 18. Model Simulations of Vertical Contributions to Withdrawal Flow (Q_w) for the Conditions of June 16, 2002, for Three Intakes (centerline positions shown), Operating Separately.

the model segment containing the intake, results in predictions of T_w and $T_{n,w.}$ The selection of intake levels and flows has a feedback affect on predictions of in-reservoir T and T_n patterns (Gelda and Effler 2006c). Iterative analyses of operation scenarios are conducted as necessary to meet the specified withdrawal goal(s). A minimal impact is sought if the specified goal cannot be met.

2.1.3.2 Specifications for example/applications of the optimization framework

Application of the optimization framework that links the reservoir simulation model with the described heuristic operations algorithm is demonstrated here in an evaluation of two MLI alternatives. The two scenarios are for the conditions of 2002 (Table 6), the year of second greatest drawdown and highest T_w goal, of the 1989-2003 period (Gelda and Effler 2006a). These example applications focus only on meeting the T_w goal. Maintenance of the observed Q_w time series for that year, as part of these example applications, reflects protection of the reservoir's primary intended use as a water supply.

Table 6: Specification of two MLI configurations for evaluation by the optimization framework.

Scenario*	Site	No. of Levels	Elevation of Intake Levels (m)†			
			I	II	III	IV
A	3	3	339.5	333.5	327.4	-
B	1.5	3	339.5	328.1	316.7	-
baseline[xx]	3	1	-	-	-	327.4

* see Figure 19

† centerline, assuming 2.45 m height for intakes

xx prevailing conditions

The development of model inputs, including the drivers for 2002 has been specified elsewhere (Gelda and Effler 2006a). The two MLI scenarios considered here include two sites, one at the existing location (site 3) and the other substantially down-reservoir in a deeper area (site 1.5, Figure 1a), both with three intakes (Table 6). Both scenario configurations (A and B) have a near-surface intake (I) at an elevation (centerline of 2.45 m high intake) of 339.5 m (Table 6). The deepest intake levels approach the reservoir bottom at the two locations (Table 6). The intermediate intake levels are positioned such that distances between them are equal.

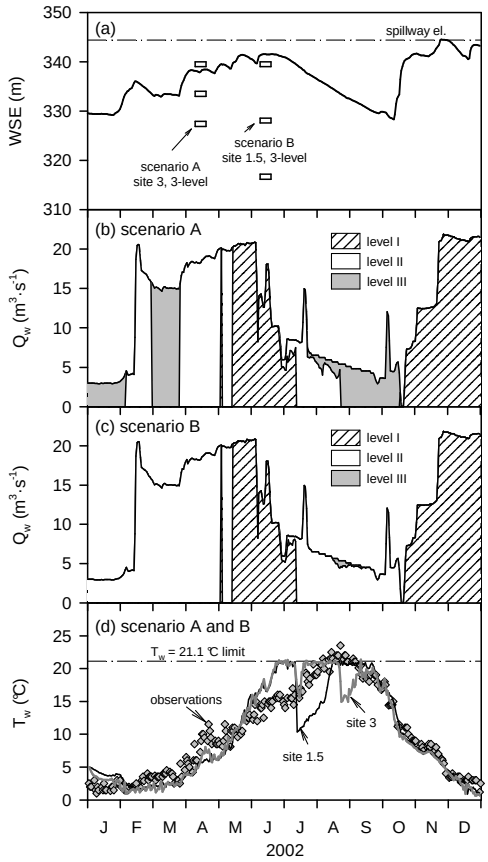

Figure 19. Results of Example Application of Optimization Framework for Two MLI Scenarios (see Table 6): (a) WSE, with Vertical Positions of Intakes Presented for Two MLI Scenarios, (b) Q_w (observed) and Simulated Apportionments for Intake Levels of Scenario A, (c) Q_w (observed) and Simulated Apportionments for Intake Levels of Scenario B, and (d) T_w, Observations and Model Predictions for Scenarios A and B.

2.1.3.3 Results for example applications of the optimization framework

Time series of simulations of apportionments of Q_w and associated predictions of T_w are presented for the two MLI scenarios; the corresponding time series of observed WSE is included for reference (Figure 19). All three intake levels were predicted to be active at some time during the year for both three-level intake scenarios (A and B; Table 6; Figure 19a and c) and all scenarios were successful in avoiding violations of the goal for T_w (e.g., Figure 19d). The timing of use of the various intake levels was highly dependent on WSE for these scenarios.

The early use of the deepest level intake through January and into February for scenario A (site 3, Figure 19b) reflects the extensive drawdown of the reservoir surface at that time. Subsequent shifts in use of the various intake levels for this scenario, including the abrupt start-up and subsequent discontinued use of the upper intake in early May, all tracked the dynamics of WSE (Figure 19a), reflecting the use of the intake positioned

highest in the water column. The upper intake was used solely for this scenario from early May through June (Figure 19b). Clear increases in T_w relative to the observations for 2002 were manifested over this interval (Figure 19d), reflecting the effects of releasing epilimnetic waters instead of the cooler waters of the lower layers at site 3. Blending, guided by the optimization algorithm, of relatively small amounts of level II with the level I withdrawal was necessary through early July to meet the T_w standard. Note that predicted T_w tracks the specified goal-during this and other intervals of blending (Figure 19d). Drawdown eliminated access to level I starting in early July. The attendant shift to level II (Figure 19b) was accompanied by a sharp decrease in T_w of ~ 5º C. Blending of withdrawals from intake levels II and III became necessary for this scenario to meet the T_w standard starting in late July, and continued until late August when access to the middle intake level was eliminated by drawdown (Figure 19a and b). The abrupt shift to level III (bottom) as the sole source of Q_w resulted in a second sharp decrease in T_w of ~ 5º C (Figure 19d). Exclusive use of this bottom level intake was required through mid-October (past the time when T_w values approached the standard), when the abrupt refilling of the reservoir (Figure 19a) from high runoff allowed access to the upper level intake (Figure 19b).

Certain features of the simulations for scenario B (site 1.5), an alternative that would position a multi-level intake facility in a deeper part of the reservoir (Figure 1b), present interesting contrasts to those presented for the shallower site (Figure 19b - d). The middle level (II) for this scenario met the entire Q_w demand through April. Thereafter, until late June, the apportionment according to levels did not differ from scenario A (site 3). Smaller contributions from level II were required in the blending interval of late June through early May for scenario B (site 1.5; Figure 19b and c), associated with the colder (e.g., deeper) waters available at level II for this scenario. This was also responsible for the even larger decrease in T_w (~ 10º C), compared to scenario A (site 3,; Figure 19d), when drawdown eliminated access to the upper level intake. Use of the deepest level intake is predicted only for about two weeks in late August (Figure 19c) to avoid exceedences of the standard for T_w (Figure 19d); the contribution from the deep intake remained less than 15% over this interval. Intake level II was used thereafter, until access to level I was acquired with the rapid increase in WSE in late October.

2.1.4. Probabilistic model for temperature and turbidity in the Schoharie Reservoir withdrawal

2.1.4.1 Introduction

Managers seek to effectively apply successfully tested models, as documented above, to predict ecosystem response to rehabilitation alternatives. Such predictions, or forecasts, are described as a priori simulations (Bierman and Dolan 1986; Gelda et al. 2001), as they correspond to environmental forcing conditions that have not occurred, but instead are specified. Model forecasts and related management perspectives can be influenced greatly by the forcing conditions specified (Bierman and Dolan 1986; Gelda

and Effler 2003). Thus it is important that the specified forcing conditions are representative.

Goals for developing representative inputs for a priori simulations should include absence of bias and appropriate description of variability. Long-term records of environmental forcing conditions, such as meteorology and operations of reservoirs, offer opportunities to represent the effects of variations in important drivers in model forecasting (Owens and Effler 1989; Owens et al. 1998; Gelda et al. 2001). The use of long-term data sets as model inputs eliminates the arbitrariness of specification of critical conditions for complex situations, as inputs described by these actual measurements are inherently representative (Owens et al. 1998; Gelda et al. 2001). Accordingly, a model's predictive capability serves to represent the effects of variability in these forcing conditions. Presentation of the simulations in a probabilistic (e.g., cumulative percent occurrence) format (Gelda et al. 2001) provides a valuable perspective on reasonable variability in water quality to be expected, and can lead to an objective identification of critical forcing conditions (Gelda and Effler 2003). Longer monitoring records are expected to more completely represent variability. For example, Gelda and Effler (2003) conducted simulations with a probabilistic model, driven by long-term (27 y) monitoring data for key drivers, to describe variability to be expected in the status of an urban lake with respect to ammonia toxicity criteria, and to identify critical (e.g., one in ten years) runoff conditions.

2.1.4.2 Description of Probabilistic Modeling Framework

The central feature of the overall probabilistic model framework is the water quality model (Figure 20), composed of the submodels described above. It is capable of simulating transport within the reservoir, features of the thermal stratification regime, T_w, patterns of T_n within the reservoir, and $T_{n,w}$. The required inputs for the overall model dictate the data types for which long-term records or estimated values must be accessed or developed to drive the probabilistic framework (Figure 20). The optimization framework (Figure 20) supports automated and optimized selection of intake levels to meet water quality goals. A minimal impact is sought if a goal cannot be met (Gelda and Effler 2006c).

2.1.4.2.1 Specification of Drivers of Probabilistic Framework

2.1.4.2.1.1 Meteorology

Regional (e.g., off-site) meteorological data (Table 7) have been successfully used to support simulation of the stratification regime of Schoharie Reservoir with W2/T (Gelda and Effler 2006a), as well as another reservoir in the region (Gelda et al. 1998). On-site hourly (consistent with time step of model inputs) meteorological measurements

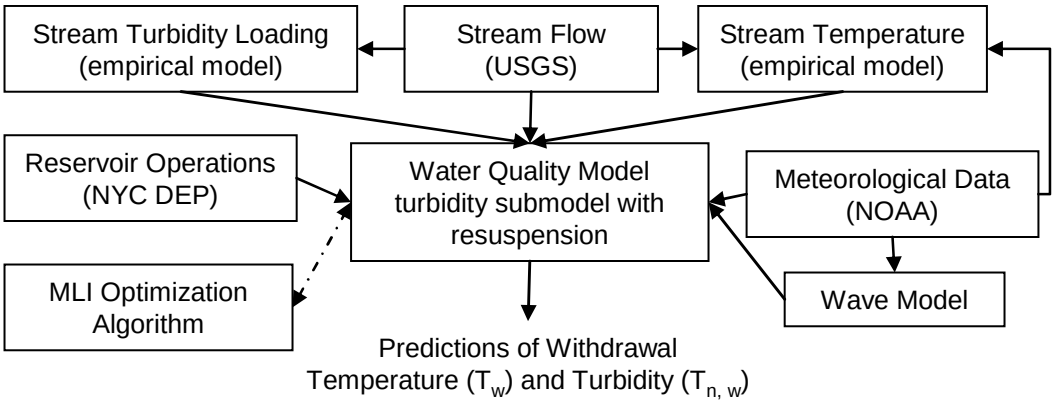

Figure 20. Probabilistic Model Framework for A Priori Simulations of Withdrawal Temperature (T_w) and Turbidity ($T_{n,w}$) for Schoharie Reservoir.

Table 7: Monitoring Data Supporting Probabilistic Modeling Framework for Schoharie Reservoir.

Model Driver Type	Items	Specifications for Data
meteorology	air T, dewpoint T, solar radiation[1], wind speed and direction	on-site, 1997 - 2002; off-site, Albany airport, since 1948 (NOAA)
inflows (gaged)	tributary flows	Schoharie Creek since 1948; Manor Kill since 1986; Bear Kill since 1998 (USGS)
inflows (ungaged)	minor tributary flows	estimated from hydrologic budget[2]
outflows	withdrawal	1948 - 1996, NYCDEP; 1997 - 2004, USGS
	spill	computed from rating curve
loads[3]	based on TSS, T_n and $\mathbf{c}_{660}$ measurements	TSS for 1996 - 2001; paired TSS and T_n for 2003 - 2004; paired $\mathbf{c}_{660}$ and T_n for 2003
stream T	Schoharie Creek, as a function of T_{air} and Q	Schoharie T, Albany T_{air}, Q 1998, 2002 - 2004
light attenuation coefficient	-	average of patterns for 1993 – 2003

[1] from cloud cover data (Cole and Wells 2002)
[2] conducted outside of the probabilistic framework
[3] from combined Q and $\mathbf{c}_{660}$ information

were available for 6 y (Table 7) of the 14 y of hydrothermal model testing (Gelda and Effler 2006a). Simulations for the other 8 y were instead supported by regional data collected at a National Weather Service station located ~ 60 km (the most proximate) northeast of the reservoir at Albany, NY. No significant difference in model performance was observed for the years of on-site versus off-site meteorological measurements (Gelda and Effler 2006a).

Strong linear least-squares regression relationships ($r^2 > 0.95$) have prevailed between on-site and off-site measurements of air T (T_{air}; Schoharie T_{air} = 0.964·Albany T_{air} - 0.45 ºC, $r^2 = 0.968$) and dewpoint T. The relationship for solar radiation (I, $w \cdot m^{-2}$) was also strong (Schoharie I = 0.853·Albany I + 8.45 $w \cdot m^{-2}$; $r^2 = 0.849$). In contrast, the relationship for wind speed (v, $m \cdot s^{-1}$) was much weaker ($r^2 = 0.31$; Schoharie v = 0.272·Albany v + 1.46 $m \cdot s^{-1}$). The regression relationships were used in specifying inputs to W2/T with the off-site meteorological data (Figure 20). The available meteorological record for Albany (since 1948, Table 7) set the duration limit (1948 - 2004; 57 y) for the probabilistic framework for this system.

2.1.4.2.1.2 Stream flows and loads

A flow gage was established by the United States Geologic Survey (USGS) for the mouth of Schoharie Creek before the reservoir was filled (Table 7). The quality of flow measurements at this gage (No. 01350000), to specify flow of the primary tributary for the probabilistic framework (Figure 20), has been described as good by the USGS (e.g., 95% of daily discharge values are within 10% of true value). Gages (USGS) were added to two smaller tributaries in 1986 and 1998; 95% of the watershed is presently gaged (Table 7). These measurements for the smaller tributaries supported development of linear least-squares regression relationships with Schoharie Creek flows that were used to specify these smaller inputs for the 57 period.

Levels of $\mathbf{c}_{660}$ were specified in Schoharie Creek hourly from the stream's flow (Q, $m^3 \cdot s^{-1}$) according to a relationship (Figure 21) developed from system-specific monitoring. This relationship is based on three components that function in series: (1) the concentration of total suspended solids (TSS) as a function of Q (unpublished data, 1996 - 2001, NYCDEP), (2) the relationship between T_n and TSS for this stream (e.g., Effler et al. 2006a), and (3) the relationship between $\mathbf{c}_{660}$ and T_n for the system (Effler et al. 2006b). Uncertainty and variability in the overall relationship (Figure 21) is primarily associated with the first of these components, as the second and third components are strong by comparison. In particular, the strong $\mathbf{c}_{660}$ - T_n relationship (Effler et al. 2006b) is expected as these are both measures of light scattering (Kirk 1994). A portion of the scatter in the $\mathbf{c}_{660}$ - Q relationship (Figure 21) apparently reflects systematic shifts that occur irregularly in response to extremely high runoff events (e.g., Smith 2002), behavior that is consistent with the poorly armored nature of the banks along Schoharie Creek. Loads of $\mathbf{c}_{660}$ (Gelda and Effler 2006b) were specified hourly as the product of hourly values of $\mathbf{c}_{660}$ and Q.

2.1.4.2.1.3 Stream temperature

Representation of the dynamics of stream T (T_s, ºC) is necessary for this system (Figure 20) because the density differences responsible for the turbid density currents

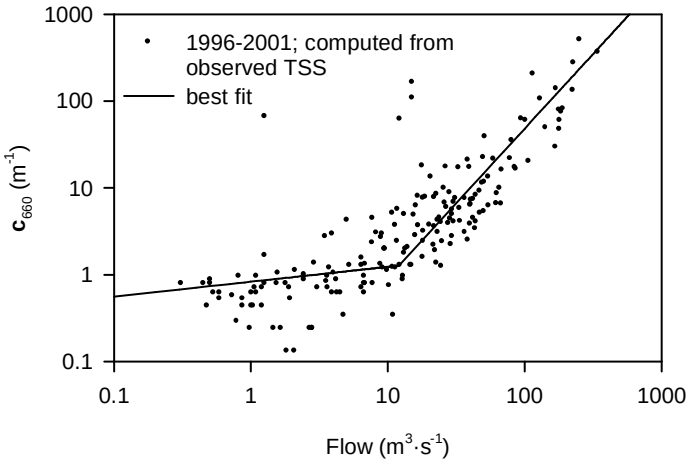

Figure 21. Evaluation of Relationship for Schoharie Creek to Support Specification of $\mathbf{c}_{660}$ Levels from Q.

and related vertically structured T_n (and $\mathbf{c}_{660}$) patterns in the reservoir are attributable to differences in temperature (Effler et al. 2006a). Moreover, wide variations in T_s occur in this stream within individual days (O'Donnell and Effler 2006). Empirical polynomial relationships were developed for individual months to specify T_s hourly as a function of Q and Albany T_{air}, according to the polynomial

$$T_{s,i} = a_0 + a_1 \cdot T_{air,i-3} + a_2 \cdot \log(Q_i) \quad (4)$$

where $T_{s,i}$ = stream temperature for Schoharie Creek for hour i, $T_{air,\ i-3}$ = air temperature 3 h before hour i, Q_i = stream flow for Schoharie Creek for hour i (interpolated values based on daily mean Q_s), and a_0, a_1, and a_2 are coefficients. The analysis was based on paired values in 1998 and 2002-2004, intervals for which measurements of $T_{s,i}$ were available (Table 7).

The empirical model(s) generally performed well at time scales of within a day and day-to-day for the various months, as illustrated for August (a_0 = 13.831, a_1 = 0.395, and a_2 = 2.408) of 1998 (Figure 22). The monthly relationships explained from 65 (October) to 82% (July) of the substantial variability in $T_{s,i}$. The same predicted time series of $T_{s,i}$ obtained for Schoharie Creek for the 57 y period was adopted for the other smaller tributaries.

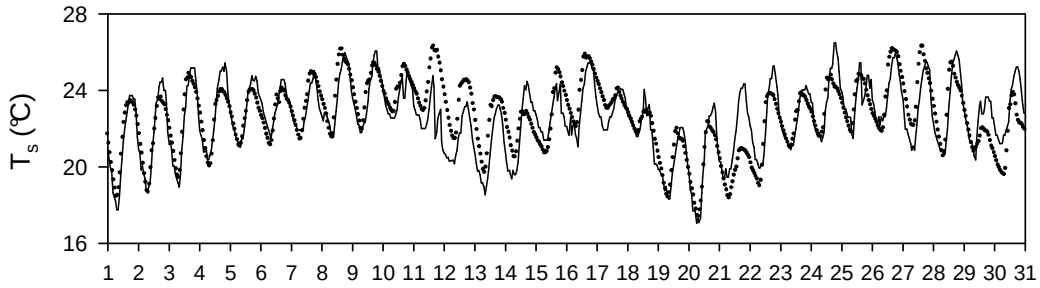

Figure 22. Performance of Empirical Temperature Model for Schoharie Creek for Hourly Observations in August 1998.

2.1.4.2.1.4 Operations

The effects of reservoir operations are mediated by the imbalance between tributary inputs and the withdrawal flow Q_w. This outflow pathway, as well as spill over the dam, as monitored by NYCDEP since the initial filling of the reservoir, is specified in the probabilistic framework for the 1948-2005 period (Figure 20; release through the dam structure has not been operative over the portion of the record represented in the probabilistic framework). A primary manifestation of the operations of this reservoir is variations in WSE. This fundamental change in the physical dimensions of the reservoir influences its thermal stratification regime (Owens et al. 1998; Gelda and Effler 2006a), vertical patterns of T_n ($\mathbf{c}_{660}$) relative to the intake depth following runoff events (Effler et al. 2006a), and related features of water quality in the withdrawal.

Substantial drawdown has been a common occurrence over the 57 y record; e.g., the annual average WSE was within 2 m of the full reservoir elevation in only 9 y of the period, and was > 5 m in 25 y (Figure 23a). The wide interannual variations reflect the effects of natural variations in runoff in the watershed. Wide variations also occur seasonally, with maximum drawdown observed on average (~ 15 m) in September and October, and minimum in April and May (Figure 23b).

2.1.4.3 Evaluation of the sources of variability of withdrawal water quality for prevailing conditions

The performance of the probabilistic framework in simulating the observed variability in T_w and $T_{n,w}$ was evaluated by comparing the predicted seasonal bounds to the population of observations for the 1987 - 2004 interval (Figures. 24 and 25), a period for which comprehensive monitoring data were available. The range of observations was quite broad for T_w (Figure 24a), but particularly for $T_{n,w}$ (Figure 25a; note logarithmic scale). The pattern for the upper bound of the T_w distribution of observations is similar to that of the epilimnion of the reservoir, while the lower bound is akin to hypolimnetic conditions (Gelda and Effler 2006a). Values approaching or exceeding the T_w goal (21.1 ^oC) have been observed over the late July through early September interval (Figure 24a).

The temporal pattern of $T_{n,w}$ has generally lacked a recurring seasonality, consistent with the more random occurrences of runoff events, that are the primary drivers of elevated turbidity in this reservoir (Effler et al. 2006b; Gelda and Effler 2006b).

No single year can represent the variability that has prevailed for both T_w and $T_{n,w}$, as illustrated by the predictions for 2003 (Figure 24a and 25a), a relatively high runoff year for the spring to fall interval in which the reservoir remained nearly full (Figure 23b). Predictions of T_w for 2003 tended to track the lower bounds

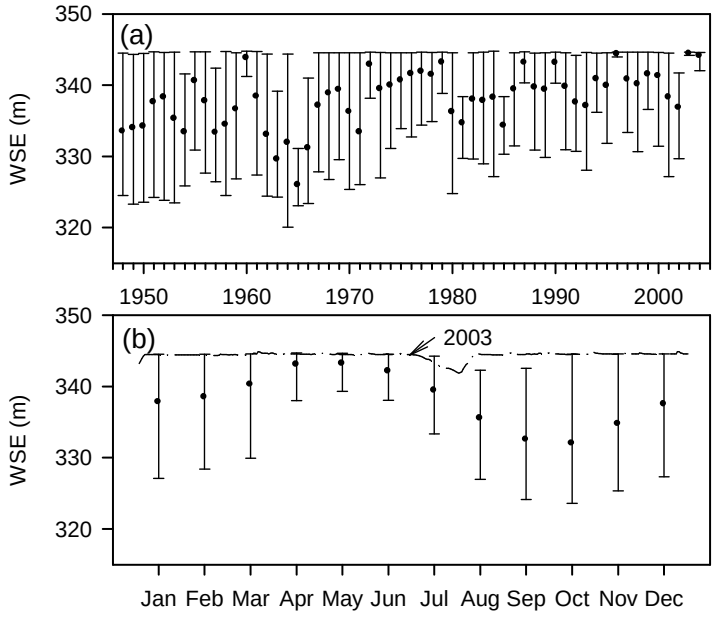

Figure 23. Historic WSE Patterns for Schoharie Reservoir, 1948 - 2004: (a) Annual Mean and 10th and 90th Percentiles, and (b) Seasonality, Monthly Mean and 10th and 90th Percentiles, with the time series for 2003 conditions included.

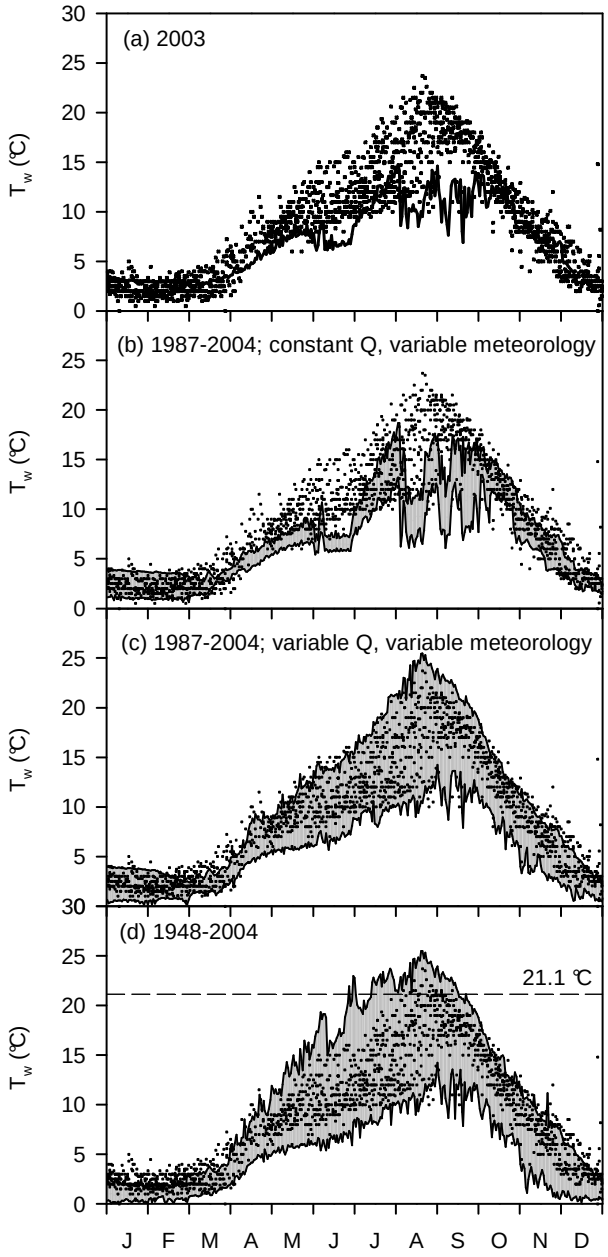

Figure 24. Comparisons of Simulations and Observations (1987-2004) of T_w: (a) Simulations for Conditions of 2003, (b) 2003 Hydrology with Meteorological Conditions for 1987-2004, (c) Simulations for Meteorological and Hydrology/Operations Conditions for 1987 - 2004, and (d) as in (c), but for 1948-2004. Line in (a) is simulations for conditions of 2003, bounds of Envelopes in (b), (c) and (d) are Ranges of Model Predictions.

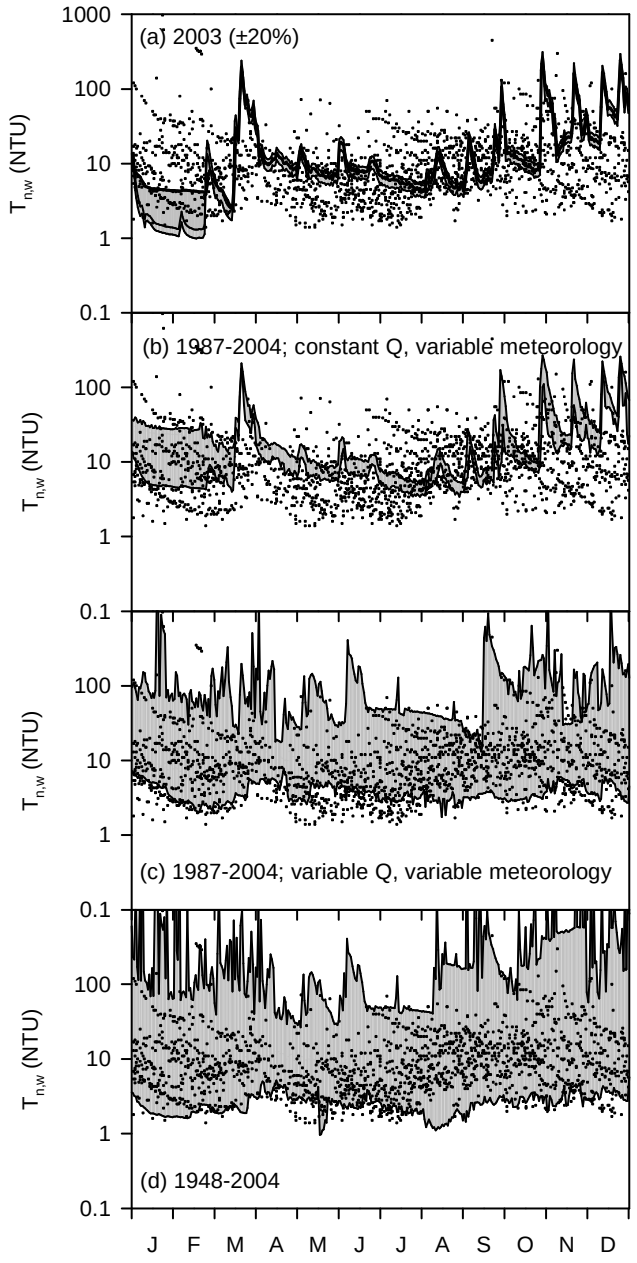

Figure 25. Comparisons of Simulations and Observations (1987 - 2004) of $T_{n,w}$: (a) Simulations for Conditions of 2003, (b) Simulations for 2003 Hydrology with Meteorological Conditions for 1987 - 2004, (c) Simulations for Meteorological and Hydrologic/Operations Conditions for 1987 - 2004, and (d) as in (c), but for 1948 - 2004. Bounds of Envelopes in (b), (c) are (d) and Ranges of Model Predictions.

of observations for the 1987 - 2004 period (Figure 24a). A number of short-term increases in $T_{n,w}$ were predicted for 2003 (Figure 25a) in response to runoff events and well-predicted (Gelda and Effler 2006b) increases in T_n levels in the reservoir's water column. The relative contributions of variations in meteorological conditions and hydrology/operations are depicted here by sequential (cumulative) inclusion of their effects for the 18 y of observations. Meteorological conditions drive not only the transport/hydrothermal submodel, but also stream T (i.e., the occurrence and depths of plunging during runoff events) and wave action (i.e., near-shore sediment resuspension; Figure 20). Hydrologic conditions, as reflected in runoff levels, are inextricably coupled to operations in this reservoir, particularly as manifested in the occurrence, timing and magnitude of drawdown (Figure 23).

Accommodation of meteorological variations, as measured over the 1987 - 2004 period, under the nearly full reservoir (hydrologic) conditions of 2003 (i.e., held constant), explain only a modest amount of the observed variability in T_w (Figure 24b) and $T_{n,w}$ (Figure 24b). Moreover, the range in predictions of T_w extend below observations in portions of the June through September interval. This feature suggests such meteorological variability did not occur for nearly full reservoir conditions, such as prevailed in 2003.

Inclusion of the effects of variability in hydrology/operations observed over the 1987 - 2004 interval resulted in much improved simulation of the observed variability (Figure 24c and 25c). Eighty five percent of the observations of T_w and 75% of the measured $T_{n,w}$ values were bounded by these predictions with the probabilistic framework. The broadening and upward shift of T_w bounds in summer (Figure 24c) is largely attributable to the common occurrence, but variable magnitude, of drawdown during that 24 y interval (Figure 23b). The highest T_w values correspond to major drawdown intervals when the intake withdrew epilimnetic waters. The lower values reflect withdraws from the hypolimnion, such as in 2003 (Figure 24a). There was some tendency to overpredict the lowest $T_{n,w}$ (and water column T_n) values (e.g., < 5 NTU; Figure 25c). This is not deemed to be a substantive short-coming as these turbidity levels are well below those of management concern. Peak occurrences of $T_{n,w}$ were somewhat over-represented by the predictions. In part, this is an artifact of the temporary shutdown of the withdrawal following certain large runoff events to avoid discharge of particularly turbid water in Esopus Creek. Comparisons of the distributions of the predictions and observations in a cumulative percent occurrence format (Figure 26) provide a more rigorous test of the representativeness of the probabilistic framework. The predictions track the observations for T_w (Figure 26a) and $T_{n,w}$ (Figure 26b) closely. For example, the probabilistic framework predicted $T_{n,w}$ exceeded 15 NTU 23% of the 1987-2004 interval, very similar to the observations (24%, Figure 26b). Yet wider season bounds of T_w and $T_{n,w}$ were predicted with the probabilistic model when the variations in drivers for the 57 y (1948-2004) record were incorporated (Figures 24d and 25d), depicting the added benefit in representing variability by considering the longer record.

2.2. Evaluation of Multi-Level Intake Scenarios with Probabilistic Modeling Framework

The developed and tested probabilistic modeling framework is applied here to evaluate the potential benefits of five selected MLI configurations in Schoharie Reservoir (Table 8). The prevailing intake configuration (single intake at site 3) is included for

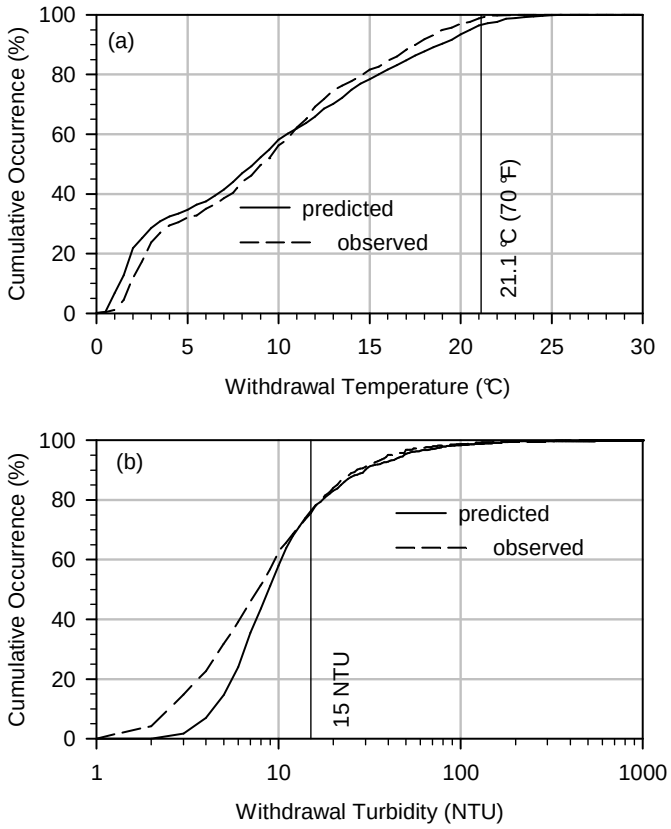

Figure 26. Performance of the Probabilistic Modeling Framework in Simulating the Observed Water Quality of the Withdrawal from Schoharie Reservoir for the 1987-2004 Interval, as Cumulative Occurrence Plots: (a) Temperature (T_w), and (b) Turbidity ($T_{n,w}$).

Table 8. Specification of five MLI configuration alternatives for evaluation with probabilistic modeling framework.

MLI Site[+]	No. of Levels	Elevation of Intake Levels (m)			
		I	II	III	IV
3	3	339.9	333.8	327.1	-
2	3	339.6	331.9	324.3	-
2	4	339.6	334.	329.5	324.3
1.5	3	339.6	330.	321.3	-
1.5	4	339.6	333.5	327.4	321.3

[+] see Figure 1b

reference. These scenarios emerged based on consideration of an array of factors (e.g., Gannett Fleming & Hazen and Sawyer 2004). The site 3 MLI alternative (Table 8) would position a MLI facility at, or adjoining, the existing intake. Both the site 2 and site 3 alternative would have greater water depths available, with the deepest depths of the alternatives (i.e., greatest access to the entire water column) available at site 1.5 (Table 8). Both three and four intake options were considered for the site 2 and site 1.5 alternatives. The applications of the probabilistic framework presented here incorporate historic operations (57 y). Thus these do not accommodate changes in operating strategies, such as may be adopted in the future to meet both water supply and SPDES permits needs. Applications of the probabilistic modeling framework to address such cases are presented elsewhere in this report.

The T_w goal is predicted to be met for essentially the entire range of conditions of the 57 y embedded within the probabilistic framework for all five of MLI scenarios (Figure 27). The short-term exceptions for certain scenarios could be eliminated by modest adjustments in operation of the intakes. Note the elimination of occurrences of $T_w > 21.1$ º C for these scenarios (Figure 27b-f) compared to the predictions for existing single fixed-depth intake (Figure 27a). T_w would tend to increase more rapidly in spring and early supper with a MLI (Figure 27b-f), reflecting an operating strategy of using warmer epilimnetic waters (i.e., upper intake) earlier in the year, thereby saving colder hypolimnetic waters for late summer withdrawal. This would result in a shift to the increased occurrence of colder T_w values in late summer (Figure 27). A wide range of T_w values (but < 21.1 º C) would continue to be encountered following the installation and operation of a MLI facility.

There are three noteworthy features of the $T_{n,w}$ prediction for the MLI scenarios (Figure 28): (1) a very wide range of values would continue to occur (e.g., the withdrawal may be shutdown for particularly high levels), (2) exceedences of the $T_{n,w}$ goal of 15 NTU would continue, though these occurrences would decrease by ~ 30% (e.g., ~ 18% occurrence > 15 NTU, instead of 25% occurrence > 15 NTU), and (3) performance at the three sites and three and four intake options would be nearly equal. The lack of greater benefit from a MLI facility for $T_{n,w}$ levels is in part a result of the substantial depth intervals impacted by runoff events (e.g., thickness of turbid density currents; Effler et al. 2006b) and that contribute to inflow into an intake (Martin and McCutcheon 1999); Gelda and Effler 2006c). Moreover, the turbid reservoir strata become thicker following runoff event in response to natural mixing processes (Effler et al. 2006a). Accordingly, the hypothetical MLIs provided only modest avoidance benefits for turbid reservoir strata (Figure 28).

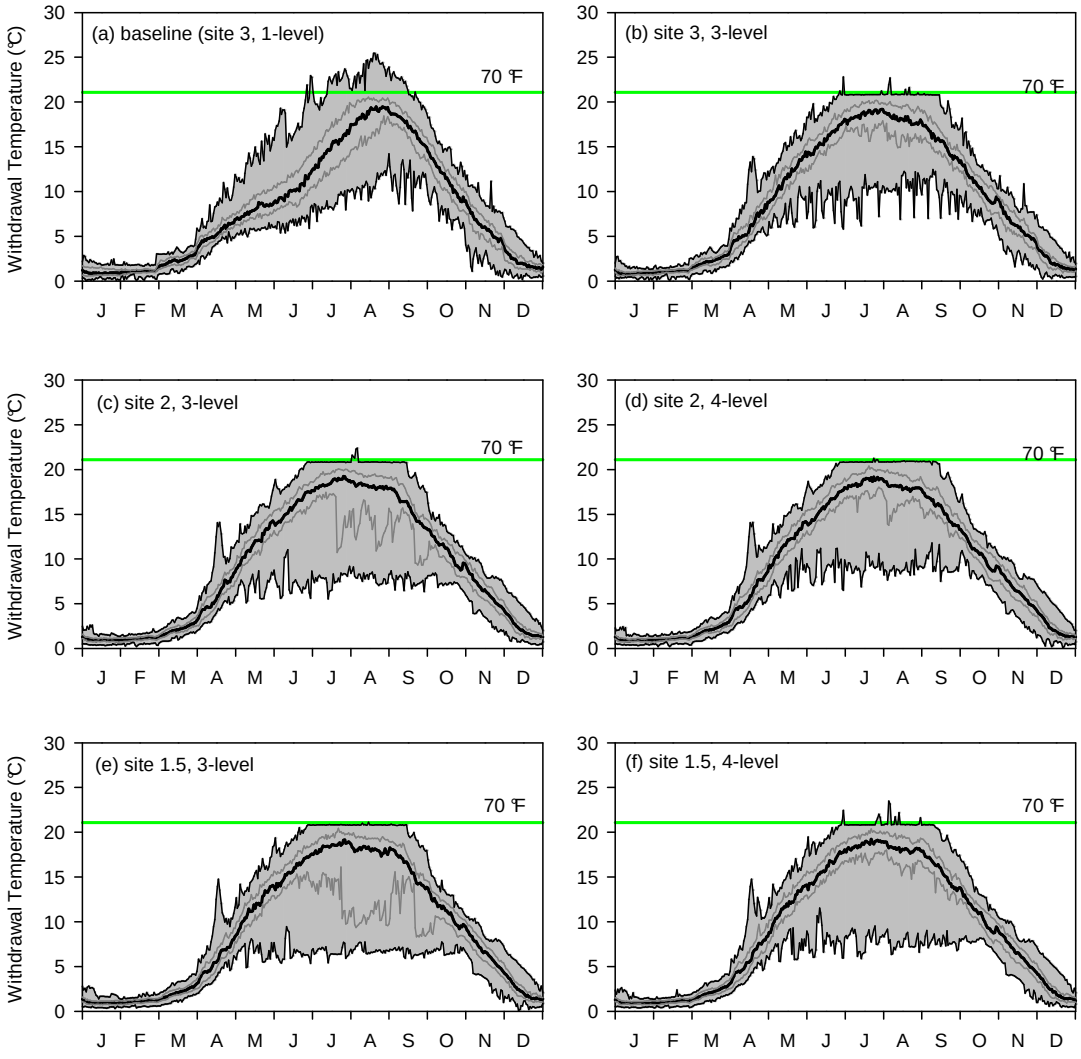

Figure 27. Predictions of the Seasonality of the Temperature of Withdrawal (T_w) of Schoharie Reservoir by the Probabilistic Framework (57 years of conditions): (a) Prevailing Conditions, (b) MLI Scenario, site 3, 3-level, (c) MLI Scenario, site 2, 3-level, (d) MLI Scenario, site 2, 4-level, (e) MLI Scenario, site 1.5, 3-level, and (f) MLI Scenario, site 1.5, 4-level.

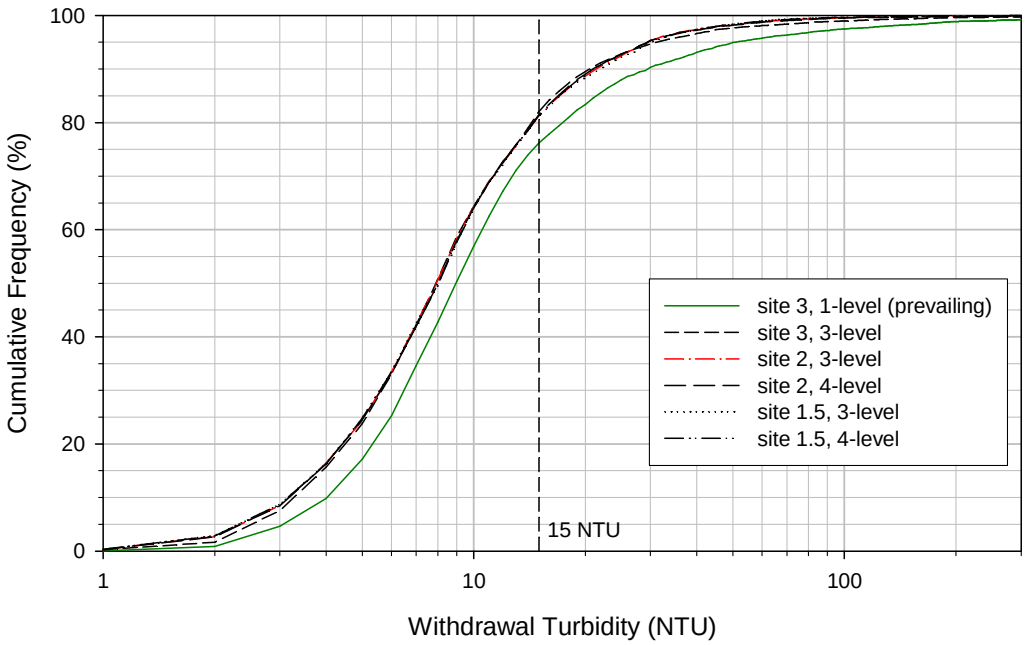

Figure 28. Predicted Distributions of the Level of Withdrawal Turbidity ($T_{n,w}$) of Schoharie Reservoir by the Probabilistic Framework (57 years of conditions) for the Prevailing Case and Five MLI Scenarios (Table 8). Note the Near-Equivalence of Performance of the MLI Scenarios.

may be shutdown for particularly high levels), (2) exceedences of the $T_{n,w}$ goal of 15 NTU would continue, though these occurrences would decrease by ~ 30% (e.g., ~ 18% occurrence > 15 NTU, instead of 25% occurrence > 15 NTU), and (3) performance at the three sites and three and four intake options would be nearly equal. The lack of greater benefit from a MLI facility for $T_{n,w}$ levels is in part a result of the substantial depth intervals impacted by runoff events (e.g., thickness of turbid density currents; Effler et al. 2006b) and that contribute to inflow into an intake (Martin and McCutcheon 1999); Gelda and Effler 2006c). Moreover, the turbid reservoir strata become thicker following runoff event in response to natural mixing processes (Effler et al. 2006a). Accordingly, the hypothetical MLIs provided only modest avoidance benefits for turbid reservoir strata (Figure 28).

The similarity in performance of the various MLI configurations in the context of percent occurrence (daily average) > 15 NTU (Figure 28), a useful summary statistic for managers, should not be misinterpreted as depicting uniformity in response to runoff events in these portions of the reservoir. Temporally and spatially detailed monitoring in the reservoir following runoff events has established highly structured patterns for T_n, that differ according to the event and other driving conditions (Effler et al. 2006a; 2006b). Comparison of the predictions of $T_{n,w}$ at a shorter time scale for two of MLI facility scenarios provides a valuable perspective on the extent of structure embedded in the summary statistic of percent occurrence > 15 NTU. Substantial spatial differences have been predicted for the two hypothetical MLI sites at a daily time step by the

probabilistic model (Figure 29a; n = 14,831 paired predictions). More extremely high $T_{n,w}$ values (> 100 NTU) were predicted for the site 3 scenario (e.g., more proximate to Schoharie Creek), but the number of these occurrences was predicted to be extremely small relative to the size of the population and the subset > 15 NTU. This analysis of model output serves to demonstrate that wide temporal differences between the two sites in the status with respect to the $T_{n,w}$ goal are embedded in the nearly equivalent performance for the statistic of percent occurrences > 15 NTU.

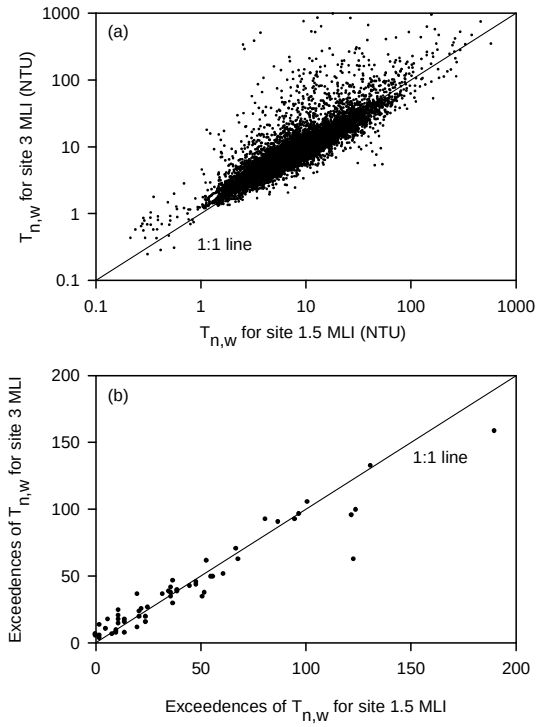

Figure 29. Comparisons of $T_{n,w}$ Values of Multi-Level Intake Facility Scenarios for Sites 3 and 1.5 (each with three intakes; Table 8) on Schoharie Reservoir for the 1948-2004 Period: (a) Daily Noontime predictions, (b) Number of Days with Average $T_{n,w}$ > 15 NTU for Each Year of the 57-Year Record.

Substantial differences in performance emerge for the same MLI scenarios in the context of the number of days for which $T_{n,w}$ > 15 NTU is predicted for each of the 57 y (Figure 29b). While the tendency towards equivalence for the entire record is apparent, rather wide differences in this metric of performance emerge for these two scenarios for many of the years. Thus one of the scenarios can be distinctly more beneficial than the other for the conditions of certain years. This analysis depicts the importance of addressing a long record of conditions to appropriately represent variability and evaluate the relative benefits of various scenarios.

3. EVALUATION OF BAFFLE ALTERNATIVE

An alternative for reduction of turbidity in the withdrawal from Schoharie Reservoir leading to the Shandaken Tunnel is the installation of an in-reservoir baffle wall. This baffle wall would divert water moving from south to north through the reservoir, causing a greater time of travel for water moving from Schoharie Creek and Bear Kill to the intake structure. This additional travel time would allow for increased mixing of turbid inflow with ambient reservoir water, and would allow for additional settling and deposition to the reservoir bottom, thereby reducing turbidity at the intake.

In order to generally evaluate this alternative and to analyze particular baffle designs, a three-dimensional hydrothermal and mass transport model of the reservoir was used. The model used is based on first principles (conservation equations for momentum, heat, and mass), has been applied to a wide variety of surface water bodies including lakes and reservoirs, and has been specifically tested for Schoharie Reservoir (Owens and Effler 2005). A three-dimensional model is required for this analysis in order to simulate the lateral variations in transport and water quality conditions that would occur as a result of installation of a baffle. This model has the capability to consider a thin, impermeable barrier through a portion of the water body.

A preliminary (Phase I) analysis of this alternative has been completed (Upstate Freshwater Institute 2004; Gannett Fleming & Hazen and Sawyer 2004). This earlier analysis was based on the following:

1. The performance of a baffle during two historic runoff events was analyzed. The reservoir was full during both of these events.
2. A conservative (non-settling) tracer was used to mimic particles or turbidity entering from the tributaries.
3. Three baffle lengths, covering a range from 1800 to 12300 ft (550 to 3750 m) were considered.

This Phase 2 analysis was designed to analyze the performance of additional baffle configurations, using a more accurate and rigorous approach. Specifically, six historic runoff events, including events that occurred during periods of reservoir drawdown, were used. Also, settling particles, rather than a conservative tracer, were predicted by the model. Using relationships established through monitoring studies, the effect of the baffle on turbidity was predicted.

3.1. Model Description

The model used in this study is a well-established and supported computer code, the Environmental Fluid Dynamics Code (EFDC). EFDC has been applied to a wide variety of surface water bodies, including applications to lakes and reservoirs (Yang et al. 2000; Jin et al. 2000; Ji et al. 2003). EFDC has received support from EPA. Region 4

EPA has recommended that EFDC be used as the hydrodynamic and transport framework for water quality modeling associated with TMDL development. The EPA Ecosystems Research Division in Athens, GA is supporting EFDC as a part of a collection of models that it recommends for use. EFDC is a mechanistic model that is based on fundamental governing equations for water mass, momentum, heat and particulate mass. The model uses sophisticated, state of the art algorithms and submodels to describe turbulence characteristics and turbulent diffusion coefficients, surface heat transfer, thermal stratification effects, and reservoir inflow and outflow.

EFDC has been applied to and tested for the particular characteristics of Schoharie Reservoir (Owens and Effler 2006). The model was applied for the historical conditions which occurred in the August-November interval of 2003. During this time, a series of four runoff events occurred in the tributaries to the reservoir. These events are representative of the conditions under which runoff results in elevated turbidity in the reservoir. As is typically the case in temperate climates in late summer and fall, Schoharie Creek was generally cooler and thus more dense than the surface waters of the reservoir. As a result, the creek enters the reservoir as a plunging inflow. Between the submerged weir at the upstream end of the reservoir and Site 4, the cool inflow passes through the plunge region, where the negative buoyancy of the stream in a sense exceeds its momentum, and the inflow sinks below the surface and flows down the sloping reservoir bottom, generally following the path of the drowned channel of Schoharie Creek. This density current continues until it reaches the depth of the thermocline, where it encounters cooler reservoir water. At a point where the inflow density is no longer greater than the reservoir, the inflow lifts off of the reservoir bottom and intrudes into the thermally-stratified layers of the reservoir.

During these events, the specific conductance (SC) of Schoharie Creek drops as a result of dilution of ionically-enriched baseflow. Monitoring of the reservoir water column during and after such events shows that the inflow from the creek follows the general pattern described above. Partially mixed stream inflow, identified by relatively low SC, can be found over the entire length and width of the reservoir following these events. The model testing described by Owens and Effler indicates that the model is capable of simulating (hindcasting) the three-dimensional patterns of SC observed in the reservoir. The baffle analysis described herein investigates the movement of water entering from tributaries through the reservoir, which is very similar to the conditions for which the model was tested. Accordingly, the successful testing described by Owens and Effler (2006) is the basis for its use in predicting the effects of a baffle.

3.2. Modeling Approach and Inputs

EFDC is a computationally complex model, so that run times are quite long. In addition, it was assumed that the baffle would only have significant effect on withdrawal turbidity during runoff events. As a result, the modeling analysis was based on simulation of individual runoff events and the period following the event as reservoir

turbidity returns to background or pre-storm levels. Observations indicate that this period is in the range of 2 to 4 weeks, depending on the characteristics of the individual event.

Six historic runoff events were selected (Table 9). These events were selected to include a representative range of the important environmental conditions which influence the impact on the reservoir. These conditions are magnitude of runoff, reservoir drawdown during the event, and magnitude of thermal stratification (quantified by the top-bottom temperature difference, Table 9). The six events selected represent a reasonable range of these conditions. Note that events 1 and 2 (Table 9) were the same events that were used in the Phase 1 analysis.

Table 9. Summary of runoff events used to analyze baffle performance.

Event Number	Year	Date of Peak Flow	Peak Daily Flow, m^3/sec	Drawdown at Start, meters	Top-Bottom Temp. Diff., ^oC	Duration of Simulation, days
1	2003	26-Oct	196	0	5	14
2	2003	4-Sep	76	0	17	14
3	2002	16-Oct	112	16	7	14
4	2001	13-Apr	187	0	4	30
5	1999	16-Sep	345	9	17	14
6	1992	6-Jun	122	5	12	20

In the 3D model simulations presented here, the model state variables used to represent water quality were three classes of particles. The following assumptions were made in simulating the particles in the reservoir:

1. Although the model equations used to simulate and quantify water quality are mass conservation equations, the values used to represent concentration were in fact values of the optical property of beam attenuation coefficient (BAC), with units of $meter^{-1}$. The use of BAC as a state variable in an mass conservation model was discussed in the 2D modeling portion of this report.
2. The total BAC of a sample or parcel of water was divided into three classes of BAC. Each of these 3 classes was treated as a state variable in the 3D model. The single distinguishing characteristic of the three classes is the settling velocity assigned to each class (Table 10). With the BAC of each class computed by the model, the total BAC was computed as the sum of the individual classes.
3. Based on available monitoring data from Schoharie Reservoir, turbidity (NTU) was computed as 2.5 time the total BAC ($meter^{-1}$).
4. The particle classes were not inter-related, so that particles in one class could not be transformed in any manner into another class.
5. A constant fraction of the total BAC of the tributary inflow was assigned to each of the three components of BAC (Table 10).

6. The only source of particles (BAC) to the water column of the reservoir is from tributary loading. Resuspension of particles (BAC) from the reservoir bottom was not considered in any three-dimensional model simulations.

The first five of these assumptions are entirely consistent with the application of the two-dimensional model described in a previous section. The last assumption is not consistent in that resuspension was considered in the 2D model.

Table 10. Particle (BAC) classes, settling velocity, and associated external loading percentages

Particle (BAC) Class	Settling Velocity, m/d	Tributary Loading, %
1	0.01	20
2	2.5	45
3	5.0	35

Simulations were made using the observed historical conditions as model inputs. These observed inputs included:

1. Flows for Schoharie Creek, Bear Kill, and Manor Kill as measured by the USGS.
2. Meteorological data: for events 1 through 3, on-site data from the robotic buoy deployed in the reservoir was used. For the other events, meteorological data from the Albany NY weather station was used, as described in the 2D model section.
3. Stream temperatures: values measured by UFI were used for events 1 through 3; the empirical equation described in the 2D model section was used for earlier events.
4. Initial water surface elevation at start of the event, from NYCDEP measurements.
5. Initial temperature and turbidity conditions were taken from available UFI and NYCDEP measurements. For Events 5 and 6 there were no turbidity data available, so projections from the 2D model for existing conditions were used.
6. For Events 1 through 3, the tributary BAC used was based on observations in Schoharie Creek; for the remaining events, the empirical stream flow-BAC relationship used in the 2D model application was used.

All simulations were made assuming water was withdrawn from the existing intake. The rate of withdrawal was set to a constant value of either 80 or 300 MGD (3.51 or 13.2 m^3/sec). As the intake was not operated at either of these constant withdrawal rates during any of the six events, the reservoir operation and resulting time series of storage, water surface elevation, and spill did not follow the historical pattern during these simulations. A water budget calculation, using the observed initial storage and water surface elevation, observed stream inflows, the assumed constant withdrawal rate, and a

spillway rating curve, was used to determine the variation of storage, water surface elevation, and spillway flow rate over each simulation.

3.3. Model Grid and Alternative Baffle Configurations

The 3D model used a grid of 50-meter (164-ft) squares to represent the water surface of Schoharie Reservoir (Figure 30). A total of 1812 squares were used when the reservoir was at full storage. The model allows for squares located on the shoreline under full reservoir to be "trimmed" to a triangular shape to better represent the irregular shoreline shape. During simulations, the model allows for "wetting" and "drying" of individual squares in the grid to reflect the changing water surface elevation.

The boundary between any two adjacent squares is a 50-m line oriented in either the north-south or east-west direction. A particular baffle configuration or alignment is made up of a series of such lines connected end-to-end. For all such lines between adjacent squares that are designated in model input to be part of a baffle, the model assumes that the movement of water and particles is completely blocked over the entire 50-meter length and over the entire depth of the water column.

The maximum baffle length considered here is about 1500 feet (460 m). Six baffle configurations which meet this length requirement were analyzed. These configurations were designated numbers 11 through 16 (Table 11; Figure 31). The baffle configurations were made up of either 50-m lengths along the sides of two adjacent squares, or a 70-meter length across the diagonal of an individual square. A selected 1000-foot baffle configuration is illustrated in Figure 32, that corresponds to Baffle No. 12 of Table 11.

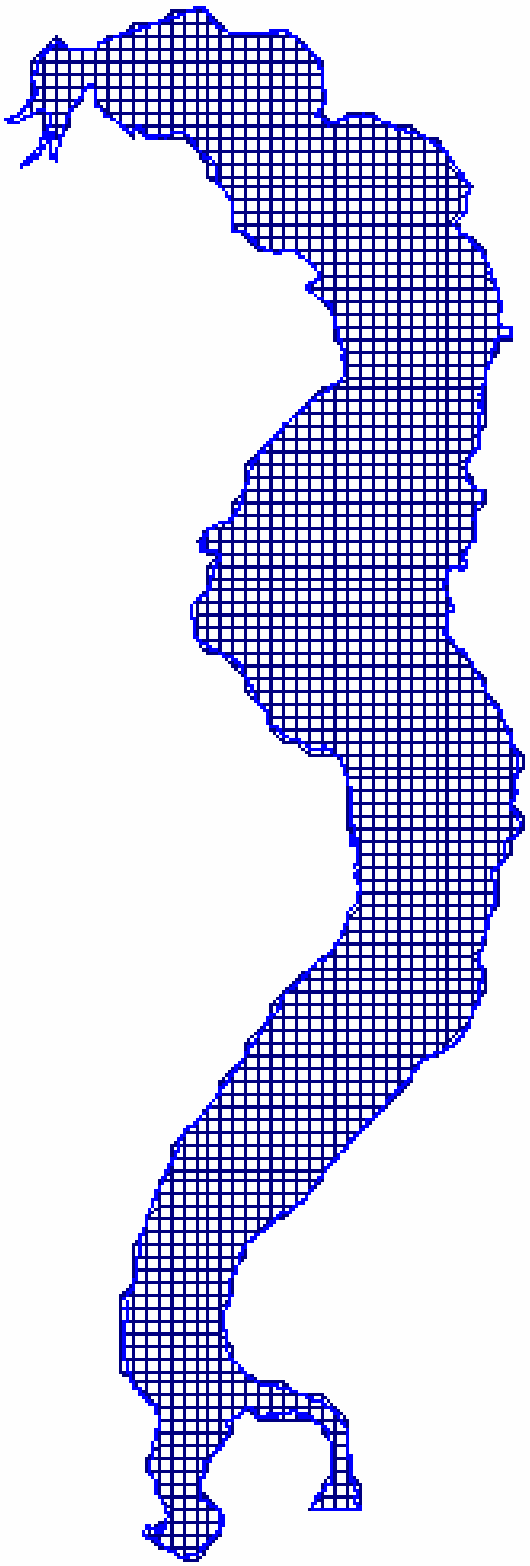

Figure 30. Grid of 50-meter squares used to represent the water surface of Schoharie Reservoir at full storage.

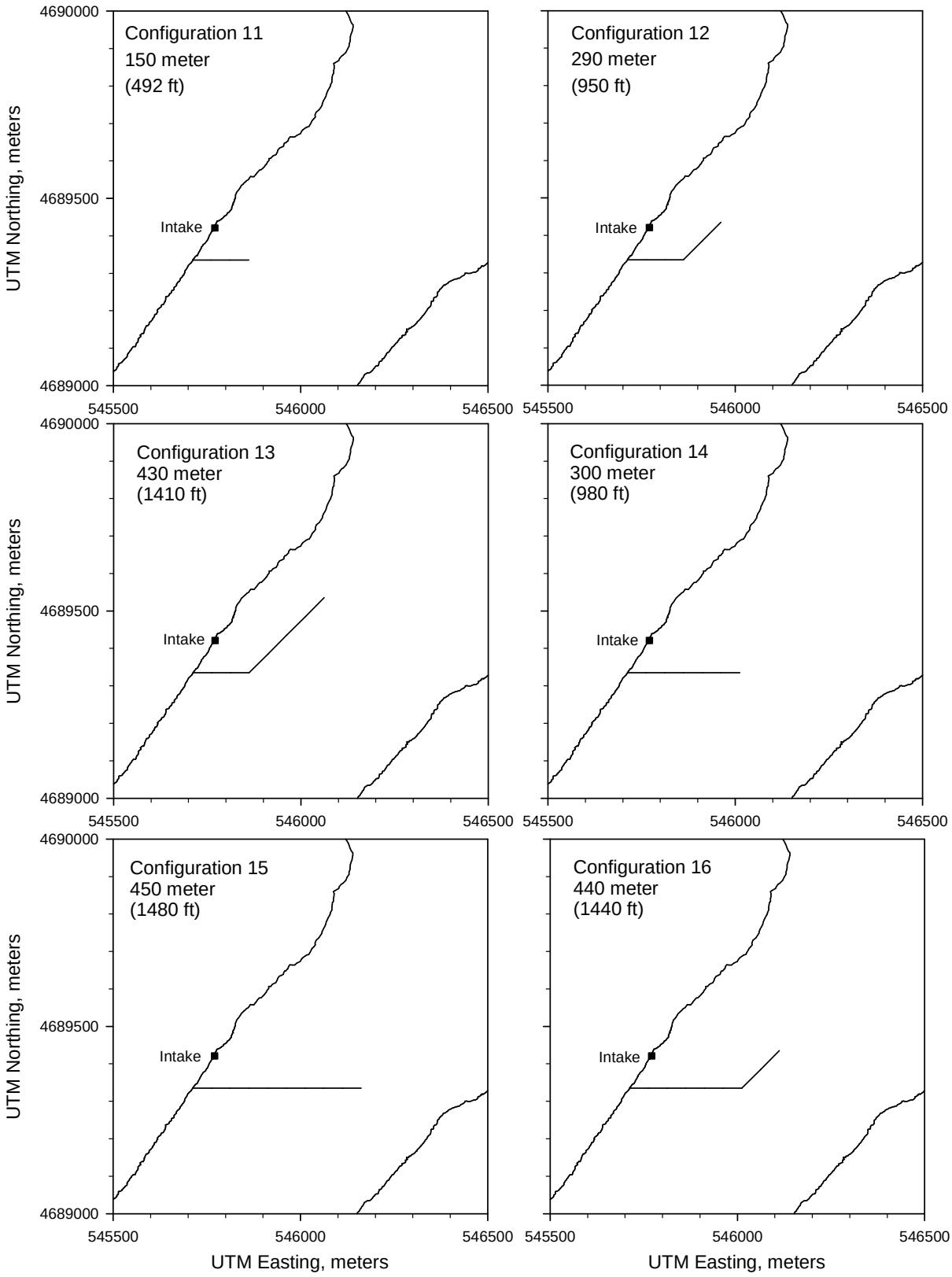

Figure 31. The six baffle configurations, numbered 11 through 16.

Table 11. Geometric properties of the six baffle configurations.

Baffle Number	Straight (S), Diagonal (D) Elements	Length, ft (m)	Surface Area, ft^2 (m^2)	Average Depth, ft (m)
11	3 S	490 (150)	25100 (2340)	51 (15.6)
12	3 S, 2 D	950 (290)	52600 (4890)	55 (16.9)
13	3 S, 4 D	1410 (430)	80200 (7450)	57 (17.3)
14	6 S	980 (300)	52300 (4860)	53 (16.2)
15	9 S	1480 (450)	79000 (7340)	53 (16.3)
16	6 S, 2 D	1440 (440)	77400 (7194)	53 (16.3)

3.4. Simulations and Results

Model runs were made for all combinations of model inputs. These include 6 runoff events, 7 baffle configurations (1 being no baffle), and 2 withdrawal flow rates, for a total of 84 model runs. These runs were arbitrarily assigned a "run number" in the range of 400 to 483. The duration of the simulation for each event (Table 9) was sufficiently long so that streamflow and the predicted turbidity at the intake structure returned to background or pre-storm levels.

The results of these simulations are shown in Figures 33 through 44. Each of these figures displays the Schoharie Creek streamflow, reservoir water surface elevation, turbidity of Schoharie Creek inflow, and predicted turbidity of the withdrawal (computed as a 24-hour moving average). In addition, summary statistics of the baffle performance are displayed in Tables 12 through 17. Table 18 specifically gives statistics for Baffle 12, the 1000-foot baffle. Some of these statistics, such as peak turbidity are self-explanatory. "Contaminated water volume" refers to the volume of water withdrawn from the reservoir whose turbidity exceeds 15 NTU. "Particle mass" refers to the total "mass" of particles in the withdrawn water whose turbidity exceeds 15 NTU; because particle mass was simulated as BAC (m^{-1}) and then converted to turbidity (NTU), the units of particle mass are the product of volume (million gallons) and turbidity, or MG-NTU. This statistic is intended to represent the total quantity of particles in "contaminated" (turbidity>15 NTU) water withdrawn from the reservoir during an event. Other summary statistics are the duration of exceedence (time period where the withdrawal turbidity exceeds 15 NTU), time to peak (interval from the start of the storm to the peak turbidity in the withdrawal), and time to turbidity (Tn) goal (interval from the start of the storm to when the withdrawal turbidity first exceeds 15 NTU).

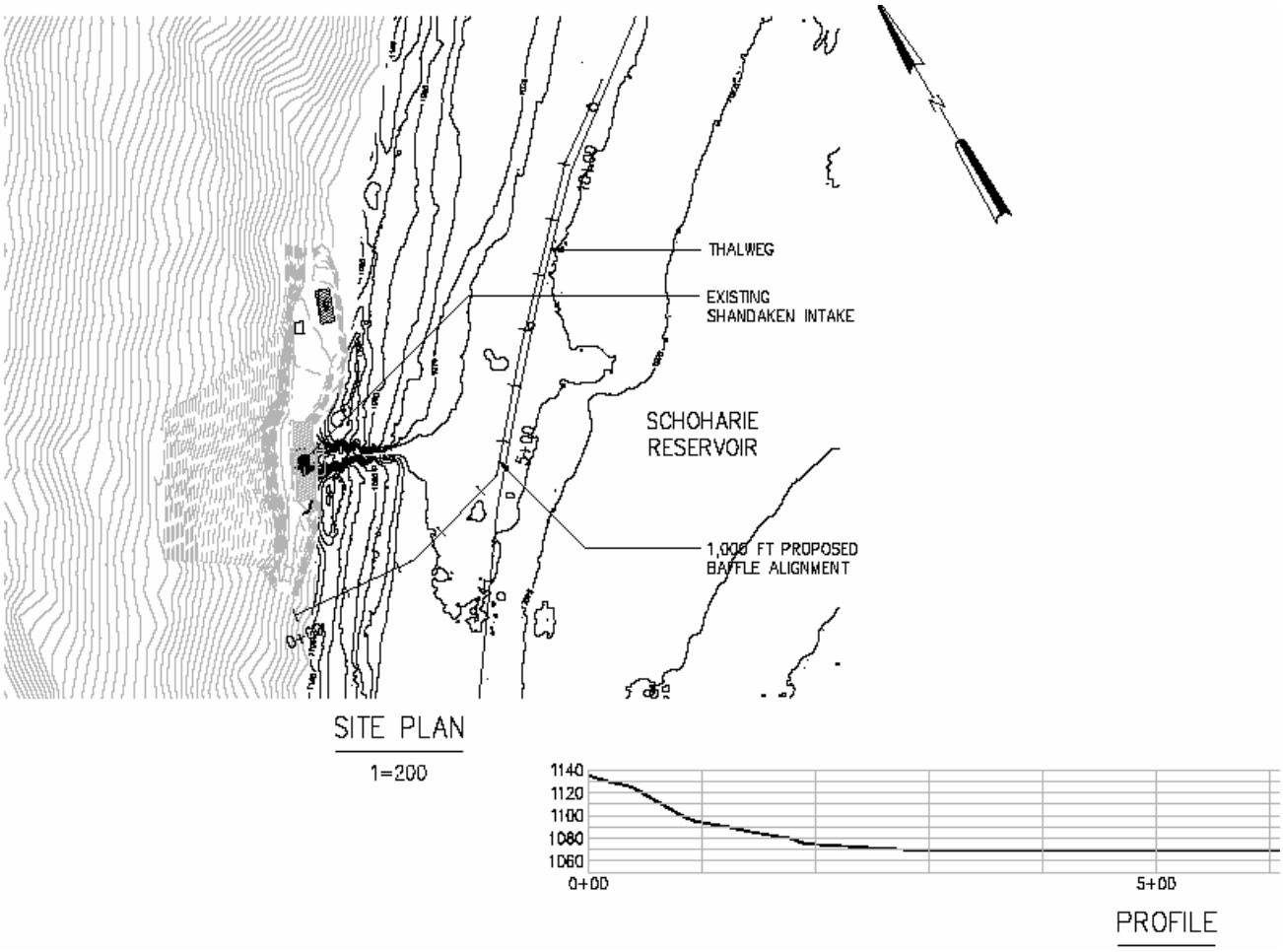

Figure 32. Baffle configuration received from Hazen & Sawyer in June 2006.

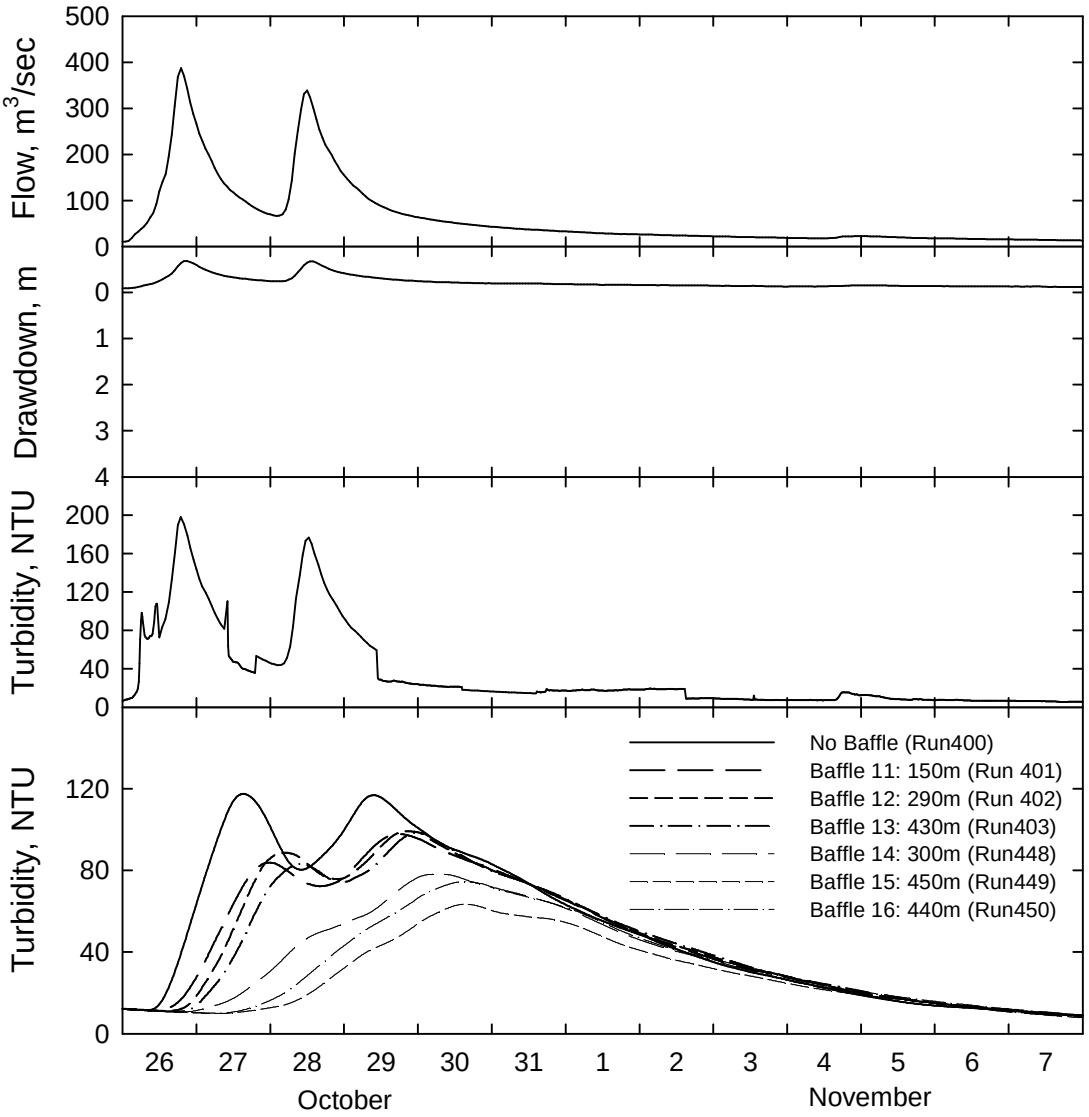

Figure 33. Predictions for Event 1, 26 October – 7 November 2003, withdrawal rate 300 MGD: Schoharie Creek streamflow, Schoharie Reservoir drawdown below spillway crest, Schoharie Creek turbidity, and withdrawal turbidity for various baffle configurations.

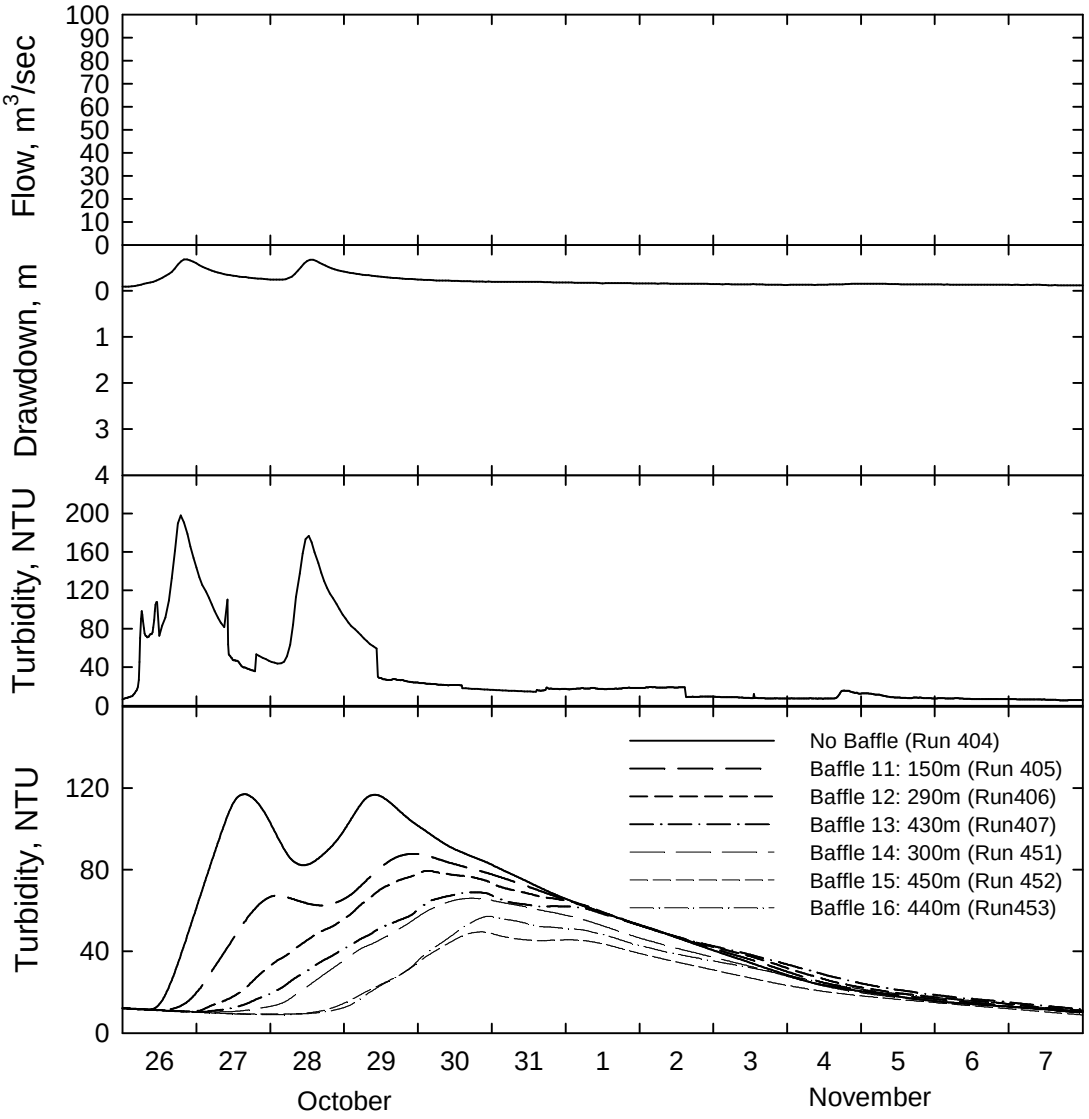

Figure 34. Predictions for Event 1, 26 October – 7 November 2003, withdrawal rate 80 MGD: Schoharie Creek streamflow, Schoharie Reservoir drawdown below spillway crest, Schoharie Creek turbidity, and withdrawal turbidity for various baffle configurations.

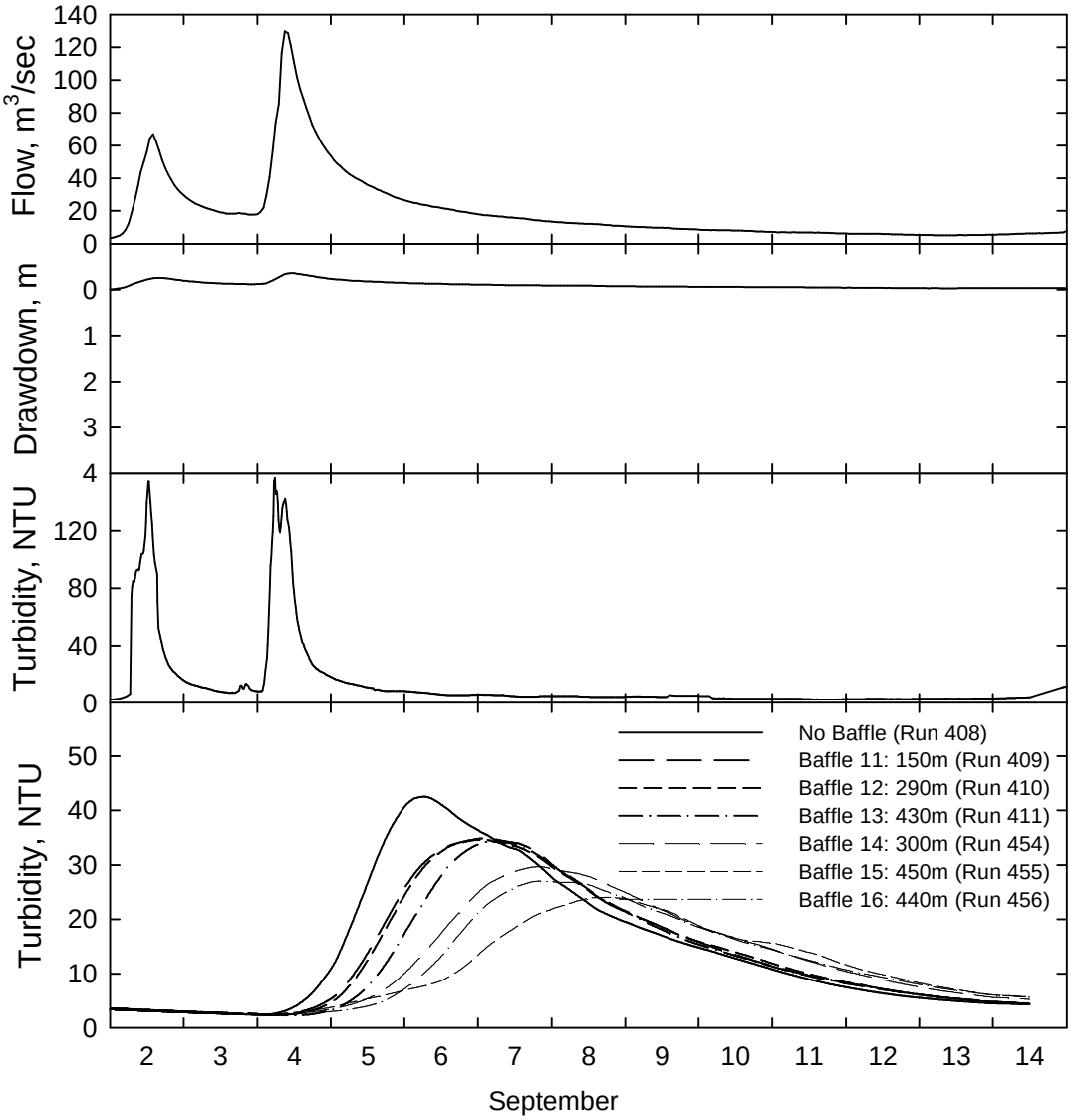

Figure 35. Predictions for Event 2, 2-15 September 2003, withdrawal rate 300 MGD: Schoharie Creek streamflow, Schoharie Reservoir drawdown below spillway crest, Schoharie Creek turbidity, and withdrawal turbidity for various baffle configurations.

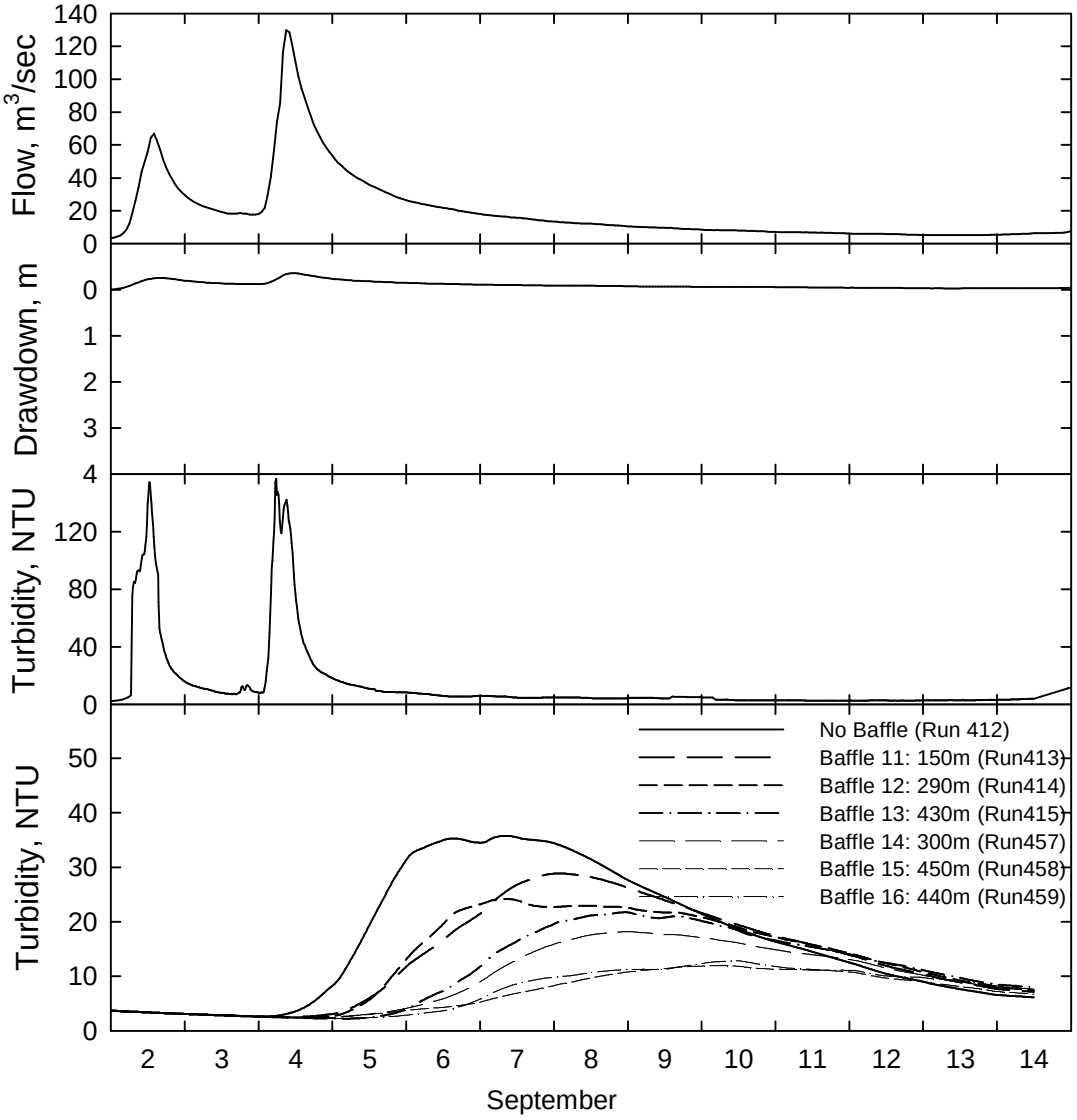

Figure 36. Predictions for Event 2, 2-15 September 2003, withdrawal rate 80 MGD: Schoharie Creek streamflow, Schoharie Reservoir drawdown below spillway crest, Schoharie Creek turbidity, and withdrawal turbidity for various baffle configurations.

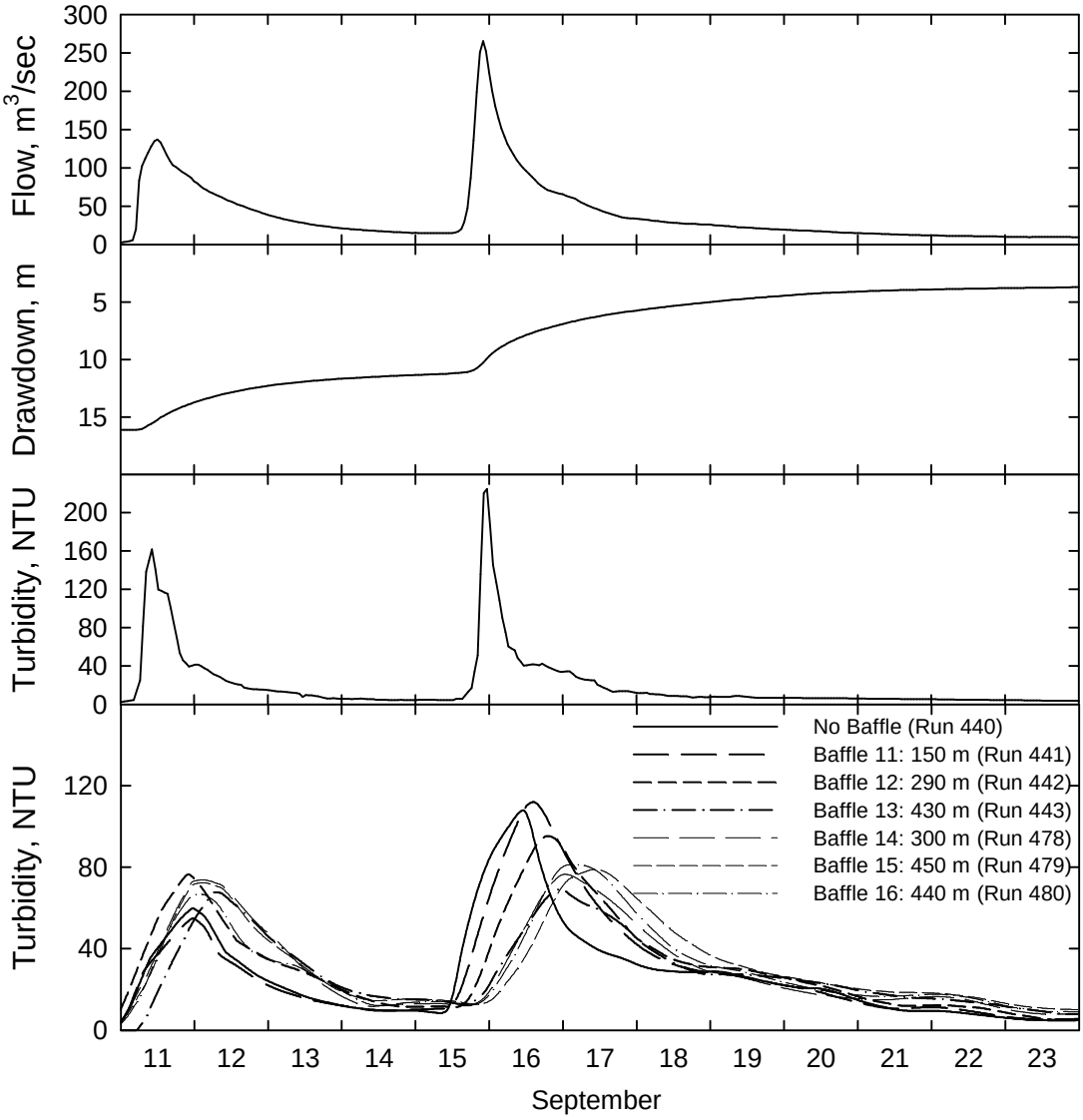

Figure 37. Predictions for Event 3, 11-23 October 2002, withdrawal rate 300 MGD: Schoharie Creek streamflow, Schoharie Reservoir drawdown below spillway crest, Schoharie Creek turbidity, and withdrawal turbidity for various baffle configurations.

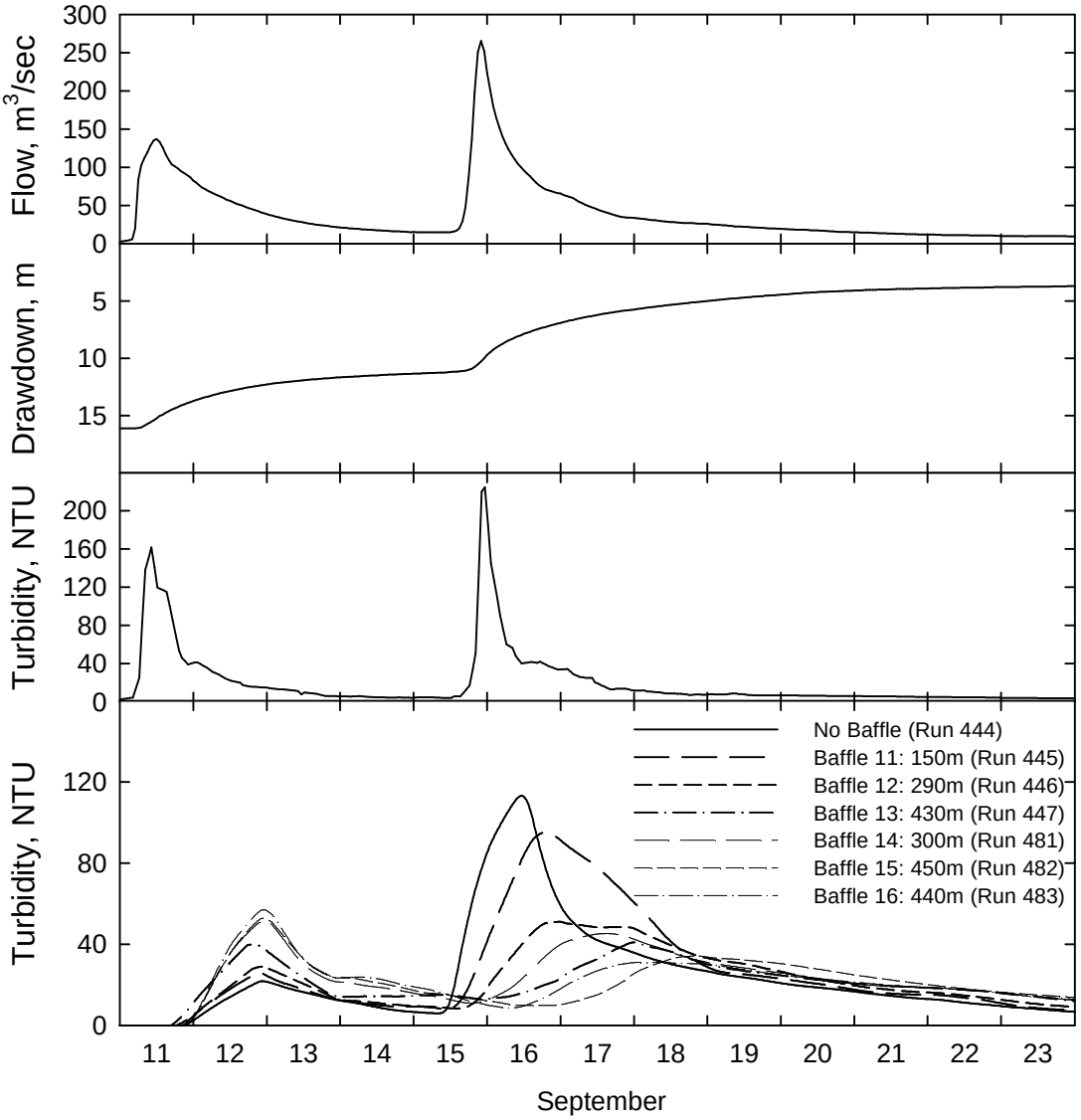

Figure 38. Predictions for Event 3, 11-23 October 2002, withdrawal rate 80 MGD: Schoharie Creek streamflow, Schoharie Reservoir drawdown below spillway crest, Schoharie Creek turbidity, and withdrawal turbidity for various baffle configurations.

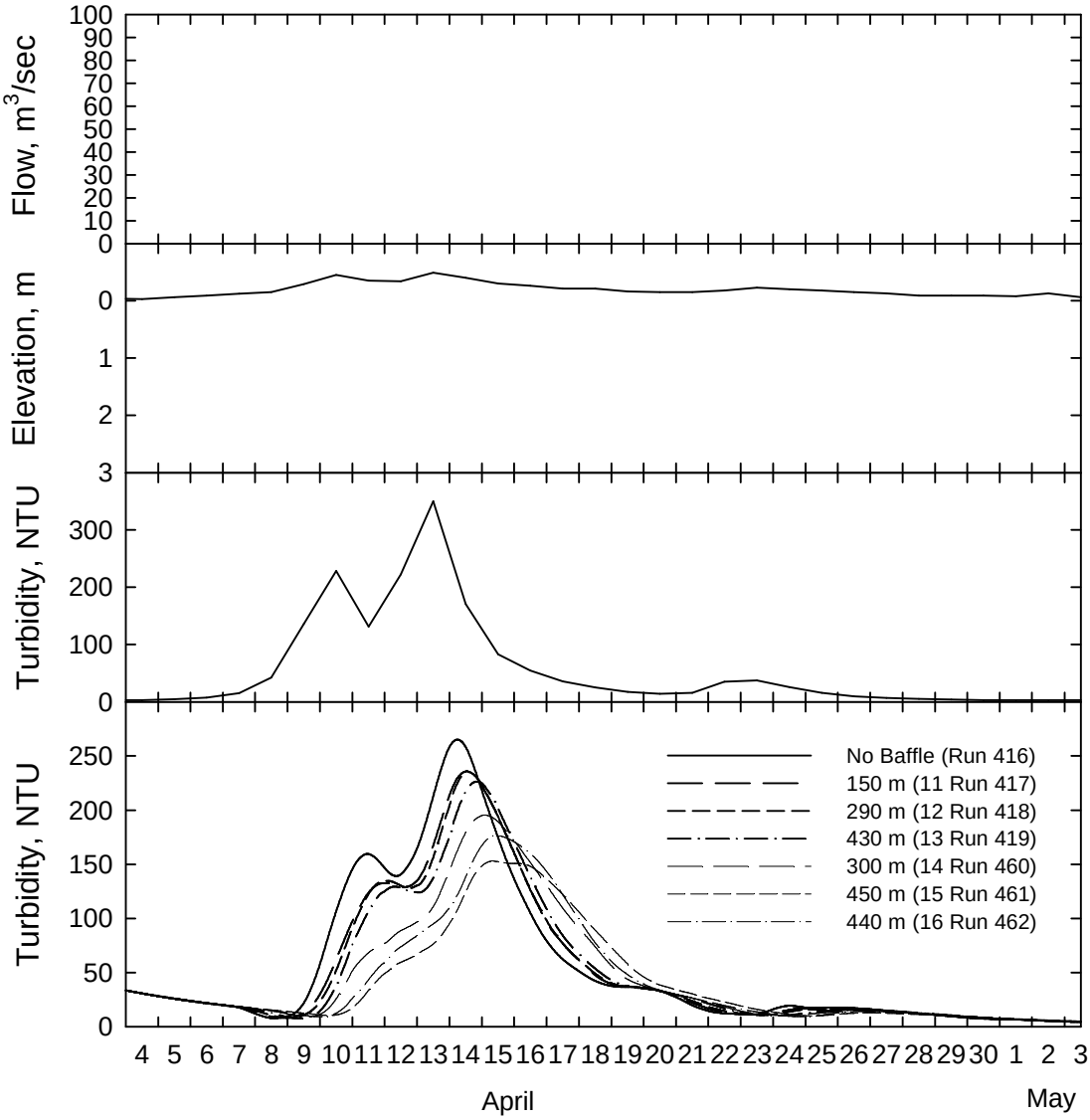

Figure 39. Predictions for Event 4, 4 April – 3 May 2001, withdrawal rate 300 MGD: Schoharie Creek streamflow, Schoharie Reservoir drawdown below spillway crest, Schoharie Creek turbidity, and withdrawal turbidity for various baffle configurations.

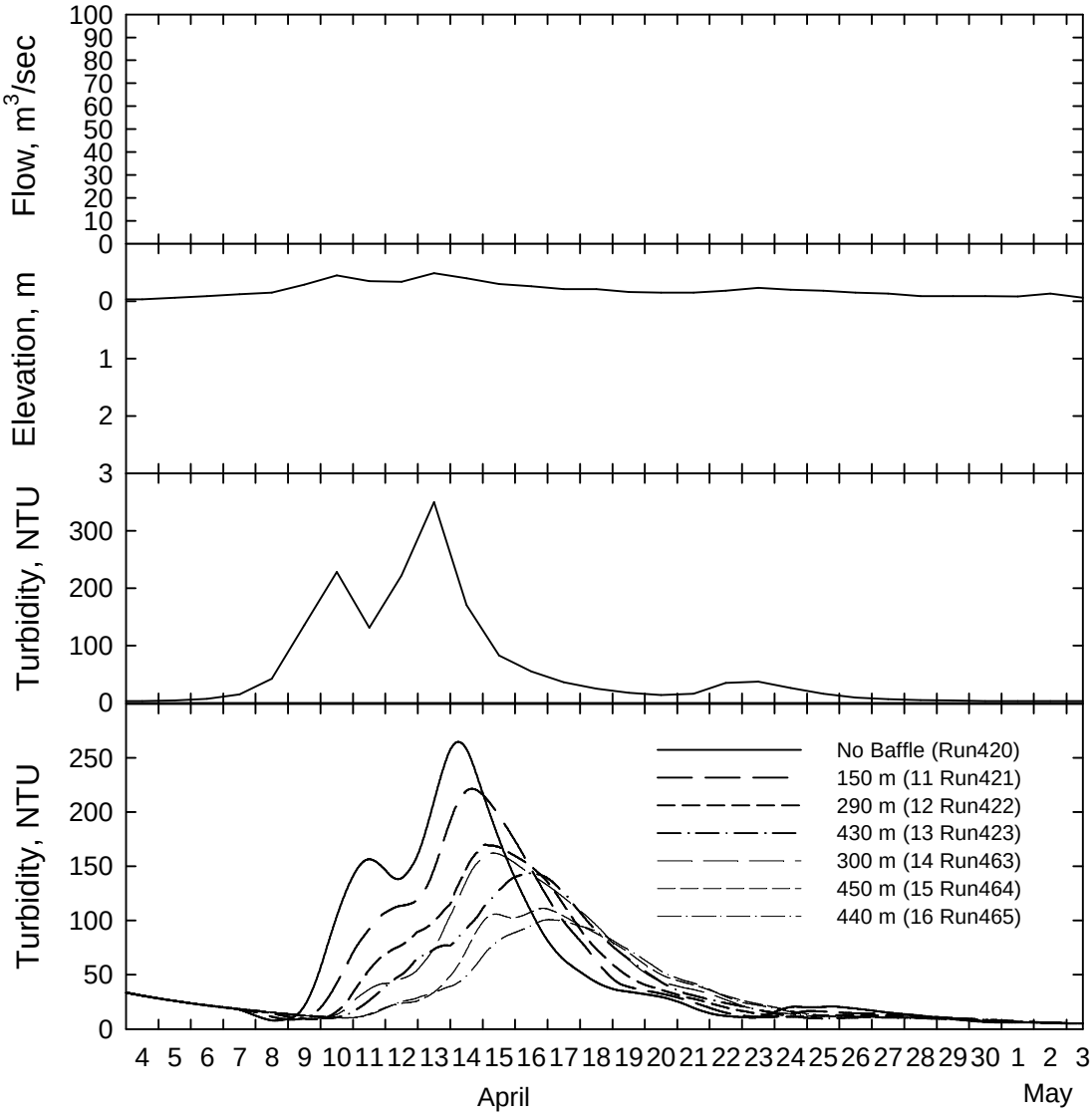

Figure 40. Predictions for Event 4, 4 April – 3 May 2001, withdrawal rate 80 MGD: Schoharie Creek streamflow, Schoharie Reservoir drawdown below spillway crest, Schoharie Creek turbidity, and withdrawal turbidity for various baffle configurations.

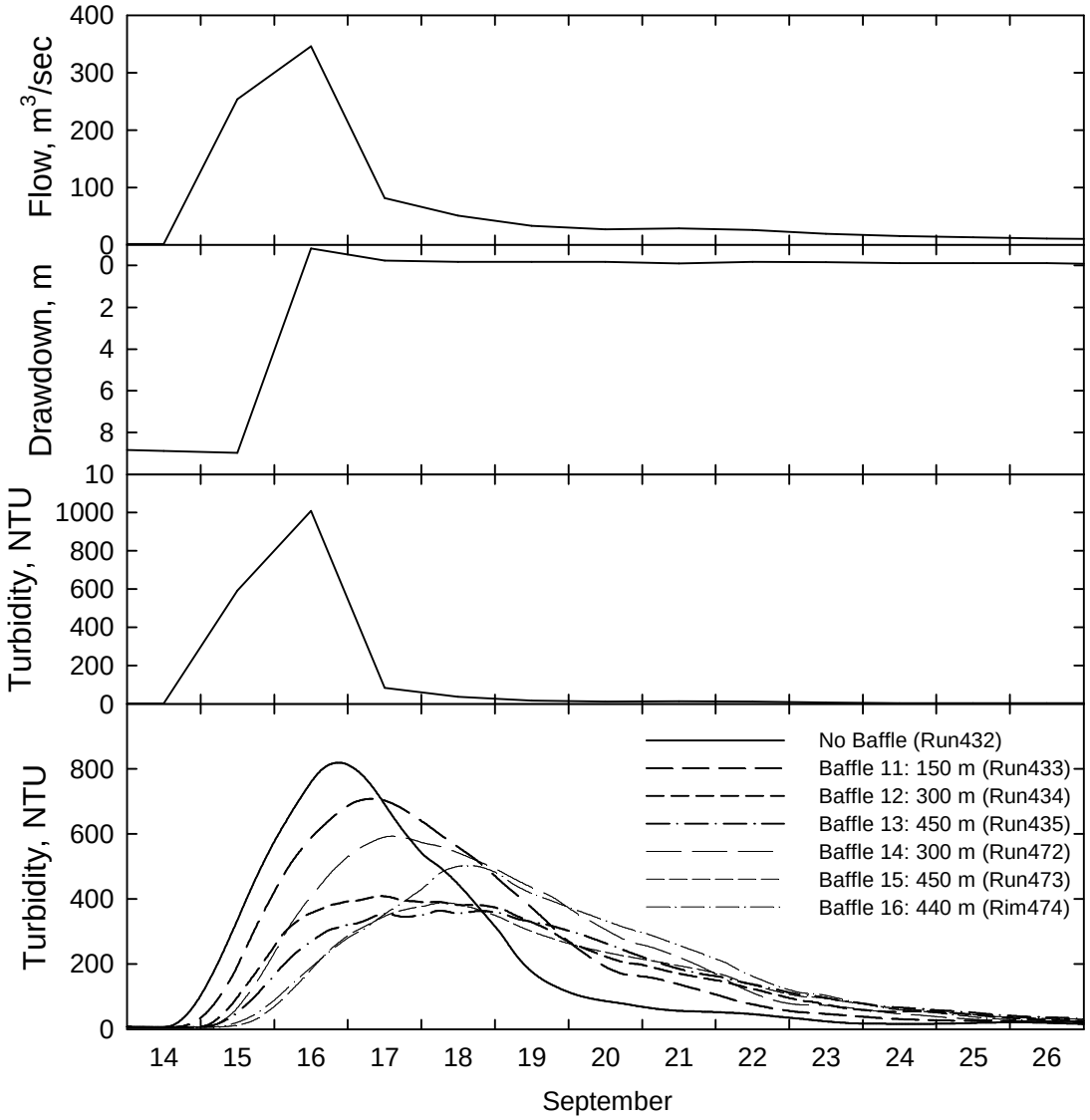

Figure 41. Predictions for Event 5, 14-26 September 1999, withdrawal rate 300 MGD: Schoharie Creek streamflow, Schoharie Reservoir drawdown below spillway crest, Schoharie Creek turbidity, and withdrawal turbidity for various baffle configurations.

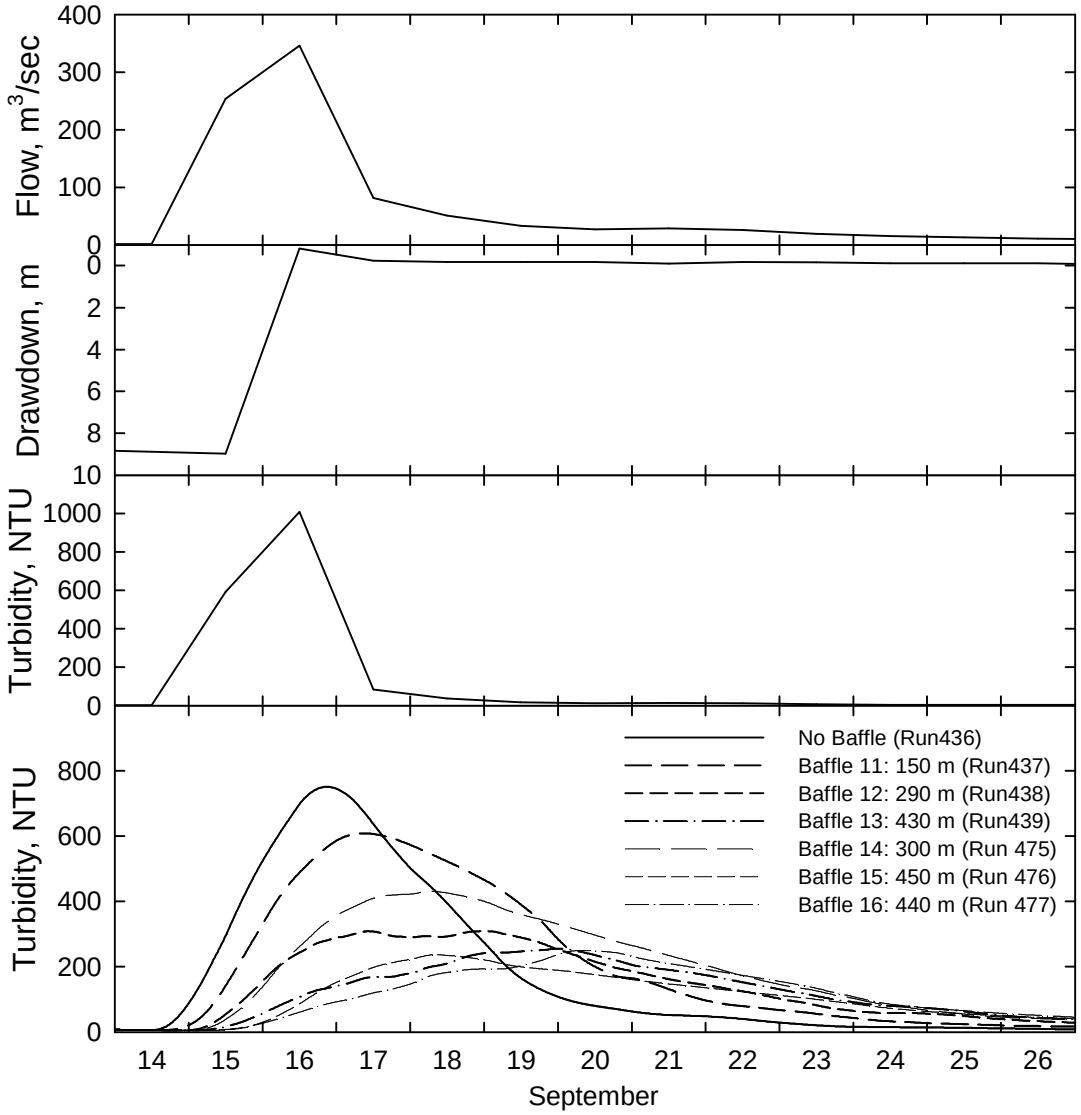

Figure 42. Predictions for Event 5, 14-26 September 1999, withdrawal rate 80 MGD: Schoharie Creek streamflow, Schoharie Reservoir drawdown below spillway crest, Schoharie Creek turbidity, and withdrawal turbidity for various baffle configurations.

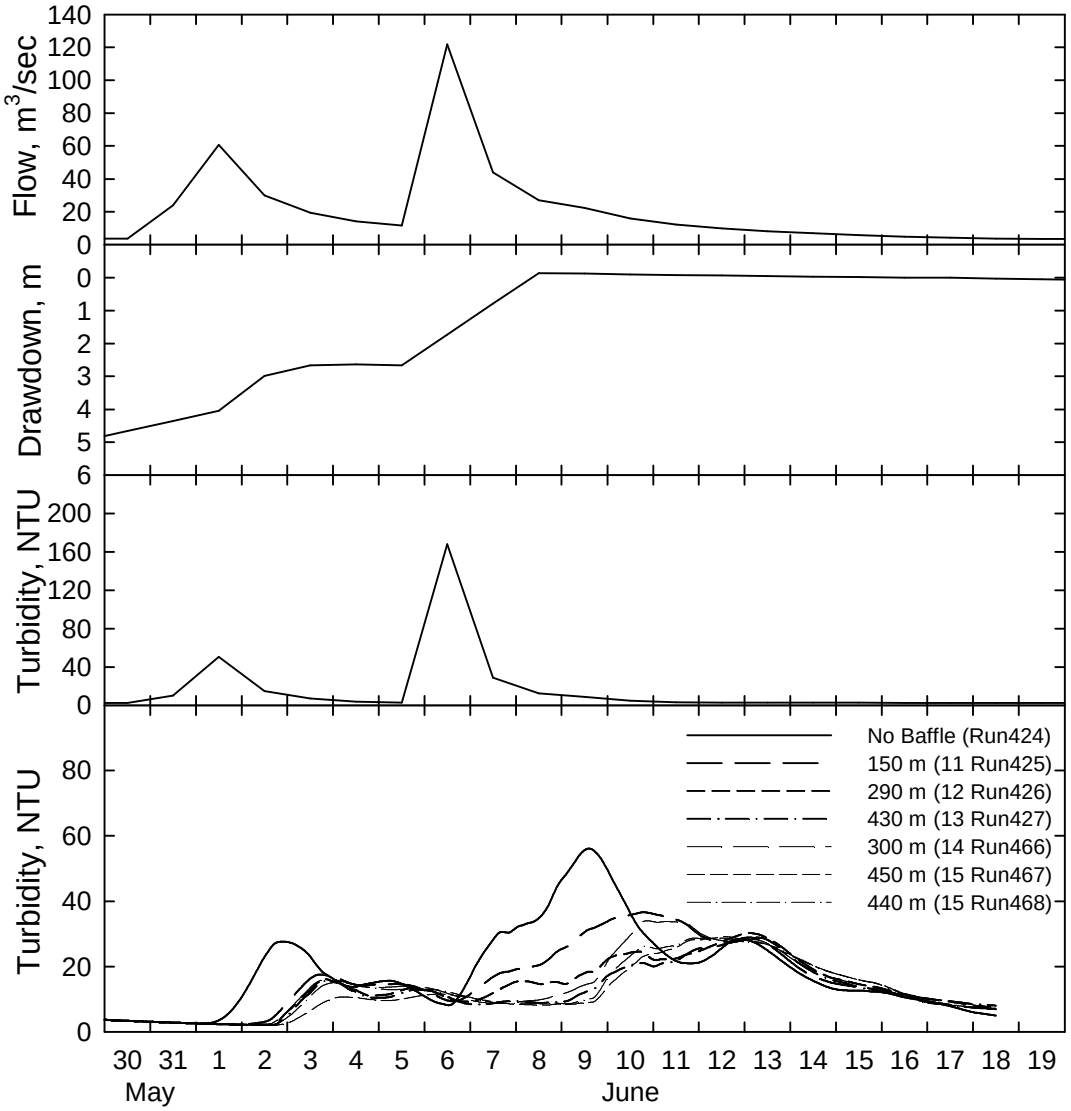

Figure 43. Predictions for Event 6, 30 May– 19 June 1992, withdrawal rate 300 MGD: Schoharie Creek streamflow, Schoharie Reservoir drawdown below spillway crest, Schoharie Creek turbidity, and withdrawal turbidity for various baffle configurations.

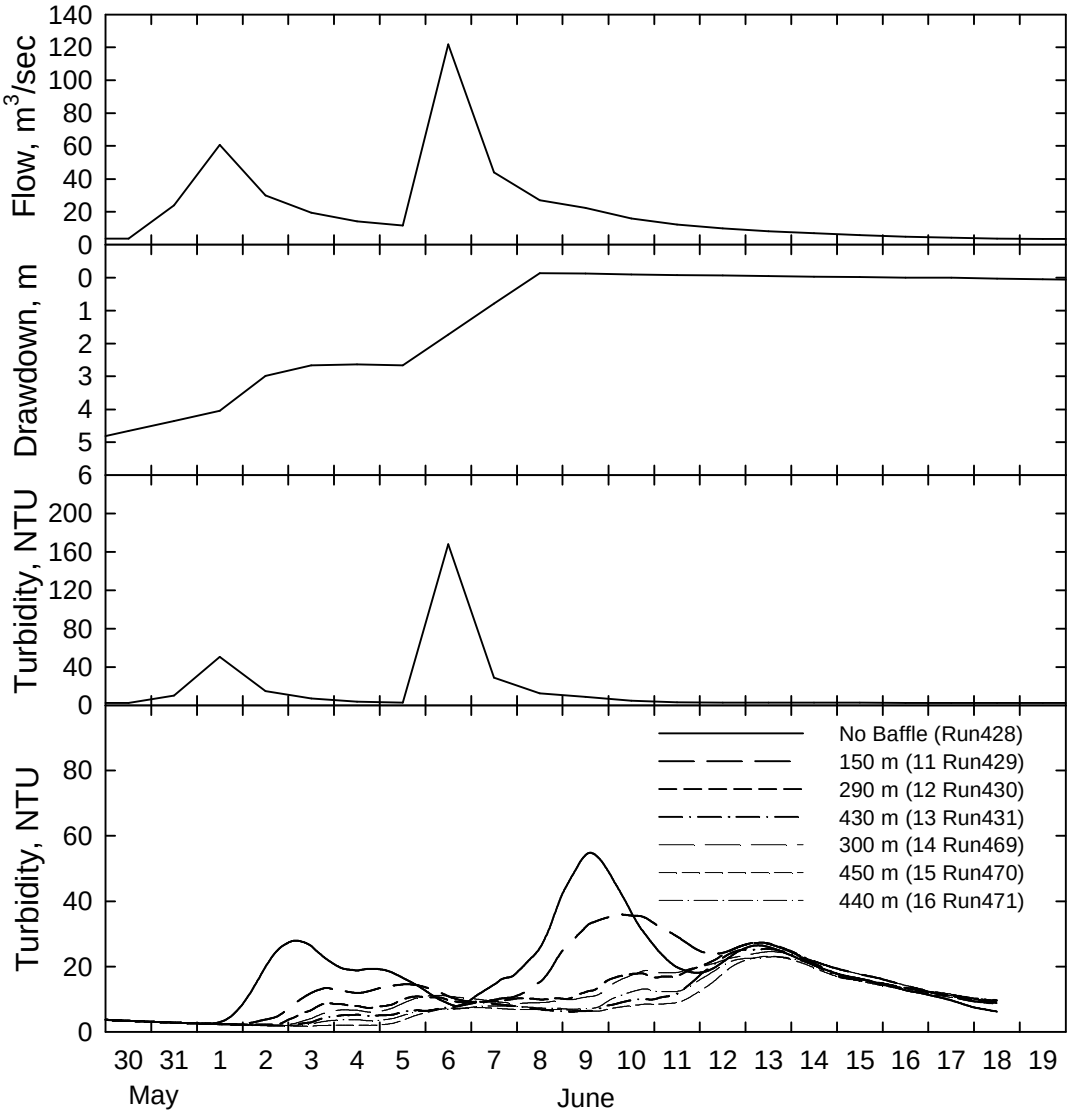

Figure 44. Predictions for Event 6, 30 May– 19 June 1992, withdrawal rate 80 MGD: Schoharie Creek streamflow, Schoharie Reservoir drawdown below spillway crest, Schoharie Creek turbidity, and withdrawal turbidity for various baffle configurations.

Table 12. Summary statistics for Event 1.

Run Number	Baffle	Withdraw MGD	Maximum Turbidity NTU	Reduction Max Turb %	Average Turbidity NTU	Reduction Avg Turb %	Contamin. Water Vol. MG	Reduction Cont. Wat Vol %	Particle Mass MG-NTU	Reduction Part. Mass %
400	No	300	117	-	49	-	3049	-	192886	-
401	11	300	98	17	43	11	3083	-1	170067	12
402	12	300	99	16	43	13	3029	1	166444	14
403	13	300	95	19	41	17	2953	3	155834	19
448	14	300	78	33	34	30	2886	5	128990	33
449	15	300	63	46	28	44	2609	14	98332	49
450	16	300	72	39	31	37	2739	10	113756	41
404	No	80	117	-	51	-	853	-	53315	-
405	11	80	88	25	41	18	850	0	43115	19
406	12	80	76	35	36	29	842	1	37040	31
407	13	80	63	46	31	39	782	8	30590	43
451	14	80	66	44	30	41	726	15	29042	46
452	15	80	49	58	23	54	636	25	20469	62
453	16	80	53	55	24	52	680	20	22424	58

Run Number	Baffle	Withdraw MGD	Period of Violation days	Reduction in Period of Viol. days	Time to Peak Hours	Increase Time to Peak %	Time to Tn Limit Hours	Increase Time to Tn Lim %
400	No	300	10.2	-	41.2	-	14.3	-
401	11	300	10.3	-0.1	91.6	122	19.9	39
402	12	300	10.1	0.1	96.9	135	24.9	75
403	13	300	9.8	0.3	99.9	142	30.5	114
448	14	300	9.6	0.5	105.2	155	34.8	144
449	15	300	8.7	1.5	113.2	175	56.7	297
450	16	300	9.1	1.0	112.7	173	52.1	266
404	No	80	10.7	-	41.7	-	14.5	-
405	11	80	10.6	0.0	96.4	131	22.8	57
406	12	80	10.5	0.1	102.3	145	34.5	138
407	13	80	9.8	0.9	120.1	188	57.5	296
451	14	80	9.1	1.6	115.3	176	54.5	275
452	15	80	8.0	2.7	118.5	184	74.5	413
453	16	80	8.5	2.2	120.9	190	79.3	446

Table 13. Summary statistics for Event 2.

Run Number	Baffle	Withdraw MGD	Maximum Turbidity NTU	Reduction Max Turb %	Average Turbidity NTU	Reduction Avg Turb %	Contamin. Water Vol. MG	Reduction Cont Wat Vol %	Particle Mass MG-NTU	Reduction Part. Mass %
408	No	300	46.3	-	15.6	-	1,543	-	46236	-
409	11	300	37.9	18	14.4	8	1,473	5	40886	12
410	12	300	37.9	18	13.8	12	1,406	9	38420	17
411	13	300	36.4	21	13.1	16	1,340	13	35107	24
454	14	300	29.7	36	12.2	22	1,360	12	31637	32
455	15	300	24.0	48	10.7	32	1,223	21	24428	47
456	16	300	27.1	42	11.5	27	1,270	18	28035	39
412	No	80	35.8	-	16.3	-	483	-	13247	-
413	11	80	28.9	19	13.2	19	429	11	9685	27
414	12	80	23.8	33	11.7	28	387	20	7856	41
415	13	80	20.1	44	10.0	38	319	34	5769	56
457	14	80	18.2	49	9.4	42	250	48	4241	68
458	15	80	12.0	67	6.9	57	0	100	0	100
459	16	80	12.9	64	7.3	55	0	100	0	100

Run Number	Baffle	Withdraw MGD	Period of Violation days	Reduction in Period of Viol. days	Time to Peak Hours	Increase Time to Peak %	Time to Tn Limit Hours	Increase Time to Tn Lim %
408	No	300	5.1	-	103.4	-	75.9	-
409	11	300	4.9	0.2	123.7	20	85.3	12
410	12	300	4.7	0.5	123.9	20	89.8	18
411	13	300	4.5	0.7	132.7	28	97.3	28
454	14	300	4.5	0.6	141.0	36	105.5	39
455	15	300	4.1	1.1	163.1	58	124.2	64
456	16	300	4.2	0.9	141.5	37	111.7	47
412	No	80	6.0	-	129.3	-	81.0	-
413	11	80	5.4	0.7	146.6	13	105.0	30
414	12	80	4.8	1.2	157.3	22	119.9	48
415	13	80	4.0	2.1	186.3	44	139.9	73
457	14	80	3.1	2.9	169.0	31	140.7	74
458	15	80	0.0	6.0	196.2	52	-	-
459	16	80	0.0	6.0	203.7	58	-	-

Table 14. Summary statistics for Event 3.

Run Number	Baffle	Withdraw MGD	Maximum Turbidity NTU	Reduction Max Turb %	Average Turbidity NTU	Reduction Avg Turb %	Contamin. Water Vol. MG	Reduction Cont. Wat Vol %	Particle Mass MG-NTU	Reduction Part. Mass %
440	No	300	107.9	-	28.3	-	1653	-	69560	-
441	11	300	111.9	-4	31.0	-10	1596	3	75408	-8
442	12	300	95.3	12	29.8	-5	1636	1	71584	-3
443	13	300	69.2	36	26.7	6	1920	-16	64503	7
478	14	300	76.5	29	27.1	4	1886	-14	65455	6
479	15	300	78.9	27	30.2	-7	2013	-22	74410	-7
480	16	300	81.3	25	29.2	-3	2010	-22	72295	-4
444	No	80	113.1	-	30.1	-	472	-	19524	-
445	11	80	94.9	16	32.4	-7	515	-9	21544	-10
446	12	80	51.0	55	25.6	15	519	-10	16472	16
447	13	80	40.9	64	22.0	27	568	-20	13945	29
481	14	80	45.3	60	24.1	20	563	-19	15514	21
482	15	80	34.2	70	20.6	31	490	-4	12121	38
483	16	80	31.0	73	20.2	33	523	-11	12242	37

Run Number	Baffle	Withdraw MGD	Period of Violation days	Reduction in Period of Viol. days	Time to Peak hours	Increase Time to Peak %	Time to Tn Limit hours	Increase Time to Tn Lim %
440	No	300	5.5	-	26.9	-	3.5	-
441	11	300	5.3	0.2	30.4	13	4.8	38
442	12	300	5.5	0.1	34.9	30	8.8	153
443	13	300	6.4	-0.9	39.2	46	12.0	246
478	14	300	6.3	-0.8	40.5	50	13.9	299
479	15	300	6.7	-1.2	50.4	87	17.1	391
480	16	300	6.7	-1.2	43.5	61	14.7	322
444	No	80	5.9	-	27.2	-	4.0	-
445	11	80	6.4	-0.5	34.7	27	8.3	106
446	12	80	6.5	-0.6	39.7	46	14.7	266
447	13	80	7.1	-1.2	63.7	134	0.0	-100
481	14	80	7.0	-1.1	54.9	102	19.7	393
482	15	80	6.1	-0.2	84.0	209	0.0	-100
483	16	80	6.5	-0.6	72.5	167	0.0	-100

Table 15. Summary statistics for Event 4.

Run Number	Baffle	Withdraw MGD	Maximum Turbidity NTU	Reduction Max Turb %	Average Turbidity NTU	Reduction Avg Turb %	Contamin. Water Vol. MG	Reduction Cont. Wat Vol %	Particle Mass MG-NTU	Reduction Part. Mass %
416	No	300	265		61	-	4855	-	429048	-
417	11	300	236	11	56	7	4679	4	393316	8
418	12	300	230	13	55	10	4316	11	375700	12
419	13	300	222	16	53	13	3996	18	359807	16
460	14	300	195	26	50	18	3816	21	334482	22
461	15	300	153	42	44	28	3839	21	290106	32
462	16	300	177	33	46	24	3772	22	306813	28
420	No	80	265	-	60	-	1297	-	113942	-
421	11	80	222	16	55	10	1128	13	99938	12
422	12	80	170	36	46	23	1027	21	82586	28
423	13	80	144	46	41	32	1035	20	72658	36
463	14	80	162	39	45	25	1083	17	80941	29
464	15	80	111	58	36	41	1055	19	61663	46
465	16	80	101	62	33	45	1034	20	56755	50

Run Number	Baffle	Withdraw MGD	Period of Violation days	Reduction in Period of Viol. days	Time to Peak hours	Increase Time to Peak %	Time to Tn Limit hours	Increase Time to Tn Lim %
416	No	300	16.2	-	135.5	-	17.3	-
417	11	300	15.6	0.6	142.4	5	24.3	40
418	12	300	14.4	1.8	147.2	9	31.5	82
419	13	300	13.3	2.9	153.1	13	37.1	114
460	14	300	12.7	3.5	155.7	15	38.4	122
461	15	300	12.8	3.4	161.3	19	54.9	217
462	16	300	12.6	3.6	164.0	21	49.1	183
420	No	80	16.2	-	135.5	-	17.9	-
421	11	80	14.1	2.1	145.6	7	29.6	66
422	12	80	12.8	3.4	155.5	15	44.5	149
423	13	80	12.9	3.3	188.5	39	56.3	215
463	14	80	13.5	2.7	161.1	19	48.3	170
464	15	80	13.2	3.0	198.1	46	72.3	304
465	16	80	12.9	3.3	202.4	49	74.1	315

Table 16. Summary statistics for Event 5.

Run Number	Baffle	Withdraw MGD	Maximum Turbidity NTU	Reduction Max Turb %	Average Turbidity NTU	Reduction Avg Turb %	Contamin. Water Vol. MG	Reduction Cont. Wat Vol %	Particle Mass MG-NTU	Reduction Part. Mass %
432	No	300	819	-	193	-	3746	-	804939	-
433	11	300	708	14	212	-10	3799	-1	886547	-10
434	12	300	409	50	165	14	3716	1	690704	14
435	13	300	364	56	159	18	3686	2	663363	18
472	14	300	593	28	205	-7	3686	2	858548	-7
473	15	300	388	53	147	24	3582	4	611536	24
474	16	300	503	39	178	8	3629	3	741967	8
436	No	80	816	-	189	-	837	-	208914	-
437	11	80	662	19	210	-11	1007	-20	234236	-12
438	12	80	336	59	150	21	984	-18	167024	20
439	13	80	278	66	128	32	964	-15	142574	32
475	14	80	469	43	196	-4	978	-17	218850	-5
476	15	80	257	69	114	39	939	-12	126905	39
477	16	80	272	67	122	35	941	-12	135386	35

Run Number	Baffle	Withdraw MGD	Period of Violation days	Reduction in Period of Viol. days	Time to Peak Hours	Increase Time to Peak %	Time to Tn Limit Hours	Increase Time to Tn Lim %
432	No	300	12.5	-	81.1	-	27.7	-
433	11	300	12.7	-0.2	92.0	13	32.3	16
434	12	300	12.4	0.1	94.7	17	38.9	40
435	13	300	12.3	0.2	114.1	41	41.3	49
472	14	300	12.3	0.2	98.7	22	41.3	49
473	15	300	11.9	0.5	115.5	42	49.6	79
474	16	300	12.1	0.4	123.2	52	45.9	65
436	No	80	10.5	-	80.8	-	28.3	-
437	11	80	12.6	-2.1	93.1	15	34.1	21
438	12	80	12.3	-1.8	131.7	63	41.1	45
439	13	80	12.1	-1.6	156.5	94	46.9	66
475	14	80	12.2	-1.8	114.7	42	42.7	51
476	15	80	11.7	-1.3	116.3	44	54.4	92
477	16	80	11.8	-1.3	164.8	104	53.9	91

Table 17. Summary statistics for Event 6.

Run Number	Baffle	Withdraw MGD	Maximum Turbidity NTU	Reduction Max Turb %	Average Turbidity NTU	Reduction Avg Turb %	Contaminated Water Volume MG	Reduction Cont. Wat Vol %	Particle Mass MG-NTU	Reduction Part. Mass %
424	No	300	56	-	19	-	3066	-	87078	-
425	11	300	37	35	16	15	2556	17	65596	25
426	12	300	30	46	14	28	2236	27	48598	44
427	13	300	29	49	13	35	1713	44	37712	57
466	14	300	34	39	14	27	1906	38	47413	46
467	15	300	29	48	12	36	1723	44	39997	54
468	16	300	29	49	13	32	1856	39	43118	50
428	No	80	55	-	19	-	938	-	23835	-
429	11	80	36	34	16	16	625	33	16053	33
430	12	80	27	50	12	37	482	49	9810	59
431	13	80	25	54	10	48	315	66	6606	72
469	14	80	25	55	12	39	491	48	9856	59
470	15	80	23	58	9	54	275	71	5390	77
471	16	80	23	58	10	49	323	65	6404	73

Run Number	Baffle	Withdraw MGD	Period of Violation days	Reduction in Period of Viol. days	Time to Peak Hours	Increase Time to Peak %	Time to Tn Limit Hours	Increase Time to Tn Lim %
424	No	300	9.2	-	242.4	-	65.9	-
425	11	300	7.8	1.4	270.9	12	96.3	46
426	12	300	5.7	3.5	326.7	35	235.2	257
427	13	300	4.9	4.3	330.7	36	250.7	281
466	14	300	5.2	4.0	273.1	13	246.7	274
467	15	300	5.2	4.0	313.9	29	256.8	290
468	16	300	5.4	3.8	303.7	25	252.0	283
428	No	80	11.0	-	242.4	-	68.5	-
429	11	80	7.4	3.6	258.1	6	218.1	218
430	12	80	5.4	5.6	332.5	37	253.9	270
431	13	80	3.3	7.6	334.4	38	298.1	335
469	14	80	5.6	5.4	337.6	39	260.0	279
470	15	80	2.8	8.1	336.0	39	309.3	351
471	16	80	3.5	7.5	339.5	40	301.1	339

Table 18. Summary statistics for Baffle 12, equivalent to the 1000-foot baffle proposed by Hazen & Sawyer in June 2006.

Run Number	Baffle	Withdraw MGD	Maximum Turbidity NTU	Reduction Max Turb %	Average Turbidity NTU	Reduction Avg Turb %	Contamin. Water Vol. MG	Reduction Cont. Wat Vol %	Particle Mass MG-NTU	Reduction Part. Mass %
Event 1										
400	No	300	117	-	49	-	3049	-	192886	-
402	12	300	99	16	43	13	3029	1	166444	14
404	No	80	117	-	51	-	853	-	53315	-
406	12	80	76	35	36	29	842	1	37040	31
Event 2										
408	No	300	46	-	16	-	1543	-	46236	-
410	12	300	38	18	14	12	1406	9	38420	17
412	No	80	36	-	16	-	483	-	13247	-
414	12	80	24	33	12	28	387	20	7856	41
Event 3										
440	No	300	108	-	28	-	1653	-	69560	-
442	12	300	95	12	30	-5	1636	1	71584	-3
444	No	80	113	-	30	-	472	-	19524	-
446	12	80	51	55	26	15	519	-10	16472	16
Event 4										
416	No	300	265		61		4855		429048	
418	12	300	230	13	55	10	4316	11	375700	12
420	No	80	265	-	60	-	1297	-	113942	-
422	12	80	170	36	46	23	1027	21	82586	28
Event 5										
432	No	300	819	-	193	-	3746	-	804939	-
434	12	300	409	50	165	14	3716	1	690704	14
436	No	80	816	-	189	-	837	-	208914	-
438	12	80	336	59	150	21	984	-18	167024	20
Event 6										
424	No	300	56	-	19	-	3066	-	87078	-
426	12	300	30	46	14	28	2236	27	48598	44
428	No	80	55	-	19	-	938	-	23835	-
430	12	80	27	50	12	37	482	49	9810	59

Table 18 (continued). Summary statistics for Baffle 12, equivalent to the 1000-foot baffle proposed by Hazen & Sawyer in June 2006.

Run Number	Baffle	Withdraw MGD	Period of Violation days	Reduction in Period of Viol. days	Time to Peak Hours	Increase Time to Peak %	Time to Tn Limit Hours	Increase Time to Tn Lim %
Event 1								
400	No	300	10.2	-	41.2	-	14.3	-
402	12	300	10.1	0.1	96.9	135	24.9	75
404	No	80	10.7	-	41.7	-	14.5	-
406	12	80	10.5	0.1	102.3	145	34.5	138
Event 2								
408	No	300	5.1	-	103.4	-	75.9	-
410	12	300	4.7	0.5	123.9	20	89.8	18
412	No	80	6.0	-	129.3	-	81.0	-
414	12	80	4.8	1.2	157.3	22	119.9	48
Event 3								
440	No	300	5.5	-	26.9	-	3.5	-
442	12	300	5.5	0.1	34.9	30	8.8	153
444	No	80	5.9	-	27.2	-	4.0	-
446	12	80	6.5	-0.6	39.7	46	14.7	266
Event 4								
416	No	300	16.2	-	135.5	-	17.3	-
418	12	300	14.4	1.8	147.2	9	31.5	82
420	No	80	16.2	-	135.5	-	17.9	-
422	12	80	12.8	3.4	155.5	15	44.5	149
Event 5								
432	No	300	12.5	-	81.1	-	27.7	-
434	12	300	12.4	0.1	94.7	17	38.9	40
436	No	80	10.5	-	80.8	-	28.3	-
438	12	80	12.3	-1.8	131.7	63	41.1	45
Event 6								
424	No	300	10.2	-	242.4	-	64.5	-
426	12	300	7.5	2.8	326.7	35	100.0	55
428	No	80	11.7	-	242.4	-	67.2	-
430	12	80	6.0	5.7	332.5	37	249.9	272

It was found in earlier simulations (not presented here) that baffle performance increases as the baffle length increases up to a length of about 1000 meters (3280 feet), at which point baffle performance begins to level off. For the shorter baffle lengths considered here, significant performance, in terms of reduction of peak turbidity and increased time to peak and time to turbidity limit, is achieved. A difference that is seen with the shorter baffle lengths is that withdrawal rate has a greater impact on baffle performance, with performance reduced at the higher (300 MGD) rate versus the lower rate (80 MGD).

Generally the performance of the baffle appears to be most strongly correlated to the baffle length for the 6 configurations considered here. It appears that Baffle 15 gives the best overall performance of these six for the various conditions considered. However, the shorter Baffle 12 provides significant improvement in turbidity conditions (Table 18).

3.5. Long-term simulation of baffle performance

Practical considerations regarding the application of the 3D model required that a relatively small number of runoff/drawdown conditions be considered; the 6 historical events used are described above. In order to allow a continuous, long-term simulation of the performance of a baffle (as was done in the analysis of a multi-level intake using the 2D model), a simple semi-empirical model was developed. The goal of this "long-term baffle model" is to estimate the effect of a baffle on withdrawal water quality using a simple framework that is less accurate than the 3D model, but is computationally much simpler.

The "long-term baffle model" assumes that a baffle creates a volume of water downstream of, or "behind", the baffle that may have a different (lower) turbidity than the water in the "main body" of the reservoir away from the baffle. If this volume is treated as completely mixed (a CSTR or continuously-stirred tank reactor), then a (particle) mass balance equation for this volume is

$$V\frac{dC_W}{dt} = Q_W\left(C_R - C_W\right) + Q_E\left(C_R - C_W\right) - Av_S C_W \tag{5}$$

where V= the volume of water "behind" the baffle, C_W = concentration (turbidity) of water in this volume, t = time, Q_W =withdrawal flow rate, C_R =concentration (turbidity) of water in the "main body" of the reservoir outside the influence of the baffle, Q_E = an exchange flow between the volume V and the "main body", A = surface area of the volume behind the baffle, v_S= settling velocity of the particles. This model assumes that water leaves the volume at a flow rate Q_W and that water enters the volume from the main body at this same rate. The exchange flow Q_E represents mixing between the volume and the main body associated with wind and water flow, but not associated with the drinking water withdrawal Q_W . This mass balance equation applies strictly to a mass constituent,

but is assumed to apply to the optical properties of BAC or turbidity, as in the 2D and 3D particle/turbidity models.

The assumptions stated above were made in order to formulate this model equation. However, it is not necessary that these assumptions hold. For example, it is not the case that, for this model to be applied successfully, the concentration (turbidity) of water behind the baffle be uniform or completely mixed. These assumptions have been made simply as a basis for formulation of the model. The model is called semi-empirical because it has a mechanistic (mass balance) basis, but requires calibration in that the parameters V, A, and Q_E cannot be independently determined. The accuracy and appropriateness of the model is judged only by its ability to approximate the predictions of the 3D model, as described below.

This model was implemented as follows. The surface area A of the volume behind to baffle and exchange flow Q_E are parameters of the model that are assumed to be constant for any particular baffle configuration. The concentration C_R is the withdrawal concentration without a baffle, while C_W is the concentration with a particular baffle. The settling velocity v_S is the average settling velocity for the 3 particle classes in the 3D and 2D models, and equal to 2.9 meters/day which is the weighted average settling velocity for the 3 classes (weighted by the fraction of tributary loading; Table 10). The volume $V = A\ (17\text{-}D)$, where D is the drawdown in meters. If D exceeds 15 meters, it is assumed that the baffle has no effect so that $C_W = C_R$. The mass balance equation above is integrated numerically using the Crank-Nicolson procedure, which works well for a time step as large as one hour.

The model was calibrated and tested using 3D model predictions with and without a baffle. Two of the six baffle configurations, numbers 12 and 13, were considered. The time series of predicted turbidity without a baffle is C_R , while the constant withdrawal rate used in the 3D model simulations is Q_W . The model equation above is integrated over time to produce a time series of C_W, which is the predicted withdrawal turbidity with the baffle in place. The time series of C_W predicted by this simple model is then compared to the time series of C_W predicted by the 3D model. The values of A and Q_E were adjusted to optimize the agreement between these two predictions. This evaluation was done for the 12 time series of 3D model predictions of C_W for Baffle 12, the six events each at Q_W equal to 80 and 300 MGD. The results shown in Figures 45 through 50 were obtained using A = 50000 m^2 and Q_E =1.0 m^3/sec. Similarly, the results for Baffle 13, obtained using A = 85000 m^2 and Q_E =1.0 m^3/sec are shown in Figures 51 through 56. While the model fits well for some of these conditions, the agreement is only fair for others. This variable performance is to be expected given the simple nature of the model.

Projections or forecasts were made with this simple model as follows. The 2D model was used to predict the time series of turbidity at the existing intake (C_R) for the period 1948 through 2004 for the actual (historical) reservoir operation using the existing intake. The resulting time series of reservoir water surface elevation, C_R , and Q_W were used to predict C_W using this simple "long-term baffle model". These predictions were

performed individually for Baffles 12 and 13. The predicted time series of C_R from the 2D model, and the two time series of C_W, were synthesized to yield Figure 57, in the form of a cumulative frequency distribution, and in Figure 58 in the form of histograms. These results consider only those times when the intake was in operation ($Q_W > 0$).

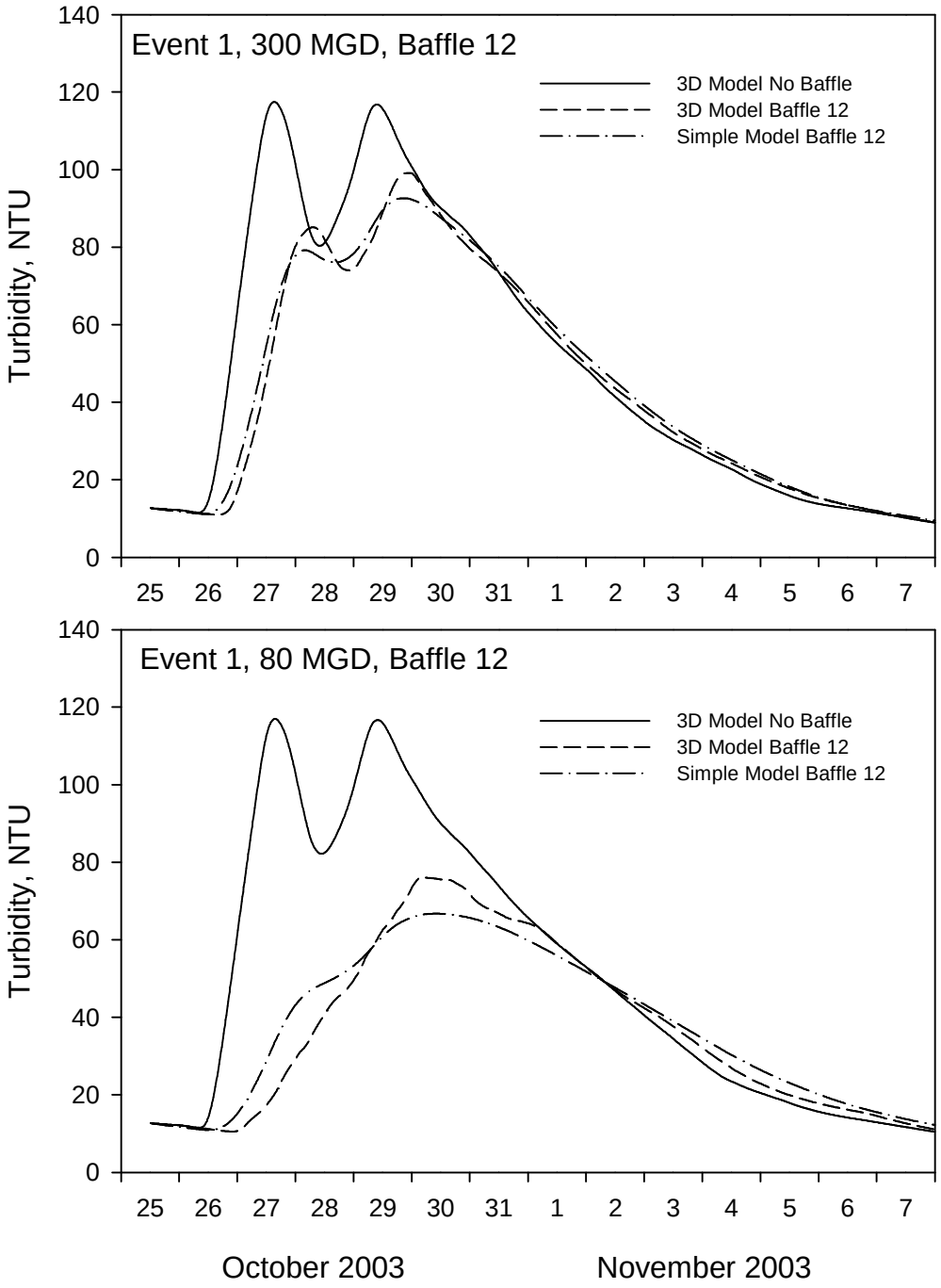

Figure 45. Comparison of simple model prediction with 3D model prediction for Event 1, Baffle 12: (a) 80 MGD, (b) 300 MGD.

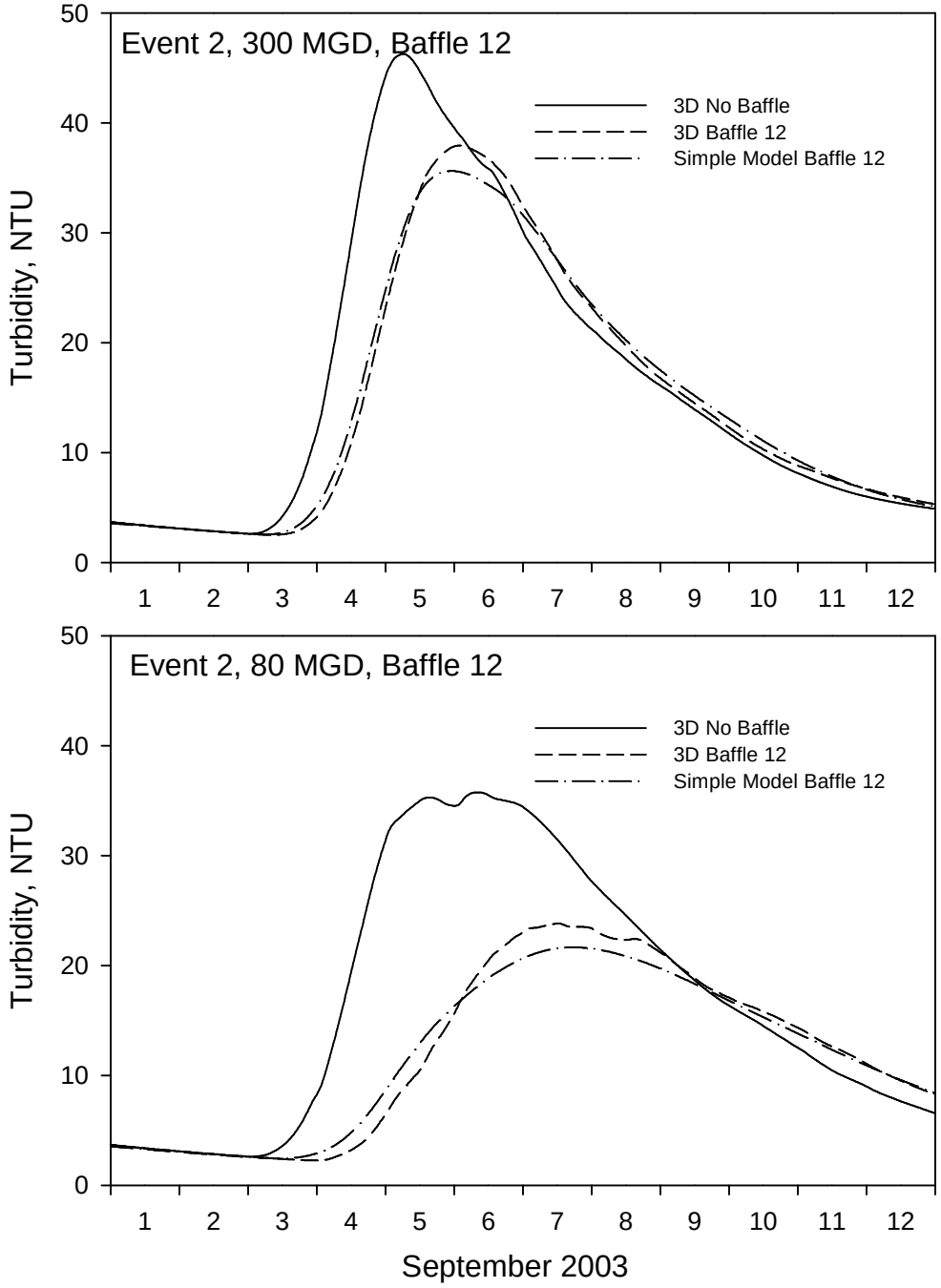

Figure 46. Comparison of simple model prediction with 3D model prediction for Event 2, Baffle 12: (a) 300 MGD, (b) 80 MGD.

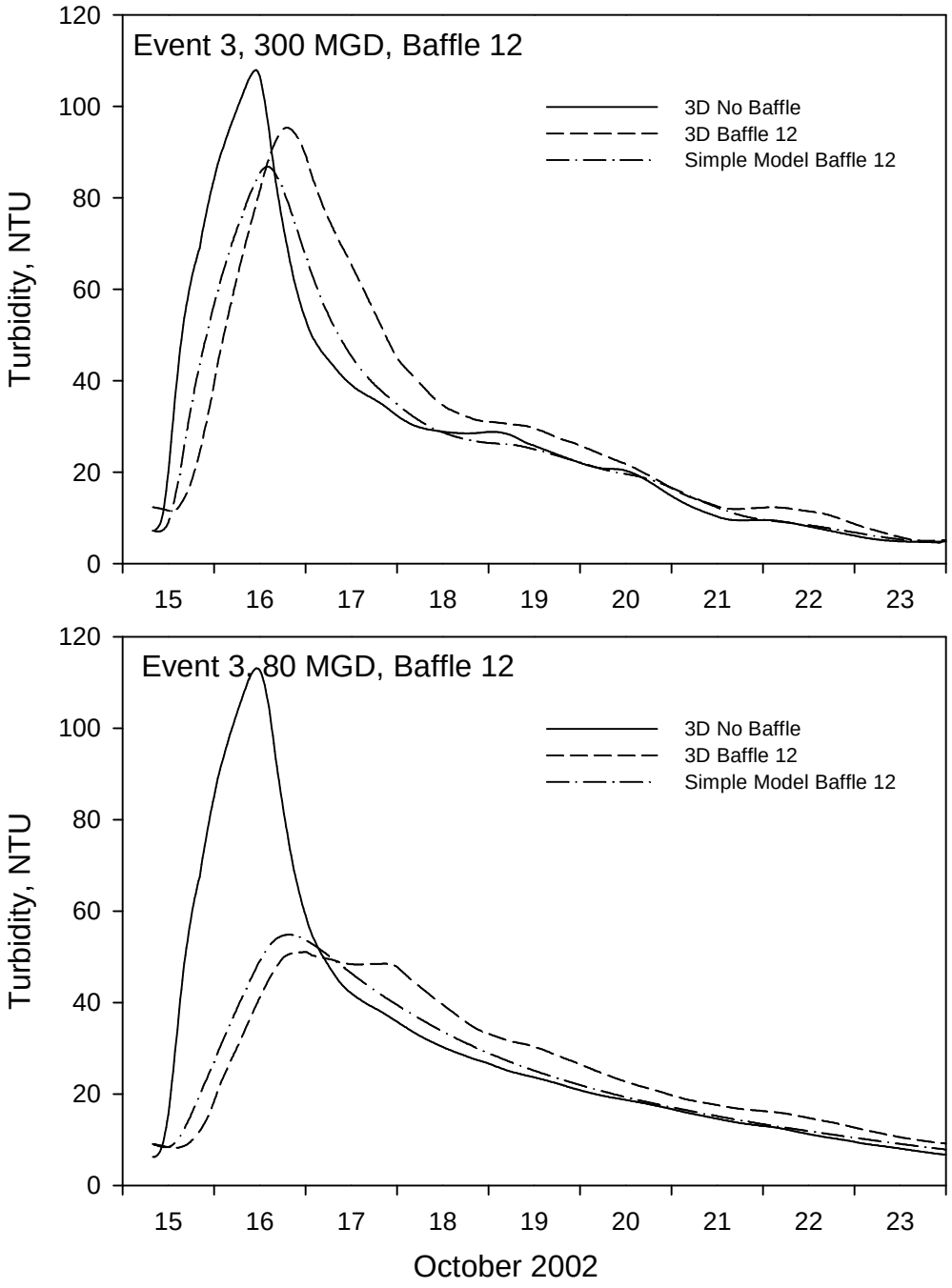

Figure 47. Comparison of simple model prediction with 3D model prediction for Event 3, Baffle 12: (a) 300 MGD, (b) 80 MGD.

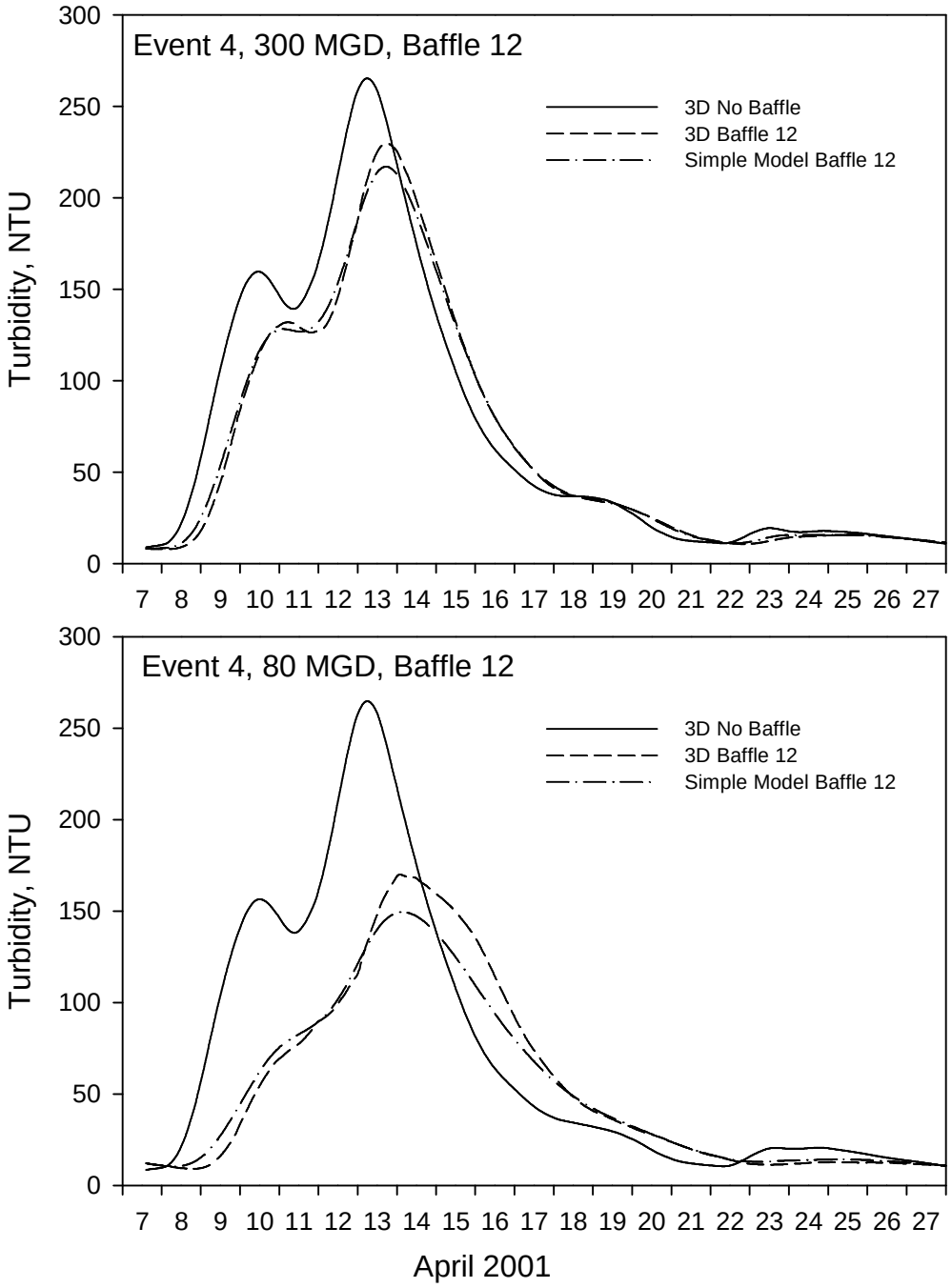

Figure 48. Comparison of simple model prediction with 3D model prediction for Event 4, Baffle 12: (a) 300 MGD, (b) 80 MGD.

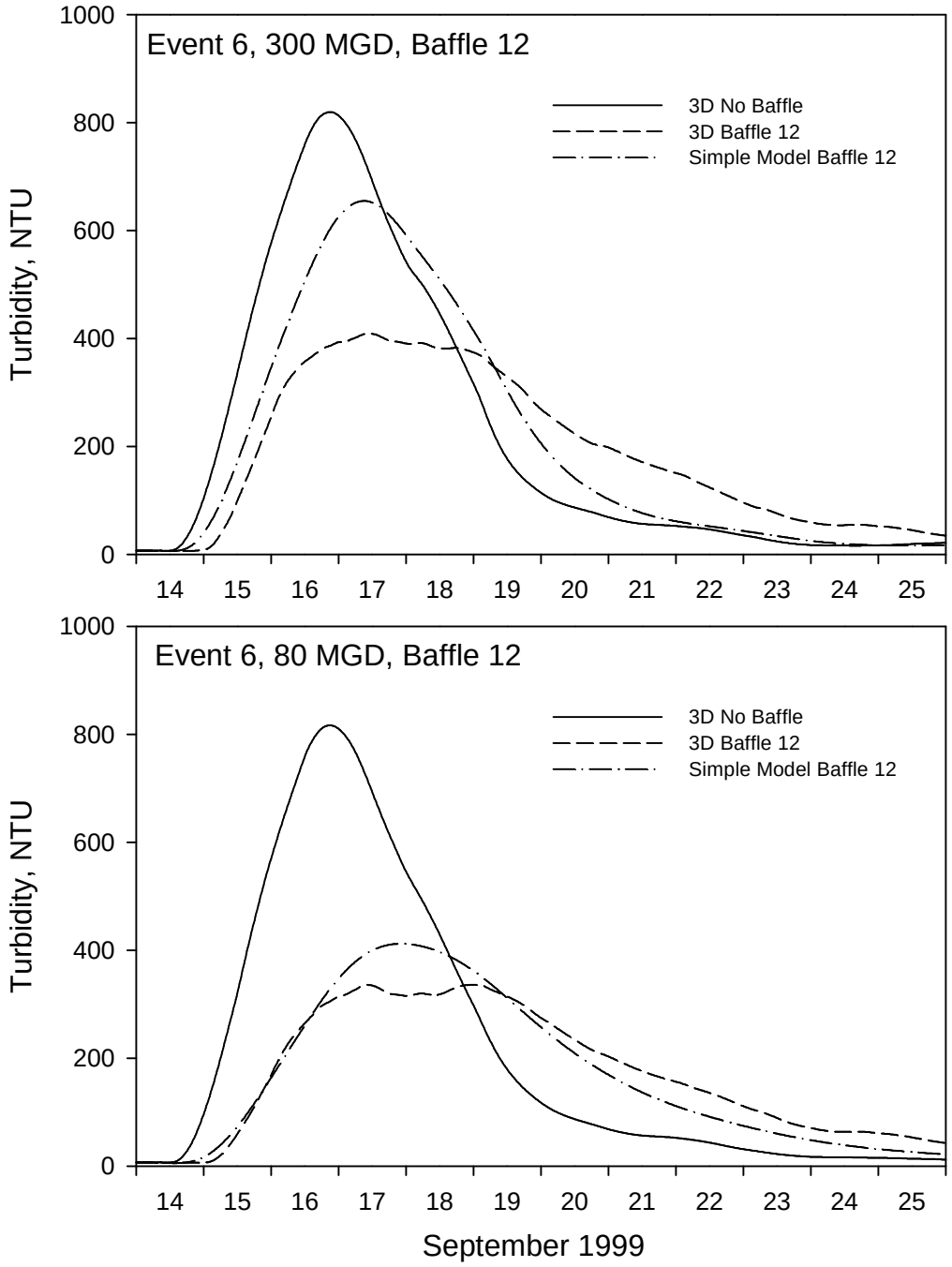

Figure 49. Comparison of simple model prediction with 3D model prediction for Event 5, Baffle 12: (a) 300 MGD, (b) 80 MGD.

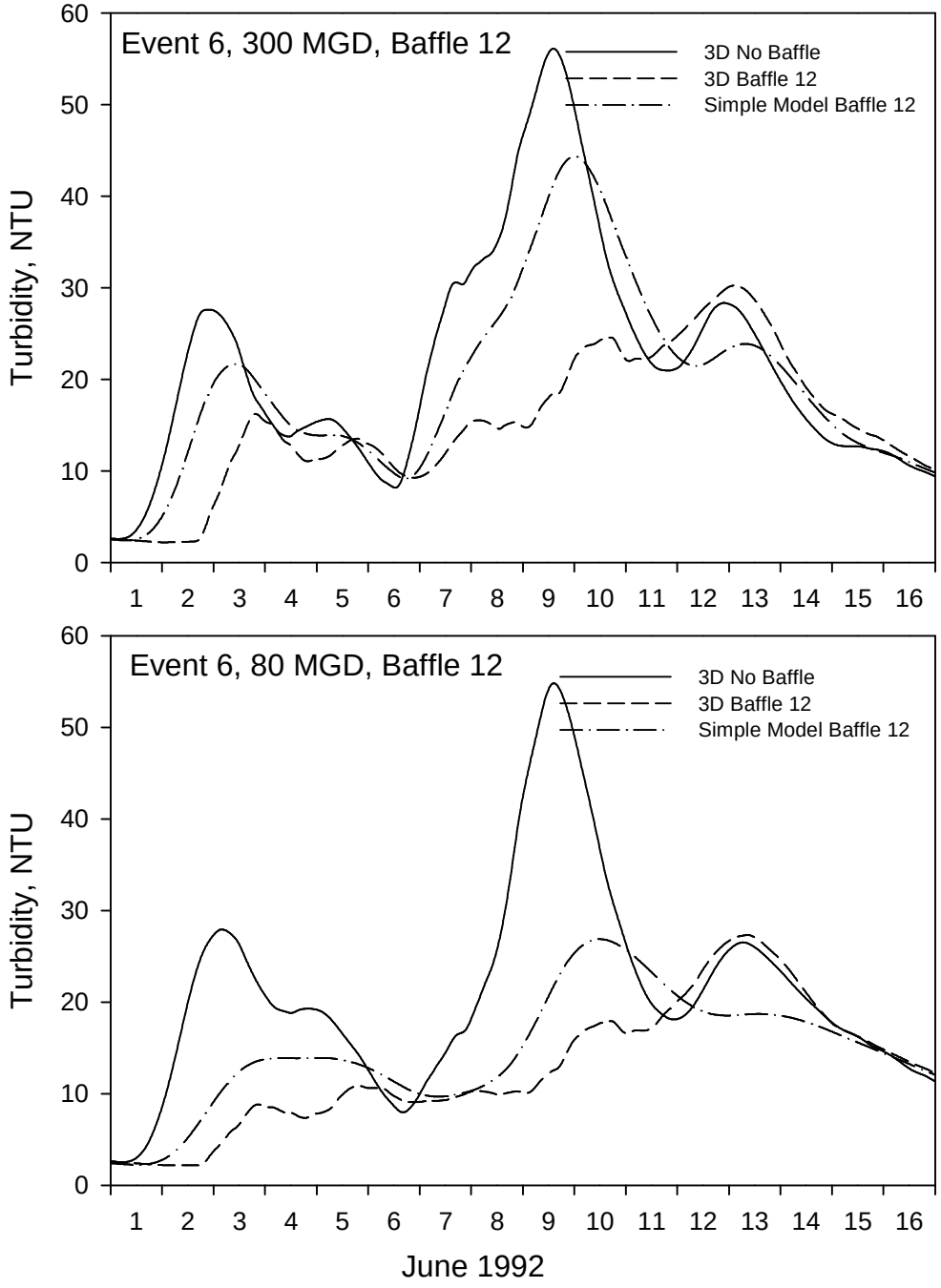

Figure 50. Comparison of simple model prediction with 3D model prediction for Event 6, Baffle 12: (a) 300 MGD, (b) 80 MGD.

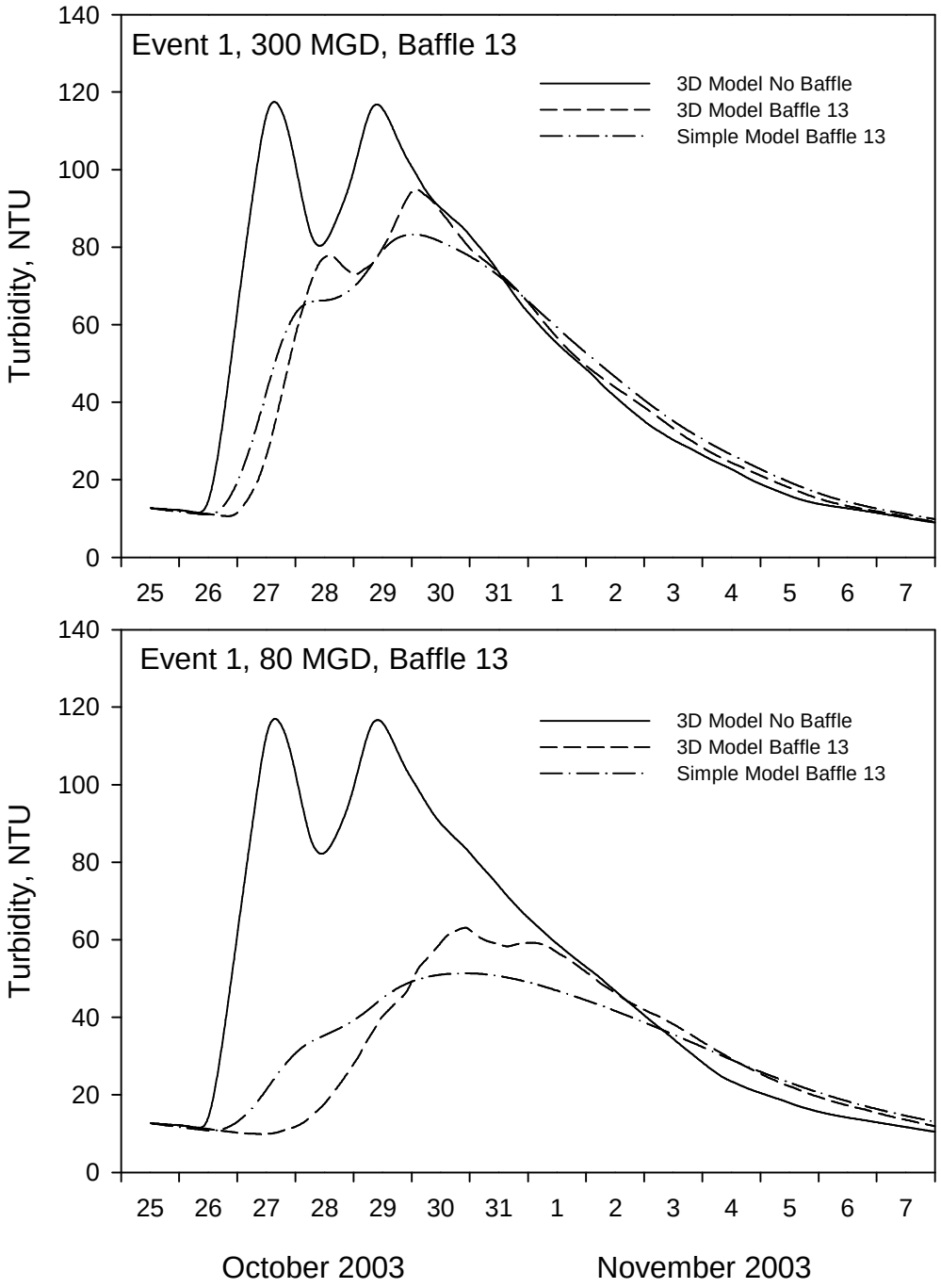

Figure 51. Comparison of simple model prediction with 3D model prediction for Event 1, Baffle 13: (a) 300 MGD, (b) 80 MGD.

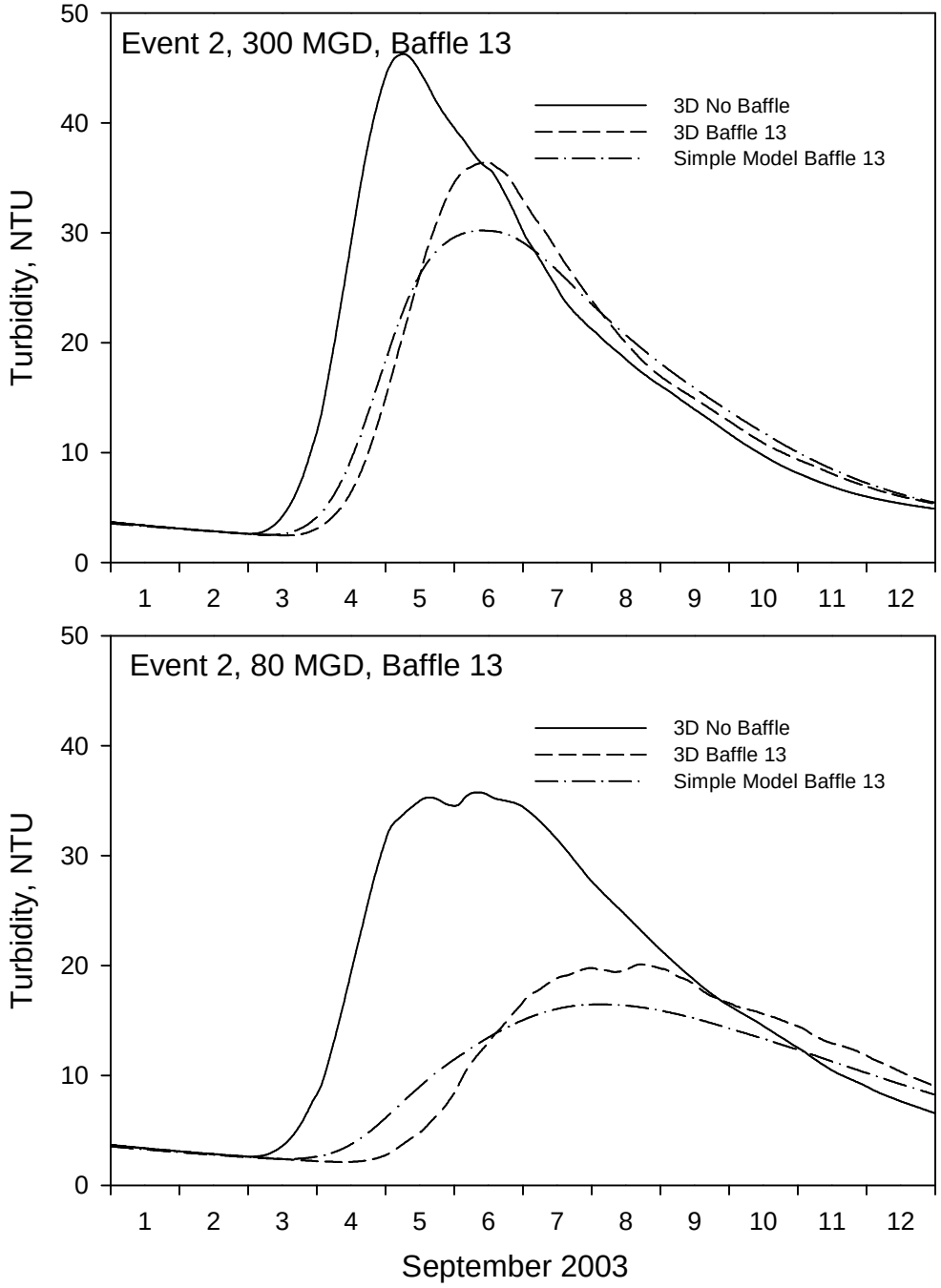

Figure 52. Comparison of simple model prediction with 3D model prediction for Event 2, Baffle 13: (a) 300 MGD, (b) 80 MGD.

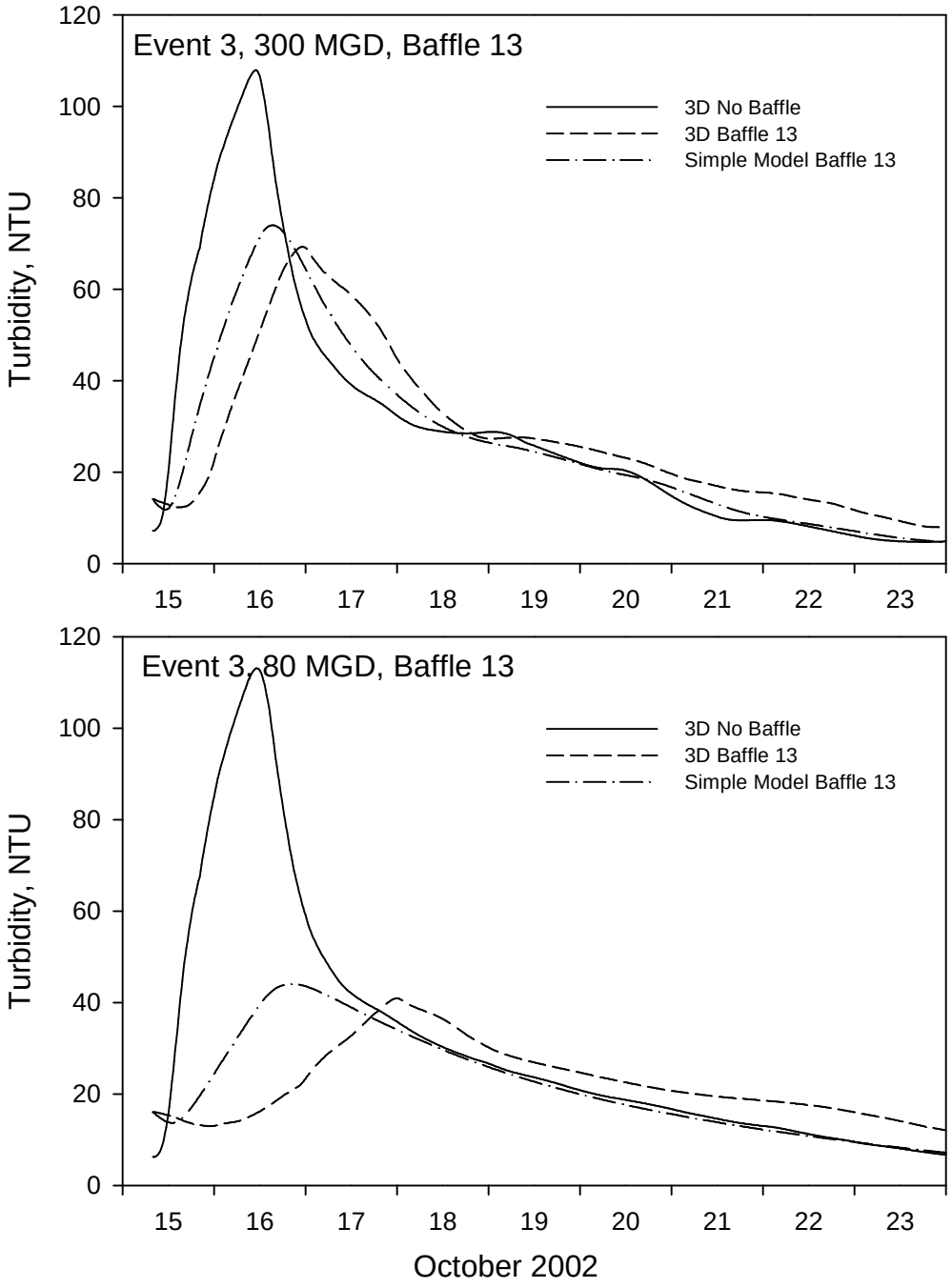

Figure 53. Comparison of simple model prediction with 3D model prediction for Event 3, Baffle 13: (a) 300 MGD, (b) 80 MGD.

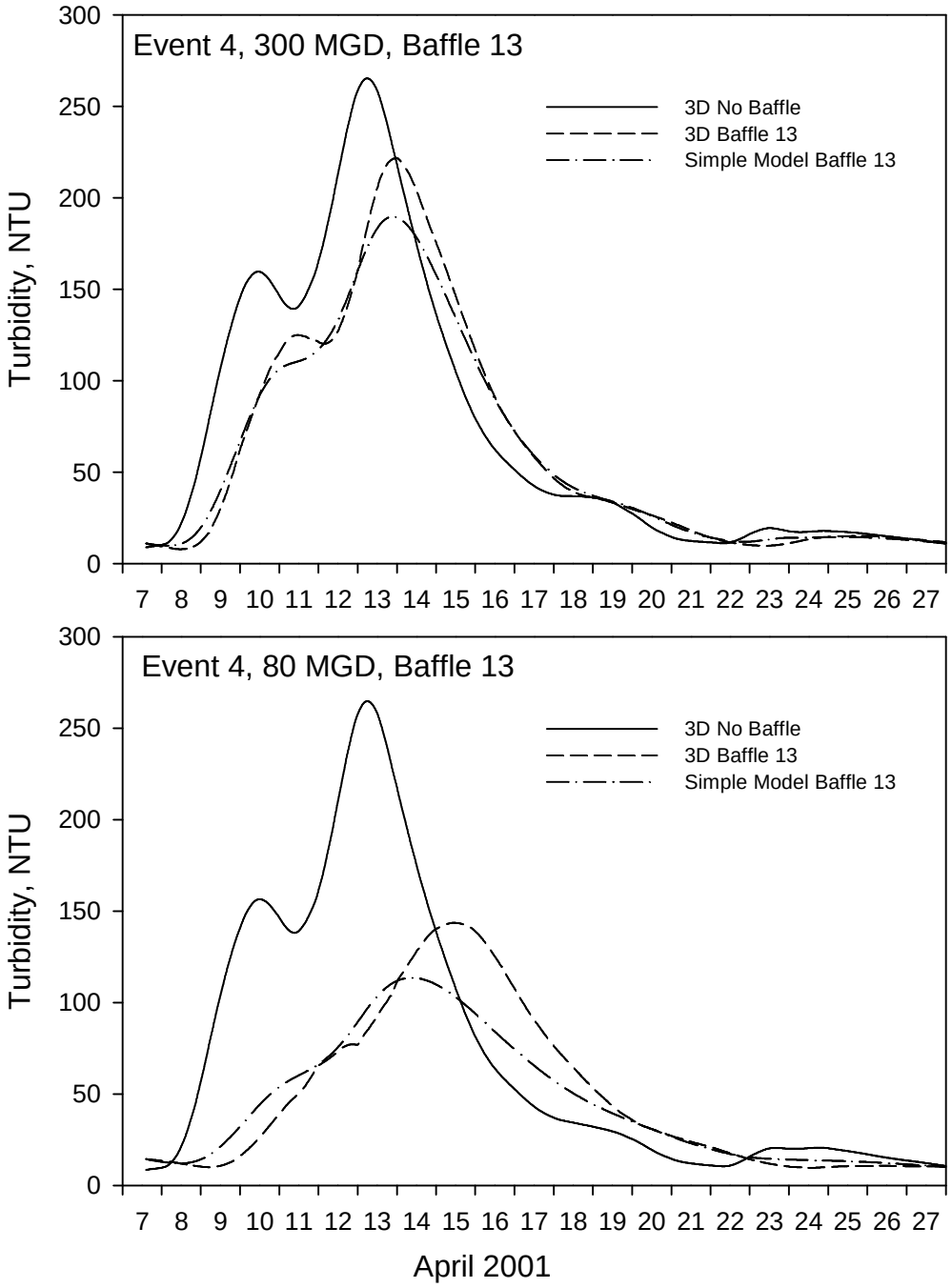

Figure 54. Comparison of simple model prediction with 3D model prediction for Event 4, Baffle 13: (a) 300 MGD, (b) 80 MGD.

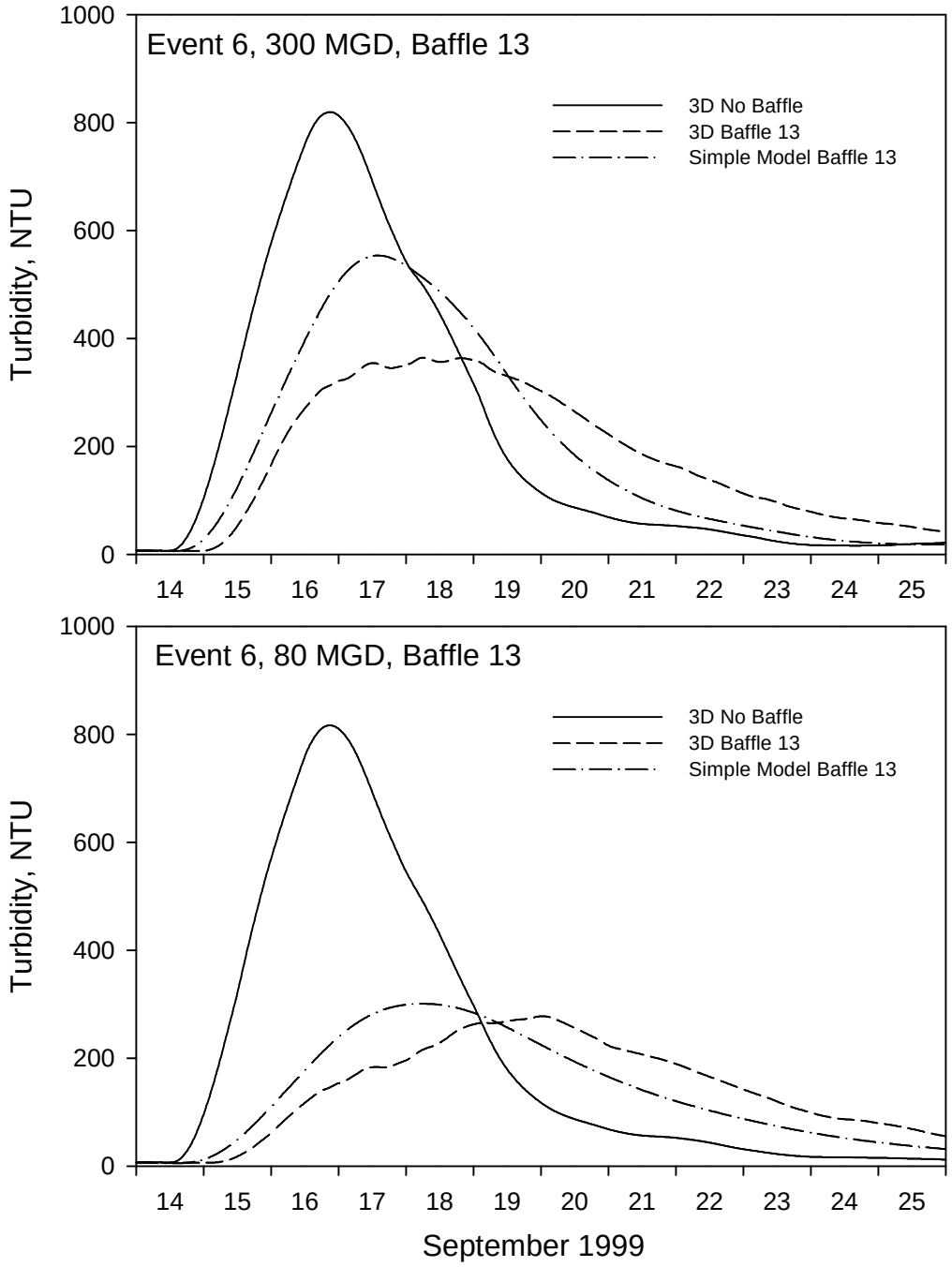

Figure 55. Comparison of simple model prediction with 3D model prediction for Event 5, Baffle 13: (a) 300 MGD, (b) 80 MGD.

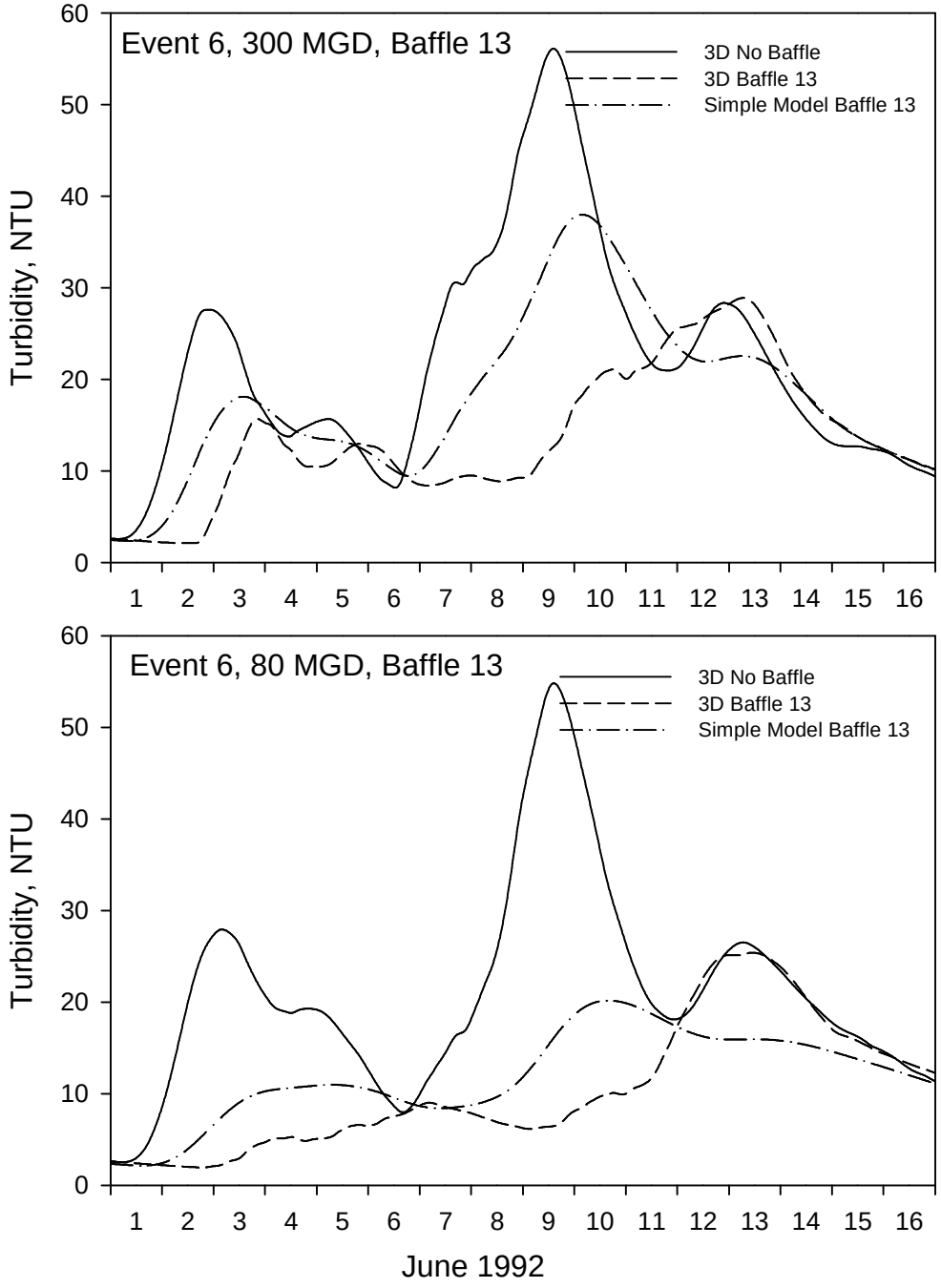

Figure 56. Comparison of simple model prediction with 3D model prediction for Event 6, Baffle 13: (a) 300 MGD, (b) 80 MGD.

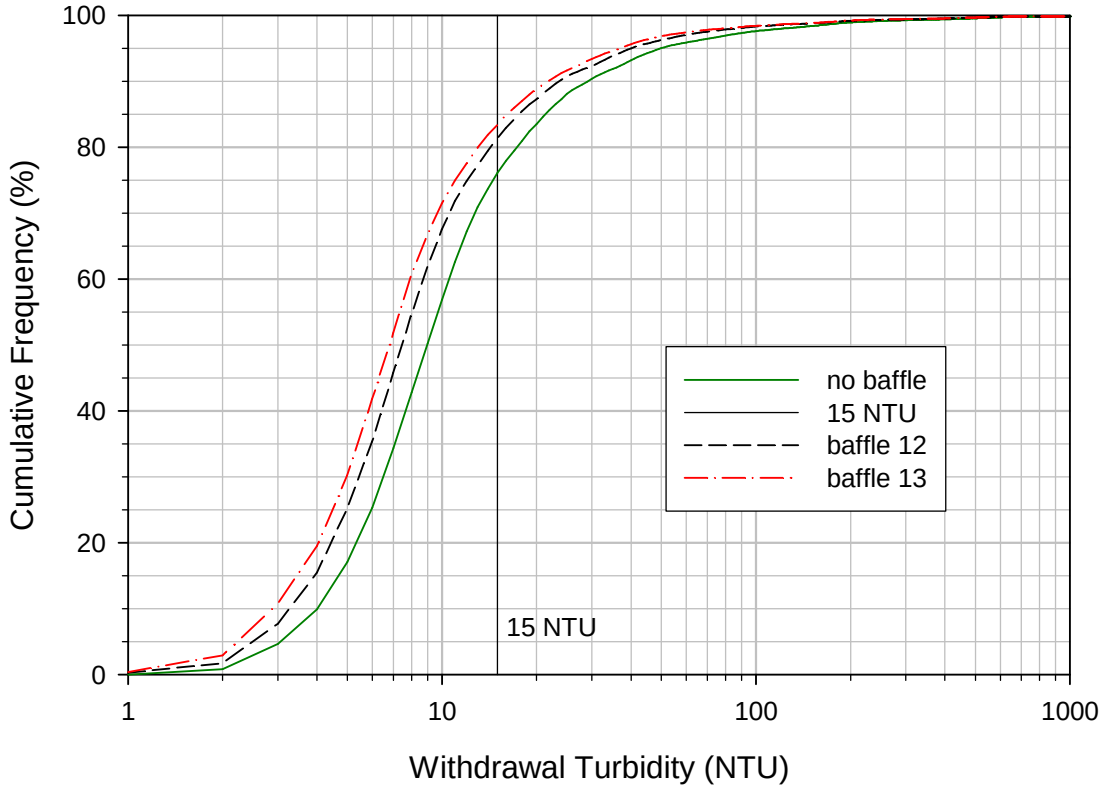

Figure 57. Cumulative frequency distribution for predictions of turbidity at the existing intake structure, Schoharie Reservoir, for the period 1948-2004, and considering only periods when the intake was in operation. The "no baffle" prediction is directly from the 2D model, while the predictions for baffle 12 and baffle 13 are from the simple baffle model.

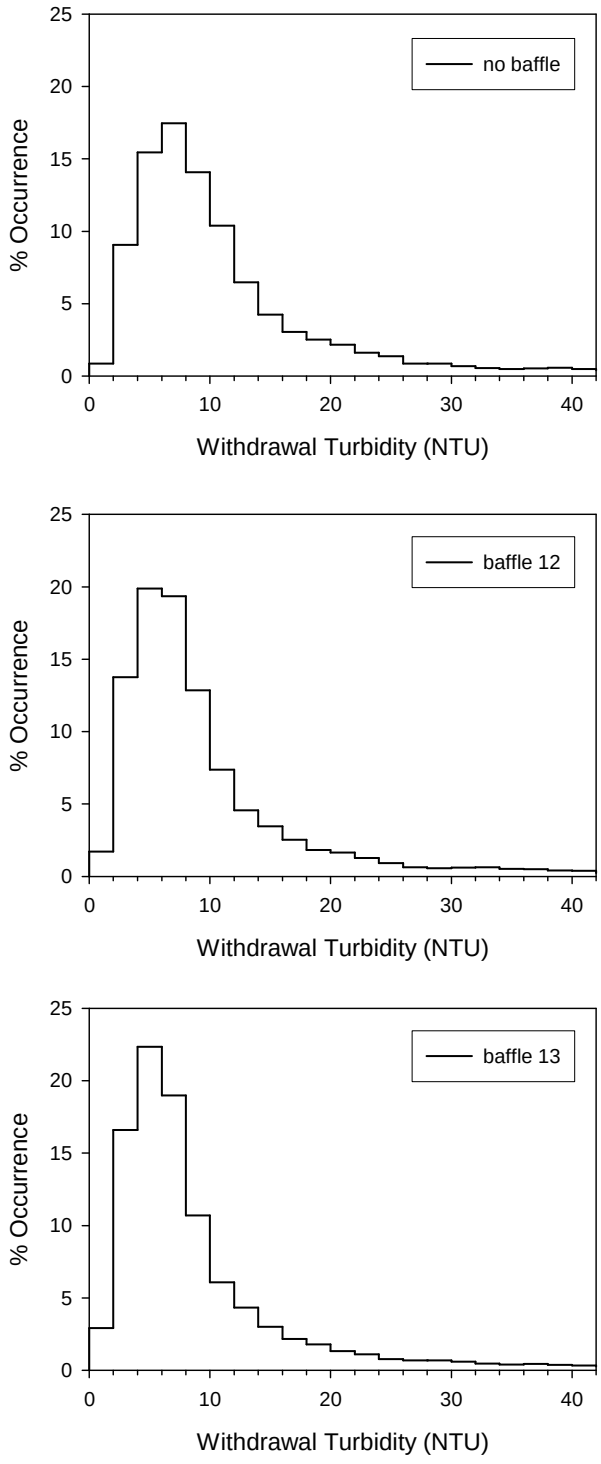

Figure 58. Histograms giving the occurrence of various levels of turbidity at the existing intake structure, Schoharie Reservoir, for the period 1948-2004, and considering only periods when the intake was in operation. The "no baffle" prediction is directly from the 2D model, while the predictions for baffle 12 and baffle 13 are from the simple baffle model.

4. ESOPUS CREEK TEMPERATURE: OBSERVATIONS, MODEL DEVELOPMENT AND APPLICATION

4.1. Background

Esopus Creek (watershed area 497 km^2) is the primary tributary to Ashokan Reservoir located in the Catskill Mountains. The present study is focused on the reach from Allaben to the mouth of the creek where it enters into the west basin of Ashokan Reservoir. The average slope of the study reach is ~ 0.6%. Stream flow in Esopus Creek is regulated by discharge from Shandaken Tunnel carrying the water from Schoharie Reservoir. The minimum flow required by NYS DEC in the creek is 160 MGD – important to the maintenance of trout fishery. The purpose of this study was to develop a temperature model for the creek so that the impact of various management actions at Schoharie Reservoir can be evaluated.

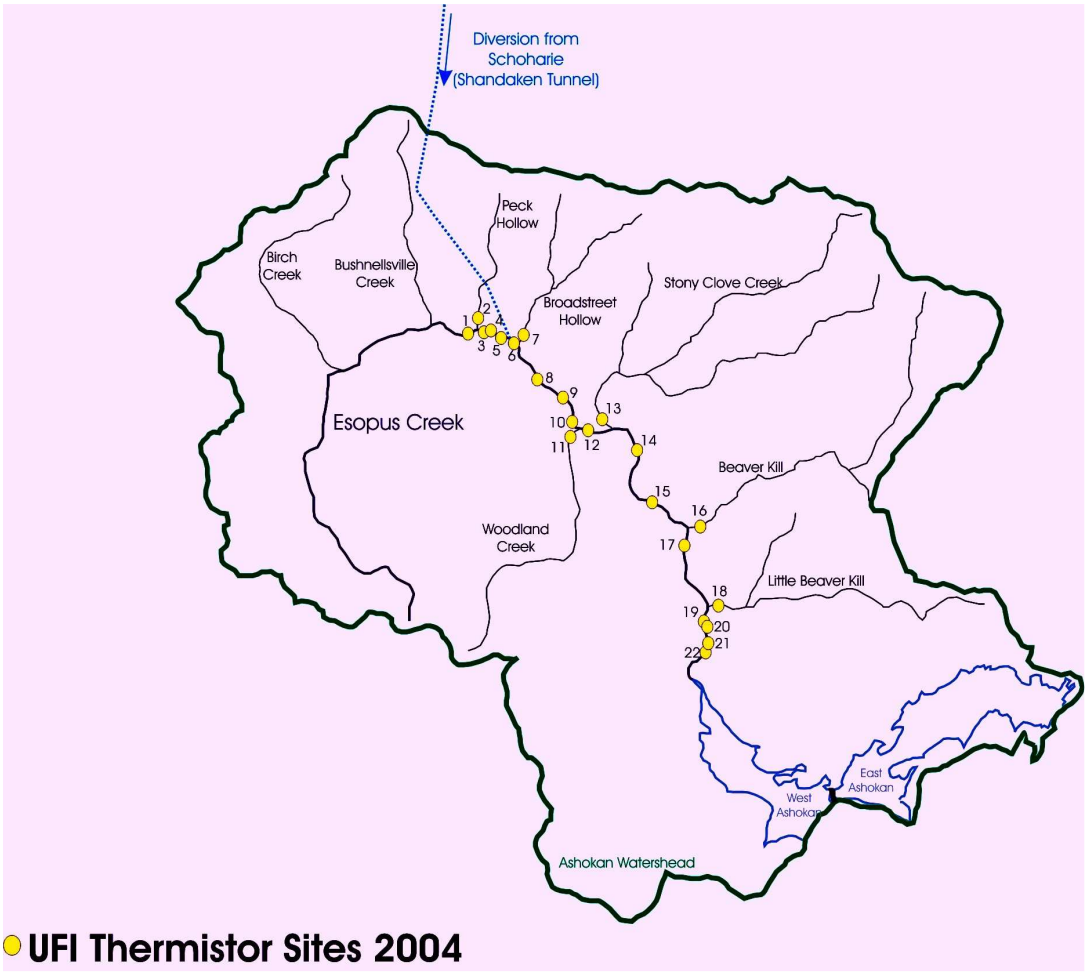

Figure 59. Esopus Creek: watershed above Ashokan Reservoir, and location of deployment of thermistors in 2004 (n = 22).

4.2. Monitoring

To support the development and testing of a temperature model for Esopus Creek, UFI conducted an intensive monitoring program during 2004. The creek monitoring program included deployment of thermistors at 22 locations (Figure 59) in the watershed and a bathymetric survey of the study reach. In addition, one thermistor was deployed in the sediments at Coldbrook and another one in the air at Boiceville monitoring hut (site E16i). Flow data for the creek and its tributaries, and Shandaken Tunnel discharge were obtained from USGS. Meteorological data were made available from robotic monitoring at Schoharie Reservoir (UFI, NYC DEP). Two other alternate meteorological data sets were also obtained from Lexington/Prattsville Airport (NOAA) and Stony Clove site (NYC DEP).

4.3. Observations

Flow from Shandaken Tunnel is compared with the upstream flow at Allaben for May-September 2004 in Figure 60. The impact of Shandaken Tunnel discharge on Esopus Creek temperature is dependent on the upstream flow and temperature, and the discharge flow and temperature. This is illustrated in the longitudinal profiles of temperature for selected days as shown in Figure 61 and 62 and in the scatter plots in Figure 63. Also shown is the diurnal temperature timeseries of temperature at the upstream site (AP; above portal) and at Coldbrook for the cases of Shandaken Tunnel being on and off in Figure 64. These observations indicate that the tunnel discharge had "cooling effect" on the Esopus Creek during summer of 2004.

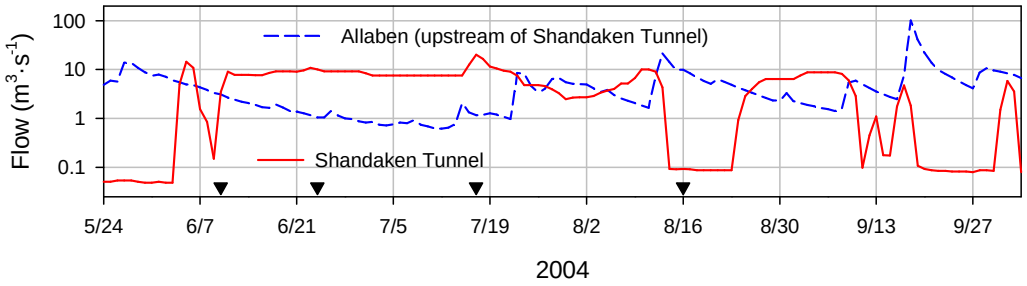

Figure 60. Timeseries of flow at Allaben and from Shandaken Tunnel for May-September 2004 (▼ indicates dates for which longitudinal profiles of temperature are presented in subsequent figures)

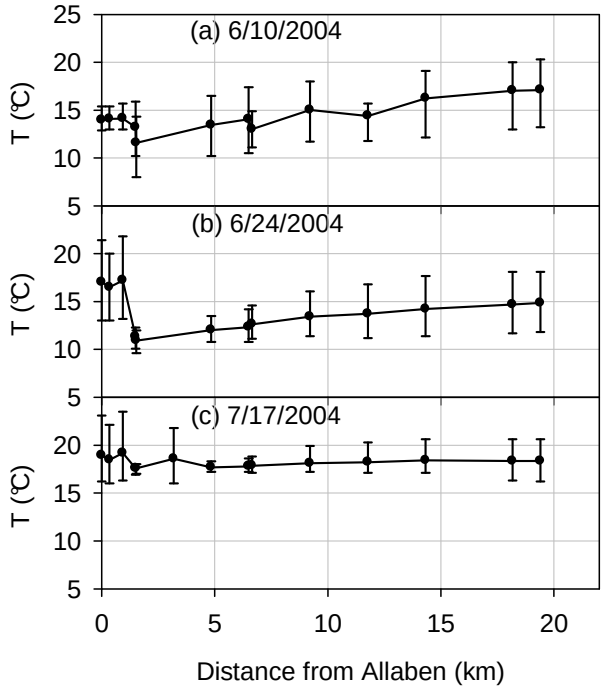

Figure 61. Longitudinal profiles of daily average temperatures (with range bars) from Allaben to the mouth of Esopus Creek for (a) 6/10/2004, (b) 6/24/2004, and (c) 7/17/2004. Shandaken Tunnel was operating in all the three cases.

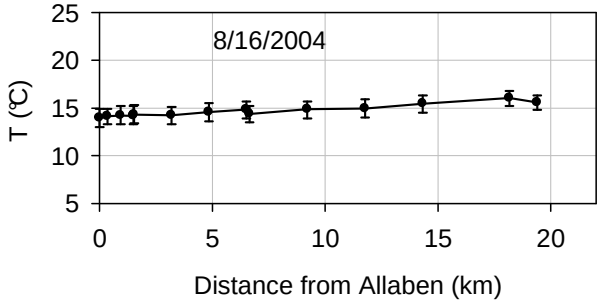

Figure 62. Longitudinal profile of daily average temperatures (with range bars) from Allaben to the mouth of Esopus Creek for 8/16/2004. Shandaken Tunnel was not operating for this case.

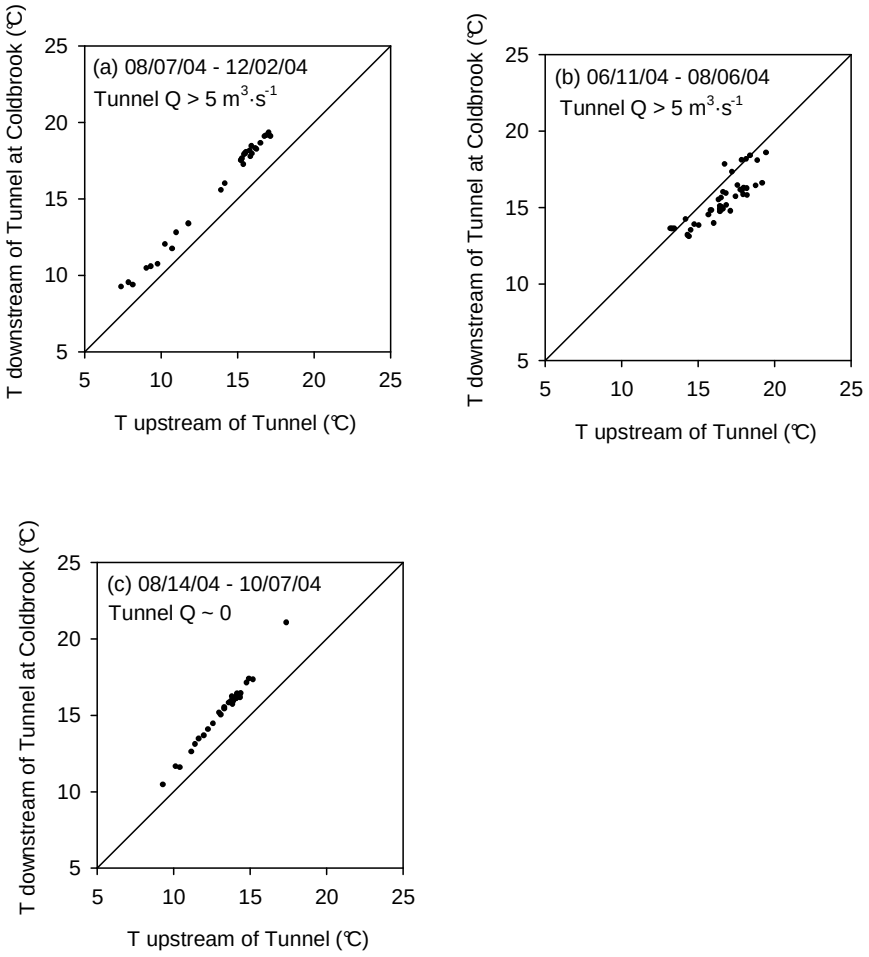

Figure 63. Comparison of daily average temperatures upstream of the Shandaken Tunnel with the temperatures downstream of the tunnel at Coldbrook.

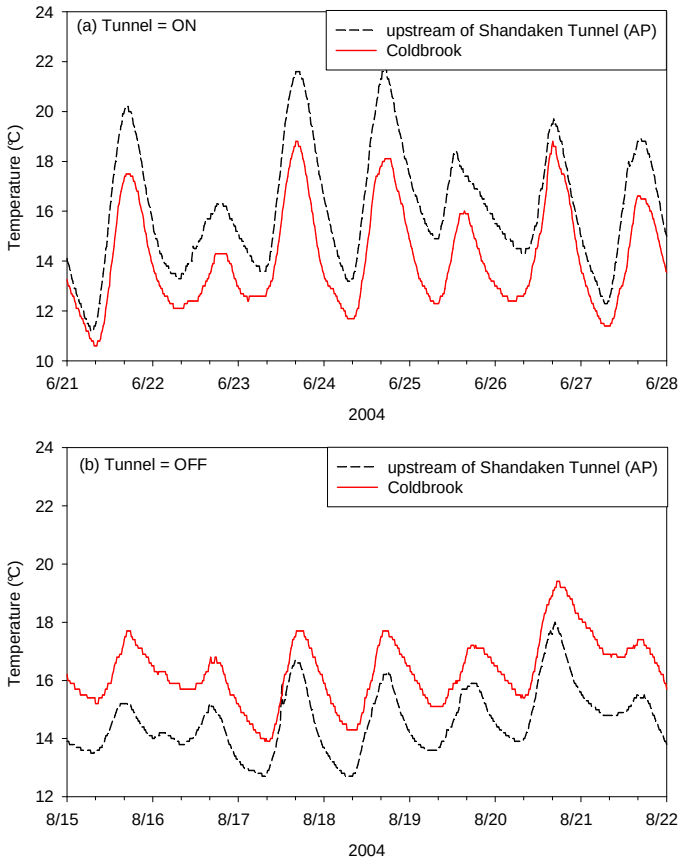

Figure 64. Comparison of diurnal temperatures upstream of the Shandaken Tunnel with the temperatures downstream of the tunnel at Coldbrook for (a) 6/21 through 6/27 when the tunnel was operating, and (b) 8/15 trhough 8/21 when the tunnel was not operating.

4.4. Model Development and Testing

We used CE-QUAL-W2, a two-dimensional hydrothermal and water quality model, to simulate temperature in Esopus Creek. We also developed a sediment heat budget submodel for the creek and included in CE-QUAL-W2. The model performed well in simulating diurnal variations in temperatures as shown in Figure 65 (RMSE = 1.1°C) and daily average variations as shown in Figure 66 (RMSE = 0.9 °C) at Coldbrook site. Performance at other sites was similar.

4.5. Model Application

The model was used to evaluate the impact of a hypothetical multi-level intake facility at Schoharie Reservoir that would divert water into Shandaken Tunnel. A linked water quantity-quality tool (OASIS-W2) was used to generate timeseries of Schoharie Reservoir withdrawal flow and temperature for (i) baseline conditions (i.e., without a multi-level intake; compliant to 6NYCRR Part 670: Reservoir Release Regulations), (ii) modified operations (compliant to SPDES Discharge Permit requirements in addition to baseline conditions), and (iii) for the case of a 3-level intake at site 3 (also compliant to 6NYCRR Part 670 and SPDES regulations). The Esopus Creek model was run with these inputs for the Shandaken Tunnel discharge. The predicted diurnal timeseries of temperature at Coldbrook site for the baseline conditions is compared with the predictions for the case of multi-level intake in Figure 66 and for the case of modified operations in Figure 67. Both, the multi-level intake and modified operations raise Esopus Creek temperature by 1-2 °C during June-July (Figures 66-69). The effect is greatest just below the Shandaken discharge as shown in Figures 70-71.

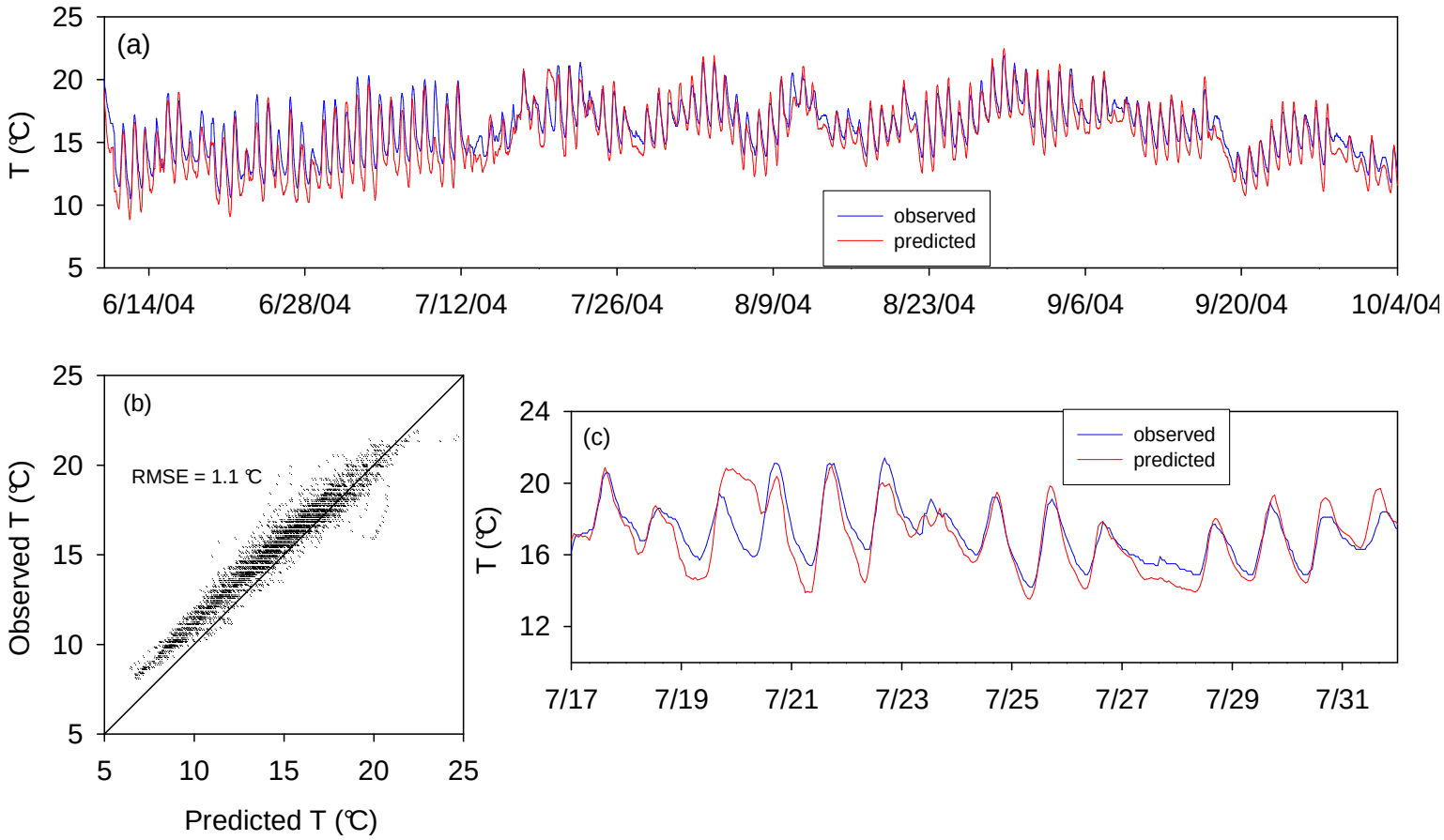

Figure 65. Model performance evaluation: Comparison of observed and predicted temperatures at Coldbrook (a) timeseries plot of diurnal temperature for June-October, (b) scatter plot of diurnal temperature for June-October, and (c) timeseries plot of diurnal temperature for 7/17-7/31.

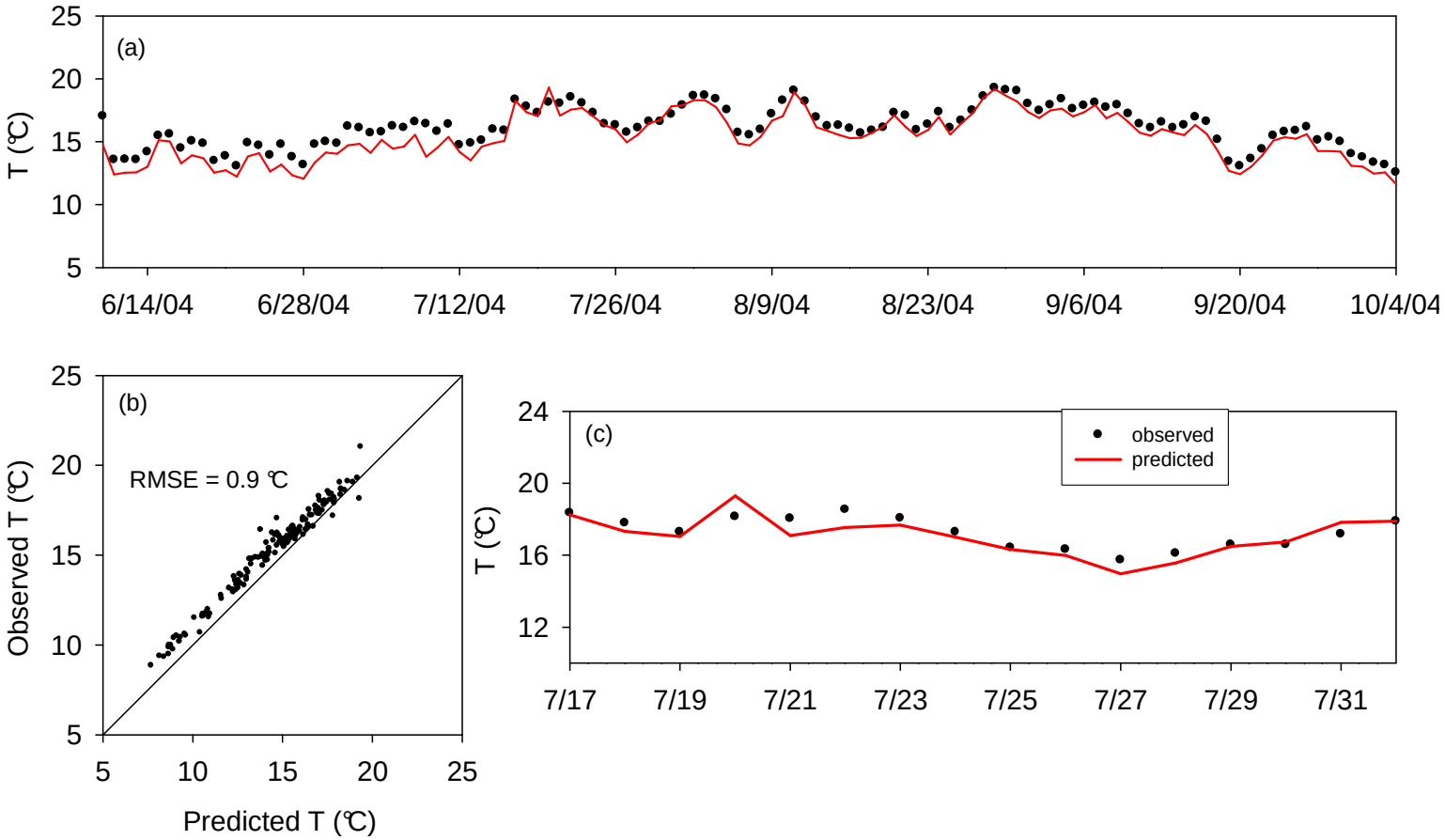

Figure 65. Model performance evaluation: Comparison of observed and predicted temperatures at Coldbrook (a) timeseries plot of daily average temperature for June-October, (b) scatter plot of daily average temperature for June-October, and (c) timeseries plot of daily average temperature for 7/17-7/31.

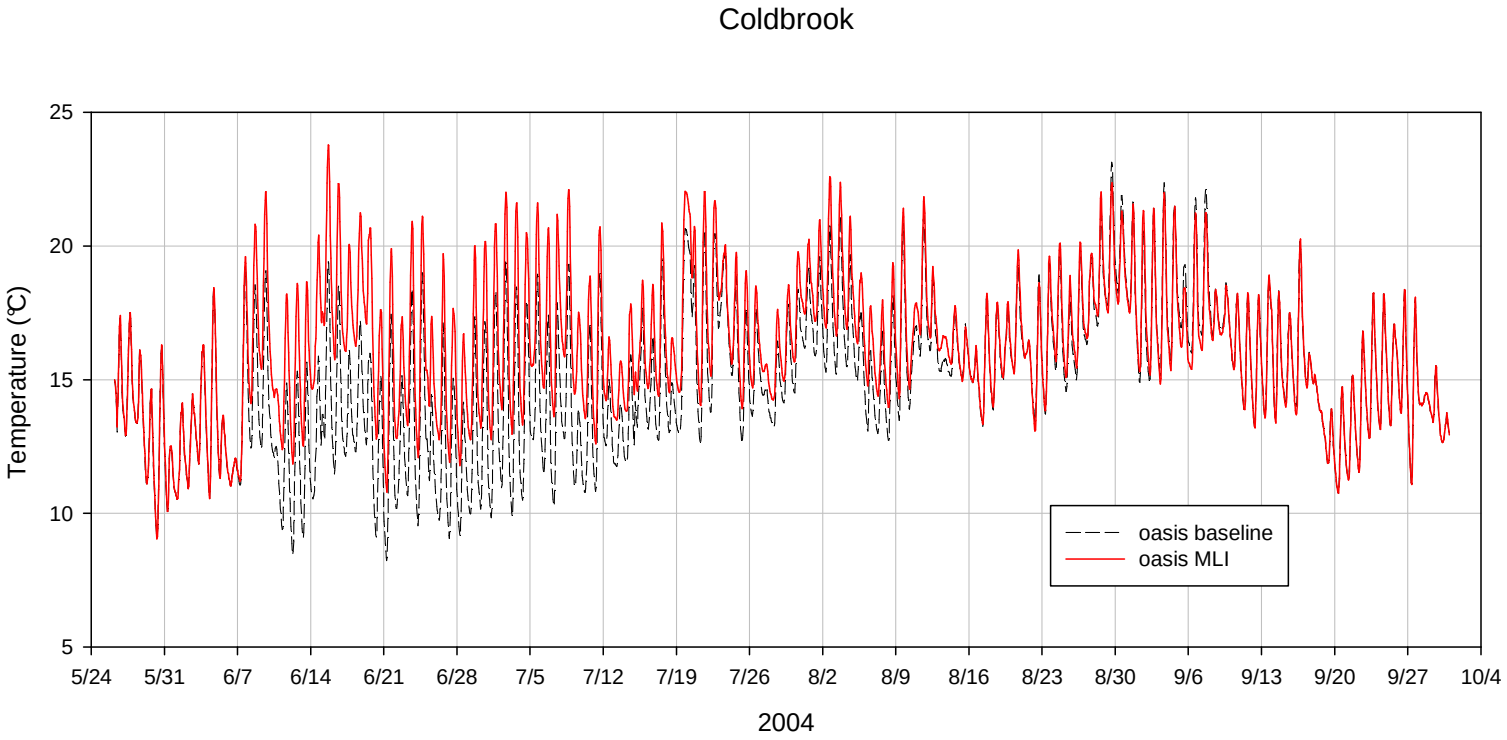

Figure 66. Timeseries of predicted diurnal temperatures at Coldbrook (Esopus Creek) for the two cases of Shandaken Tunnel discharge: (i) OASIS-baseline single level intake operation, and (ii) OASIS MLI operation

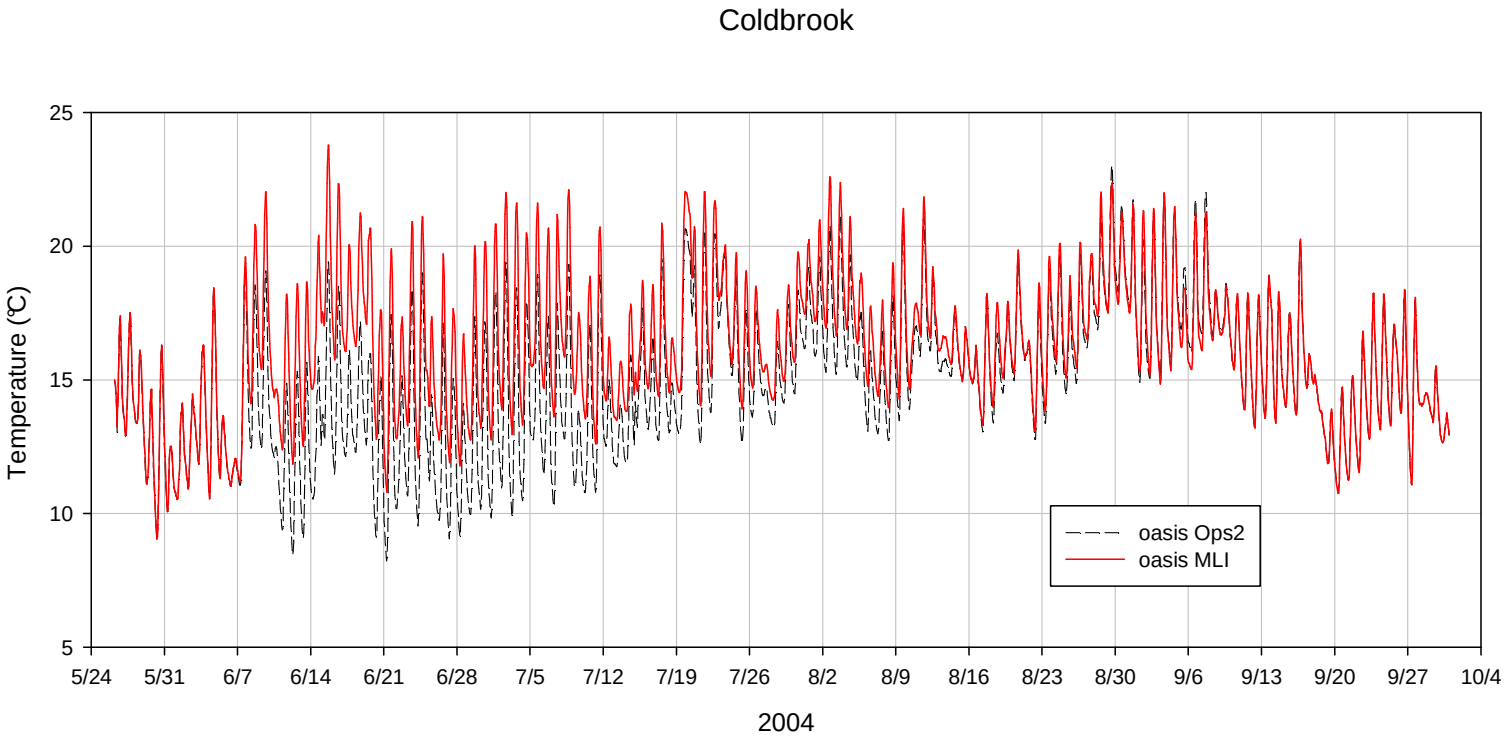

Figure 67. Timeseries of predicted diurnal temperatures at Coldbrook (Esopus Creek) for the two cases of Shandaken Tunnel discharge: (i) OASIS-baseline single level intake operation (OPS2), and (ii) OASIS MLI operation

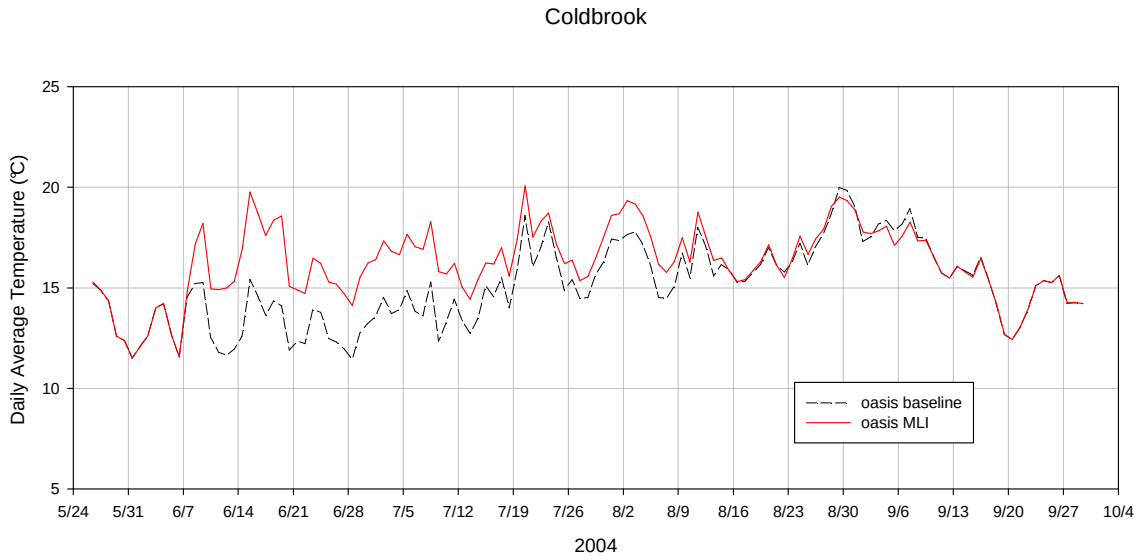

Figure 68. Timeseries of predicted daily average temperatures at Coldbrook (Esopus Creek) for the two cases of Shandaken Tunnel discharge: (i) OASIS-baseline single level intake operation, and (ii) OASIS MLI operation

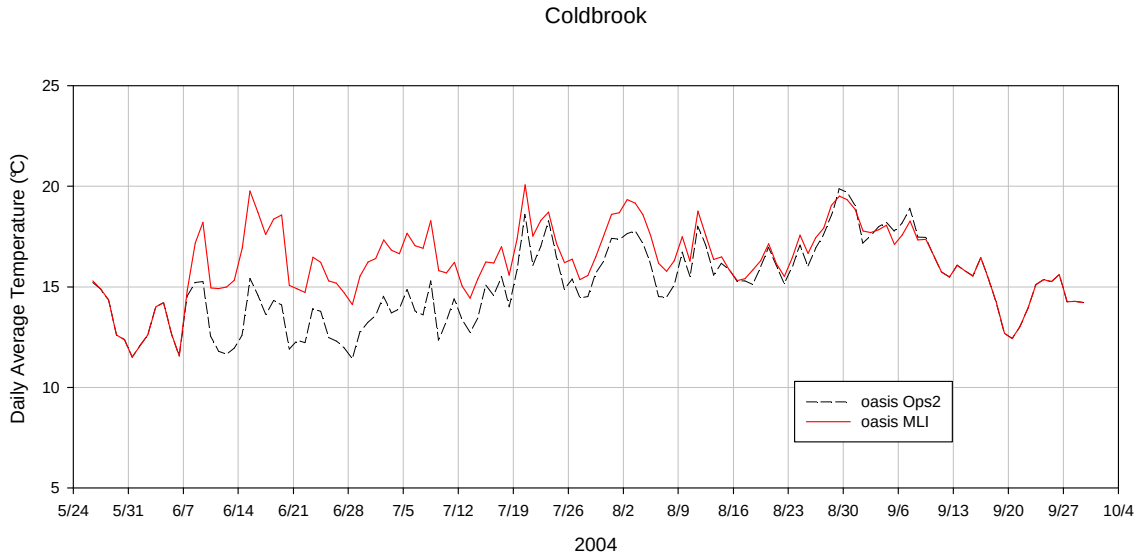

Figure 69. Timeseries of predicted daily average temperatures at Coldbrook (Esopus Creek) for the two cases of Shandaken Tunnel discharge: (i) OASIS-baseline single level intake operation (OPS2), and (ii) OASIS MLI operation

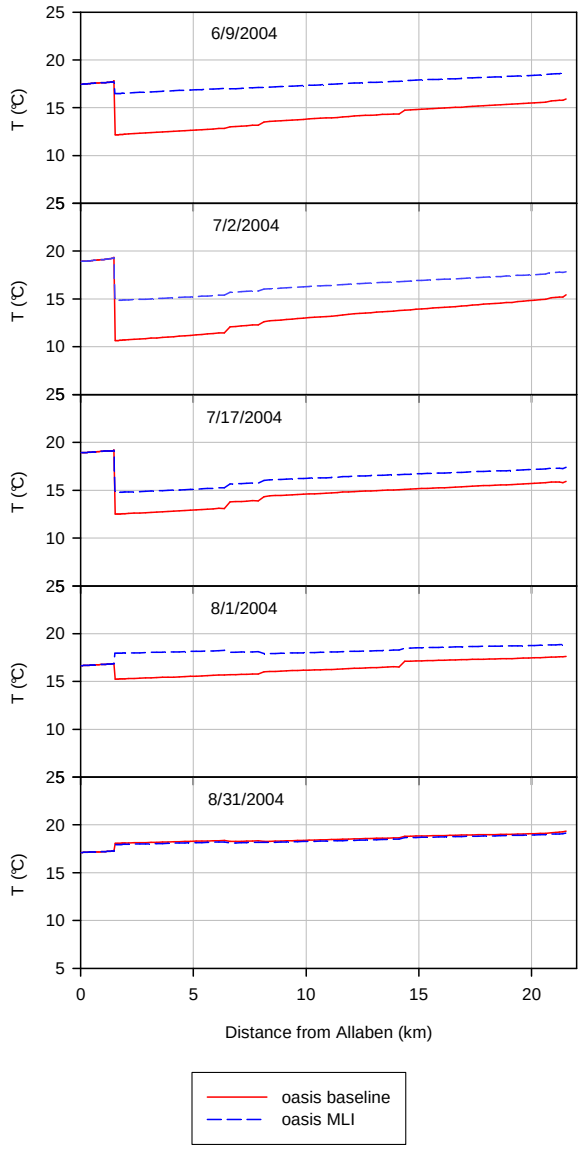

Figure 70. Longitudinal profiles of predicted daily average temperatures for selected days from Allaben to the mouth of Esopus Creek for the two cases of Shandaken Tunnel discharge: (i) OASIS-baseline single level intake operation, and (ii) OASIS MLI operation

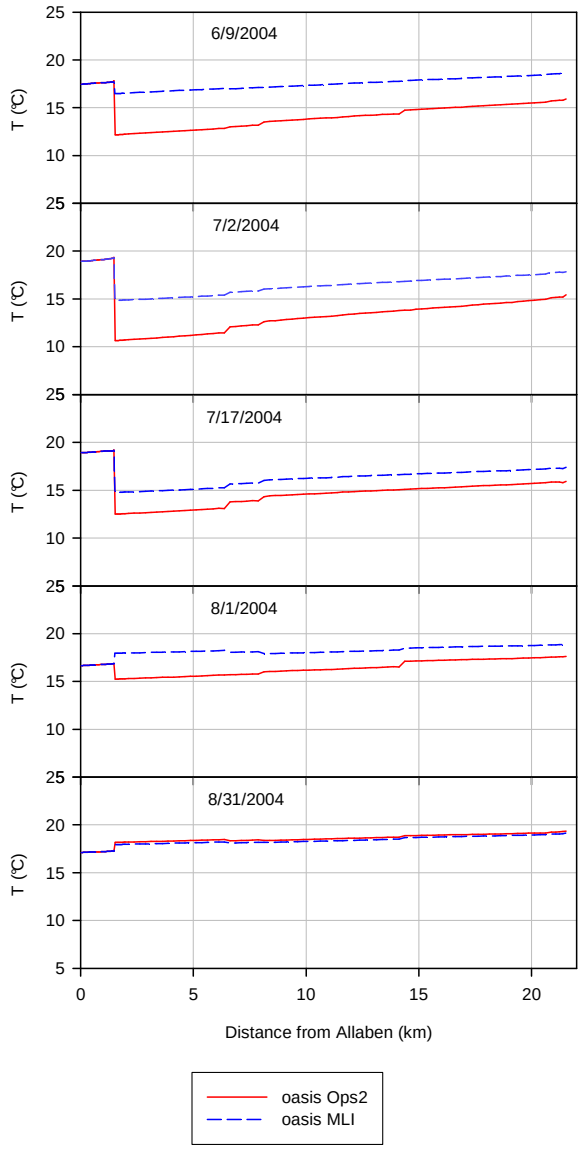

Figure 71. Longitudinal profiles of predicted daily average temperatures for selected days from Allaben to the mouth of Esopus Creek for the two cases of Shandaken Tunnel discharge: (i) OASIS-baseline single level intake operation (OPS2), and (ii) OASIS MLI operation

5. REFERENCES

Ahlfeld, D., A. Joaquin, J. Tobiason and D. Mas. 2003. Case study: Impact of reservoir stratification on interflow travel time. J. Hydraulic Engrg. Div. ASCE 129:966-975.

Babin, M., A. Morel, V. Fournier-Siere, F. Fell and D. Stramski. 2003. Light scattering properties of marine particles in coastal and open ocean waters as related to the particle mass concentration. Limnol. Oceanogr. 48:843-859.

Bierman, V. J. and D. M. Dolan. 1986. Modeling of phytoplankton in Saginaw Bay: II Post-audit phase. J. Environ. Engrg. Div. ASCE 112:415-429.

Chung, S. W. and R. Gu. 1998. Two-dimensional simulations of contaminant currents in stratified reservoir. J. Hydraulic Engrg. Div. ASCE 127:704-711.

Cole, T. M. and S. A. Wells. 2002. CE-QUAL-W2: A Two-Dimensional, Laterally Averaged, Hydrodynamic and Water Quality Model, Version 3.1. Instruction Report EL-2002-1. U.S. Army Engineering and Research Development Center, Vicksburg, MS.

Davies-Colley, R. J. and D. G. Smith. 2001. Turbidity, suspended sediment, and water clarity: A review. J. Am. Wat. Resour. Assoc. 37:1085-1101.

Davies-Colley, R. J., W. N. Vant and D. G. Smith. 1993. Colour and Clarity of Natural Waters. Ellis Horwood, New York, New York. 310 p.

Dean, R. G., and Dalrymple, R. A. (1991). Water wave mechanics for engineers and scientists. World Scientific Publishers.

Edinger, J. E. and E. M. Buchak. 1975. A hydrodynamic, two-dimensional reservoir model: The computational basis. Prepared for U.S Army Engineer Division, Ohio River, Cincinnati, OH.

Effler, S. W. 1985. Attenuation versus transparency. J. Environ. Engrg. Div. ASCE 111:448-459.

Effler, S. W., R. K. Gelda, J. A. Bloomfield, S. Quinn and D. L. Johnson. 2001. Modeling the effects of tripton on water clarity: Lake Champlain. J. Water Res. Plan. Manage. 127:224-234.

Effler, S. W. and D. A. Matthews. 2004. Sediment resuspension and drawdown in a water supply reservoir. J. Am. Wat. Resour. Assoc. 40:251-264.

Effler, S. W., D. A. Matthews, J. Kaser, A. Prestigiacomo and D. G. Smith. 2006. Runoff event impacts on a water supply reservoir: Suspended sediment loading, turbid plume behavior, and sediment deposition. J. Am. Wat. Resour. Assoc. (in press).

Effler, S. W., A. Prestigiacomo, F. Peng, K. B. Bulygina and D. G. Smith. 2006. Resolution of patterns of turbidity in a water supply reservoir from runoff events and the advantage of in situ beam attenuation measurements. Lake and Reserv. Manage. (in press).

Gannett Fleming & Hazen and Sawyer. 2004. Catskill turbidity control study: Phase I Final Report. Prepared for New York City Department of Environmental Protection, Bureau of Environmental Engineering Watershed Facilities Design.

Gelda, R. K. and S. W. Effler. 2003. Application of a probabilistic ammonia model: Identification of important model inputs and critique of a TMDL analysis for an urban lake. Lake and Reserv. Manage. 19:187-199.

Gelda, R. K. and S. W. Effler. 2006a. Testing and application of a two-dimensional hydrothermal model for a water supply reservoir: Implications of sedimentation. J. Environ. Engrg. Sci. (in review).

Gelda, R. K. and S. W. Effler. 2006b. Modeling turbidity in a water supply reservoir: Advancements and issues. J. Environ. Engrg. Div. ASCE (in review).

Gelda, R. K. and S. W. Effler. 2006b. Simulation of operations and water quality performance of reservoir multi-level intake configurations. J. Water Res. Plan. Manage. (in press).

Gelda, R. K., S. W. Effler and S. M. O'Donnell. 2001. Probabilistic model of ammonia and toxicity status for urban lake. J. Water Res. Plan. Manage. 127:337-347.

Gelda, R. K., E. M. Owens and S. W. Effler. 1998. Calibration, verification, and an application of a two-dimensional hydrothermal model [CE-QUAL-W2(t)] for Cannonsville Reservoir. Lake and Reserv. Manage. 14:186-196.

GZA GeoEnvironmental of New York. 2002. Sedimentation analysis and dredging feasibility study report: Schoharie Reservoir. Prepared for the City of New York Department of Environmental Protection and Bureau of Environmental Engineering. GZA GeoEnvironmental of New York, Buffalo, NY.

Gu, R. and S. W. Chung. 1998. Reservoir flow sensitivity to inflow and ambient parameters. J. Water Resour. Plann. Manage. Div. ASCE 124:119-128.

Hanna, R. B., L. Saito, J. M. Bartholow and J. Sandelin. 1999. Results of simulated temperature control device operations on in-reservoir and discharge water temperatures using CE-QUAL-W2. Lake and Reserv. Manage. 15:87-102.

Ji, Z., Morton, M. R., and Hamrick, J. H. 2003. Three dimensional hydrodynamic and water quality modeling in a reservoir. Proc. 8th Intl. Conf. Estuarine and Coastal Modeling, Monterey CA.

Jin, K-R., Hamrick, J. H., and Tisdale, T. 2000. Application of three-dimensional hydrodynamic model for Lake Okeechobee. J. Hydraul. Eng., 126(10), 758-771.

Kirk, J. T. O. 1994. Light and photosynthesis in aquatic ecosystems. Cambridge University, London.

Lemmin, U. and C. H. Mortimer. 1986. Tests of an extension to internal seiches of Defant's procedure for determination of surface seiche characteristics of real lakes. Limnol. Oceanogr. 31:1207-1231.

Letterman, R. D., C. E. Johnson and S. Viswanthan. 2004. Low-level turbidity measurements: A comparison of instruments. J. Am. Wat. Works Assoc. 96:125-137.

Lick, W., J. Lick and C. K. Ziegler. 1994. The resuspension and transport of fine-grained sediment in Lake Erie. J. Great Lakes Res. 20:599-612.

Luettich, R. A., D. R. F. Harleman and L. Somlyody. 1990. Dynamic behavior of suspended sediment concentrations in a shallow lake perturbed by episodic wind events. Limnol. Oceanogr. 35:1050-1067.

Martin, J. L. 1988. Application of two-dimensional water quality model. J. Environ. Engrg. Div. ASCE 114:317-336.

Martin, J. L. and S. C. McCutcheon. 1999. Hydrodynamics and transport for water quality modeling. Lewis Publishers, Boca Raton, FL. 794 p.

McCarthy, J. C., J. E. Pyle and G. M. Griffin. 1974. Light transmissivity, suspended sediments and the legal definitaion of turbidity. Estur. Coast. Mar. Sci. 2:291-299.

Newcombe, C. P. 2003. Impact assessment model for clear water fishes exposed to excessively cloudy water. J. Am. Wat. Resour. Assoc. 39:529-544.

O'Donnell, D. M. and S. W. Effler. 2006. Resolution of impacts of runoff events on a water supply reservoir with a robotic monitoring network. J. Am. Wat. Resour. Assoc. (in press).

Owens, E. M. 1998. Development and testing of one-dimensional hydrothermal models of Cannonsville Reservoir. Lake and Reserv. Manage. 14:172-185.

Owens, E. M. 2006. Observation and Simulation of Surface Waves in Two Water Supply Reservoirs. J. Hydraulic Engrg. Div. ASCE (in review).

Owens, E. M. and S. W. Effler. 1989. Changes in stratification in Onondaga Lake, NY. Wat. Resour. Bull. 25:587-597.O

Owens, E. M., and Effler, S. W. (2005). "A three-dimensional model of plunging inflow to a reservoir". *J. Hydraul. Eng.* (in review).

Owens, E. M., S. W. Effler, S. M. Doerr, R. K. Gelda, E. M. Schneiderman, D. G. Lounsbury and C. L. Stepczuk. 1998. A strategy for reservoir model forecasting based on historic meteorological conditions. Lake and Reserv. Manage. 14:322-331.

Owens, E. M., R. K. Gelda, S. W. Effler and J. M. Hassett. 1998. Hydrologic analysis and model development for Cannonsville Reservoir. Lake and Reserv. Manage. 14:140-151.

Peng, F., D. L. Johnson and S. W. Effler. 2004. Characterization of inorganic particles in selected reservoirs and tributaries of the New York City water supply. J. Am. Wat. Resour. Assoc. 40:663-676.

Schwab, D. J., J. R. Bennett, P. C. Liu and M. A. Donelan. 1984. Application of a simple numerical wave prediction model to Lake Erie. J. Geophys. Res. 89:3586-3592.

Skinner, P., C. Silver, J. Tierney and P. Lehner. 2003. Clean water - Clean creek: A proposal for a multiple level water intake structure in the Schoharie Reservoir to improve drinking water quality, protect the Esopus Creek and expand the New York City water supply. Eliot Spitzer, Attorney General of the State of New York.

Smith, D. G. 2002. Turbidity in Catskill Watershed. New York City Department of Environmental Protection, Division of Drinking Water Quality Control, Bureau of Water Supply, Valhalla, NY. 68 p.

Upstate Freshwater Institute. 2001. Calibration and verification of two-dimensional hydrothermal and eutrophication models for six Catskill/Delaware reservoirs. Submitted to the New York City Department of Environmental Protection, Valhalla, New York. Upstate Freshwater Institute, Syracuse, NY.

Upstate Freshwater Institute. 2004. Investigation of the Effects of Baffles on Features of Transport in Schoharie Reservoir. Report prepared for Hazen & Sawyer Environmental Engineers and Scientists, and New York City Department of Environmental Protection.

Wetzel, R. G. 2001. Limnology: lake and reservoir ecosystems. Academic Press, New York.

Yang, Z., Khangaonkar T., DeGasperi C., and Marshall, K. 2000. Three-dimensional modeling of temperature stratification and density-driven circulation in Lake Billy Chinook, Oregon. Proc. 6th Intl. Conf. Estuarine and Coastal Modeling, M. L. Spaulding, et al., (eds.). ASCE, New Orleans, LA, pp. 411-425.

Ziegler, C. K. and B. S. Nisbet. 1995. Long-term simulations of fine-grained sediment transport in large reservoir. J. Hydraulic Engrg. Div. ASCE 121:773-781.